LEVEL

12

AD A097641

DTIC FILE COPY

DTIC
APR 13 1981
C

DISTRIBUTION STATEMENT A
Approved for public release;
Distribution Unlimited

81 4 30 003

AVIONICS DIVISION ITT
390 Washington Avenue, Nutley, NJ 07110

(12)

FINAL REPORT: S-BAND MICROWAVE SYSTEM,

CONTRACT DAAK70-79-C-0171

NOVEMBER 15, 1980

Revised by 12/18/80

PREPARED BY:

ITT Avionics Division
Electro-Optical Systems Depart.
390 Washington Avenue
Nutley, NJ 07110

TABLE OF CONTENTS

FIGURES

1.0 INTRODUCTION

There are, at present, two significant methods available for introducing microwave energy into a plasma. Fehsenfeld etal. Ref. 7, utilizing his number 5 cavity, claims power transfer levels of the order of 100 percent. The principal difficulty lies in the rather restricted volume and can be expected to be quite inhomogeneous. Close coupling between the plasma and the cavity is involved.

The second technique espoused by Bossisio Ref. 8 and McTaggert Ref. 9 involves the use of a slow wave structure and a loose coupling. Because of this structure, there is little difficulty in operating the discharge and very large plasma volumes have been accomodated. Claims for very high coupling efficiency are also recorded for this technique.

Both these techniques involve the use of a "CW" magnetron. No "too much" is being said about the use of waveguide plasmas at present. Such plasmas can be either the central conductor of a coaxial waveguide having either cylindrical or spherical symmetry. They could also act as the outer wall of a coaxial waveguide. The principal problem lies in the need for an auxiliary starting technique since the field intensities in a normal waveguide structure are somewhat lower than those required for breakdown when higher pressure are involved. This can be overcome by the use of a lumped parameter waveguide which is essentially a set of leaky resonant cavities in series with the plasma tube as the common central conductor. A helical close coupling to the central conductor is another technique. An alternate system that permits the coupling with acoustic waves and that admits higher electric field intensities is a pulsed magnetron.

In order to implement a specific design that introduces microwave energy into a plasma, it is first necessary to identify the medium that will comprise the plasma.

This, in a complete analysis, includes the volume, shape factor, density, and temperature. In addition, the material species in terms of ionization levels and excited levels, at least, in the case of the simpler monatomic materials must be represented.

The resultant population will then be a system of charged particles including both electrons and ions with a residual fraction of un-ionized particles. All of these members of a more complex population, are in various stages of excitation.

Such a plasma structure will exhibit characteristic responses to external stimulation at certain unique frequencies which are due to the propagation velocities and the dominant characteristic dimensions of the plasma. When the parameters of the incident energy are appropriate for these plasma resonances, there are departures from the normal operation. The various states of excitation, the relative populations and the lifetimes of the species in those states determine how the applied energy is apportioned between the various internal plasma processes. The object then becomes the identification of the initial species distribution so that certain final processes are accentuated. In the present program several of these aspects are described in the succeeding sections. This program has not addressed the optimization of the potential resultant laser because the knowledge of the particular processes such as the reaction rates of the various alkali earth halides, and their various diatomic radicals are, at present, unavailable. The necessary data for these are, however, expected to

be provided in the next stage of the program.

2.0 ESTIMATE OF CAVITY TEMPERATURES

It is important to establish the anticipated steady state temperature of the microwave cavity and also the time required to attain this equilibrium. Four reasons are involved. The first is that the cavity wall acts as the thermal environment for the quartz plasma container. The second is the establishment of the expected variation in cavity dimensions as a function of temperature. The third is the assurance of maintaining the mechanical integrity of the cavity. The fourth is the reduction in the conductivity of the cavity itself due to an increase in temperature. To this end the steady state temperature is established for a variety of power losses. The power lost is, of course, a measure of the lack of laser efficiency at the cavity itself.

The brass cavity has a total surface area of 4089 cm^2. The cavity was painted black to approach a unity emissivity as closely as practical. The probable value for the spectral region that is effective, is 96%. This is largely due to the refractive index of the paint binder. The convective - conductive characteristics are dominated by the external gaseous surface film which is approximately 0.43cm thick. The gas film conductivity is temperature dependent and has the value:

2.1 $k = 1.92 \times 10^{-5} \sqrt{T}\ (1 + 2 \times 10^{-4}T)/(1 + 124/T)$ joules/cm sec ^{o}K

for air, T in ^{o}K.

Combining the resultant power transfer with the radiative contribution from $\sigma\varepsilon\ (T^4 - T_o^4)$ results in a equilibrium temperature for the cavity which is a function of the energy being lost from the laser operation. The extreme result presumes a 0.43cm air film

and a 24°C ambient temperature T_o. This is graphed in figure 1. The second aspect of the temperature consideration is the temperature that will be attained by the quartz vessel envelope. This is significant for several reasons. The first is for the maintenance of an adequate vapor pressure in the quartz enclosed cavity. This implies a certain minimum desired temperature. The second is the maintenance of a low enough electrical conductivity in the quartz so that a thermal runaway does not occur. This requires a maximum allowable temperature.

An estimate has been made for the temperature attained by the quartz tube when the cavity is losing power at a number of levels. These power losses correspond to the cavity temperatures shown in figure 1. The solution is, of necessity, empirical because of the complex effects due to the convective component being confined to the annular region defined by the concentric cylinders. These effects have been considered in reference 30 on which this estimate is based. The active portion of the quartz tube is approximately 71cm long and 2.5cm in diameter. This is a $580cm^2$ surface. As an example, in free air, the quartz tube would reach about 420°C if 1000 watts were dissipated in this manner. The existence of an enclosure, which is highly reflective, surrounding the quartz, however, reduces the heat transfer to a much lower rate. The effective emissivity may be shown to be

2.2 $E = \varepsilon_2/(\varepsilon_2/\varepsilon_1 + 1 - \varepsilon_2)$ where ε_2 is the emissivity of the hot (quartz) surface and ε_1 is the emissivity of the cold (brass) surface. In the region of 100 to 200°C polished brass emissivities ε_1 is 0.055. Quartz in the range from 300 to 500°C has an emissivity

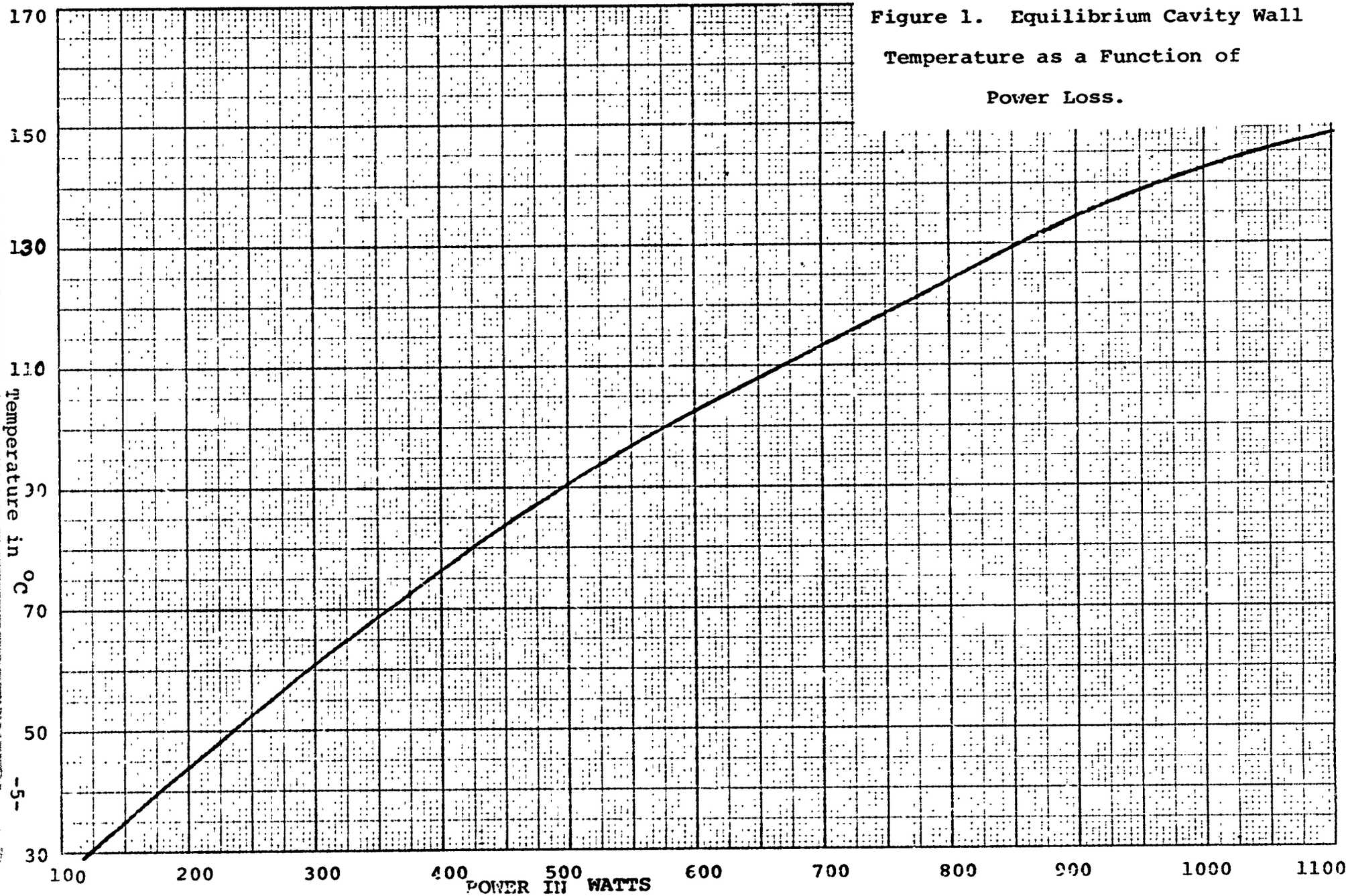

Figure 1. Equilibrium Cavity Wall Temperature as a Function of Power Loss.

ε_2 of $\sim$0.78 in thickness of 2mm. Ideally, it is most desireable to minimize the effective emissivity. This permits the maximum gradient in temperature between the plasma envelope and the cavity. Any oxidation of the brass results in its effective emissivity increasing to 0.6. Improper cleansing can leave a residual coating of body oils which will be emissive at these thermal wavelengths. The radiative coupling will be increased, due to this change in the effective emissivity, from 0.055 to 0.51. Beyond 500°C the emissivity of the quartz decreases because thermal radiation at the shorter wavelengths will not be emitted in such thin layers (2mm). The detailed analysis is functionally dependent on the particular type of quartz which, combined with the other considerations, makes the analysis overly complex. We have therefore chosen several values of E the, effective emissivity, to predict only the magnitude of the quartz envelope temperature as a function of the microwave cavity surface temperature. Figure 2 is the result.

These equilibrium temperatures of the cavity are reached only after a considerable time period because of the cavity mass. This is about 9.8 Kilograms of brass. Since the heat capacity of the brass is 0.369 joules/°C, the heat capacity of the entire cavity is 3.6×10^3 joules/°C. It is evident that the rate of temperature increase, even on the assumption that the entire 1200 watt input power was being transferred in to radiation, conduction, and convection, would not result in equilibrium in less than ½ hour. Figure 3 shows the initial rate of temperature increase.

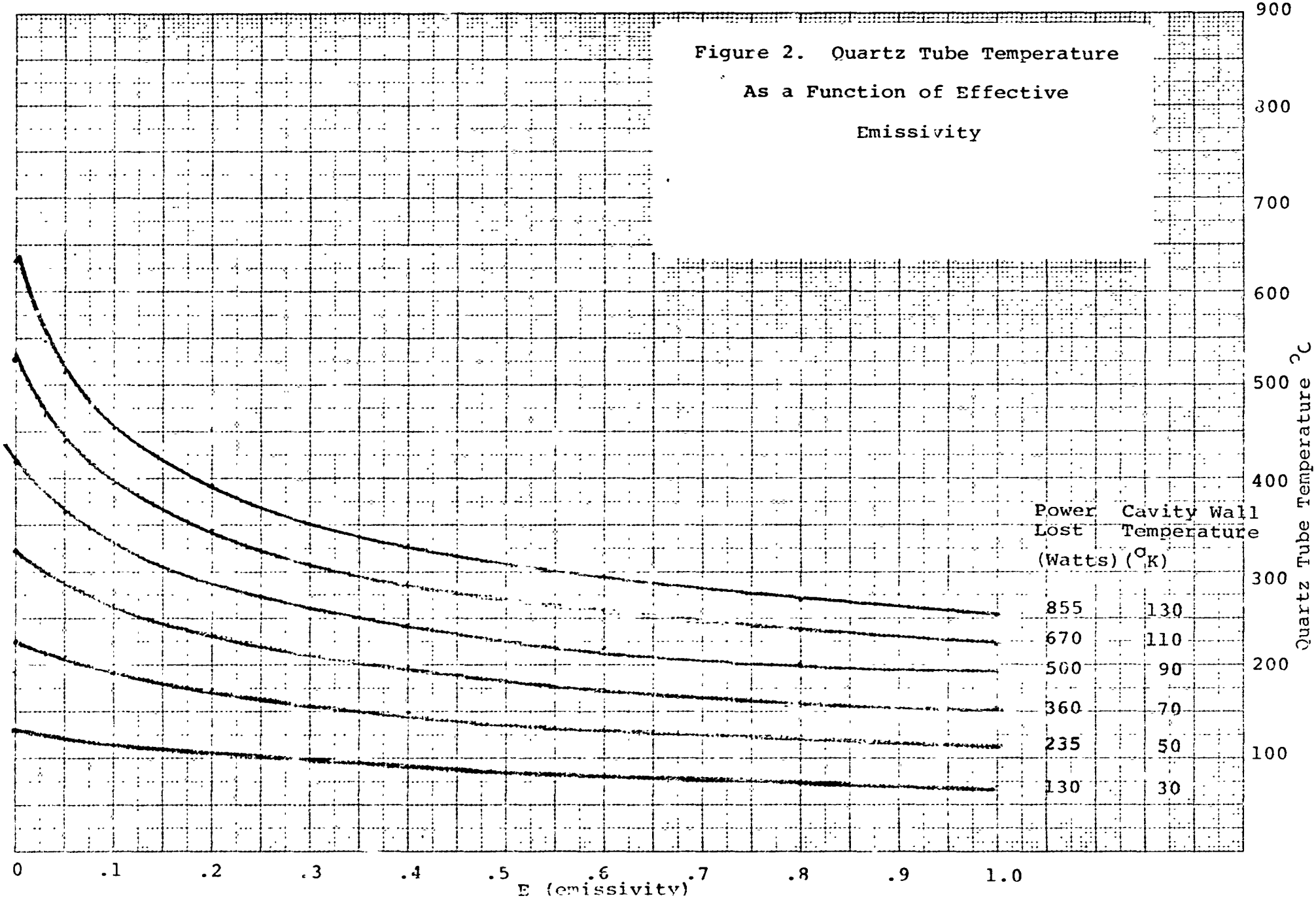

Figure 3. Initial Rate of Temperature Increase as a Function of the Power Transfer.

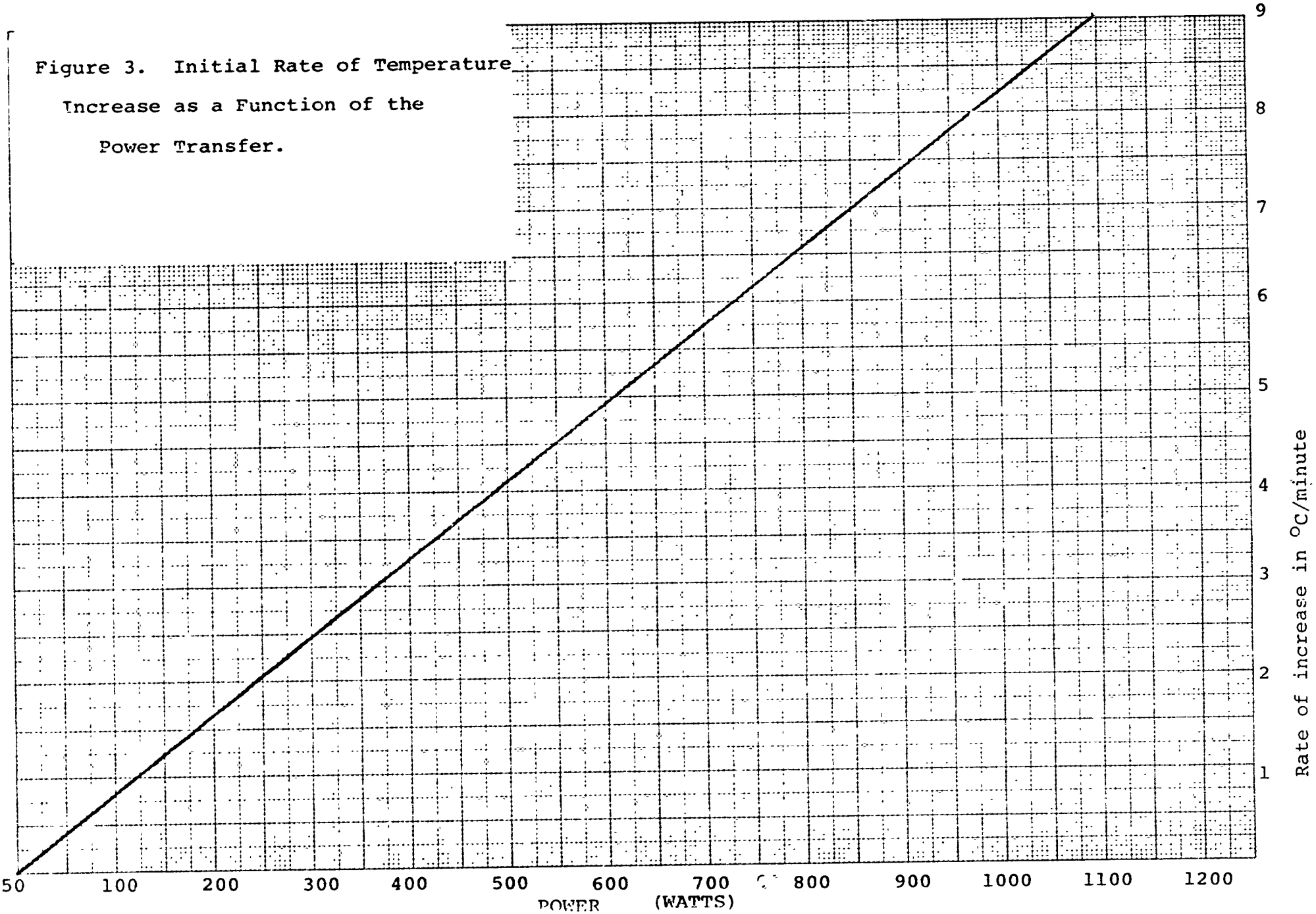

3.0 EQUILIBRIUM CHARGE DENSITY IN PLASMA

The determination of the propagation constant of a plasma requires a knowledge of the charge densities encountered. This quantity can be estimated from the Saha Equation for the specific atomic or molecular species involved at equilibrium. We have been using the form:

3.1 $$\log_{10} k = \log\left(\frac{\varepsilon^2}{1-\varepsilon^2}\right) P\ (\text{atm}) = \left(\frac{-5044 V_i}{T} + \log \frac{\omega_i \omega_e}{\omega_a} - 6.491\right)$$

Where V_i is the ionization energy in electron volts

T temperature in degrees kelvin

ω statistical weights of

atoms (ω_a)

ions (ω_i)

electrons (ω_e) = 2

P pressure in atmospheres

ε the equilibrium degree of dissociation

k the equilibrium constant

Note that:

$n_o \varepsilon = n_e$ electrons/cm^3 where

LP $= n_o$ particles/cm^3 and

L = Loschmidts' number

This equation has been programmed onto a TI59 program card to allow a convenient population estimate as a function of temperature. See Appendix I for format. Any need for a more detailed energy level populations of the excited states can be introduced by the utilization of the analytic techniques suggested in Ref. 1-3. Figure 4 is representative of the results obtained. The particular case

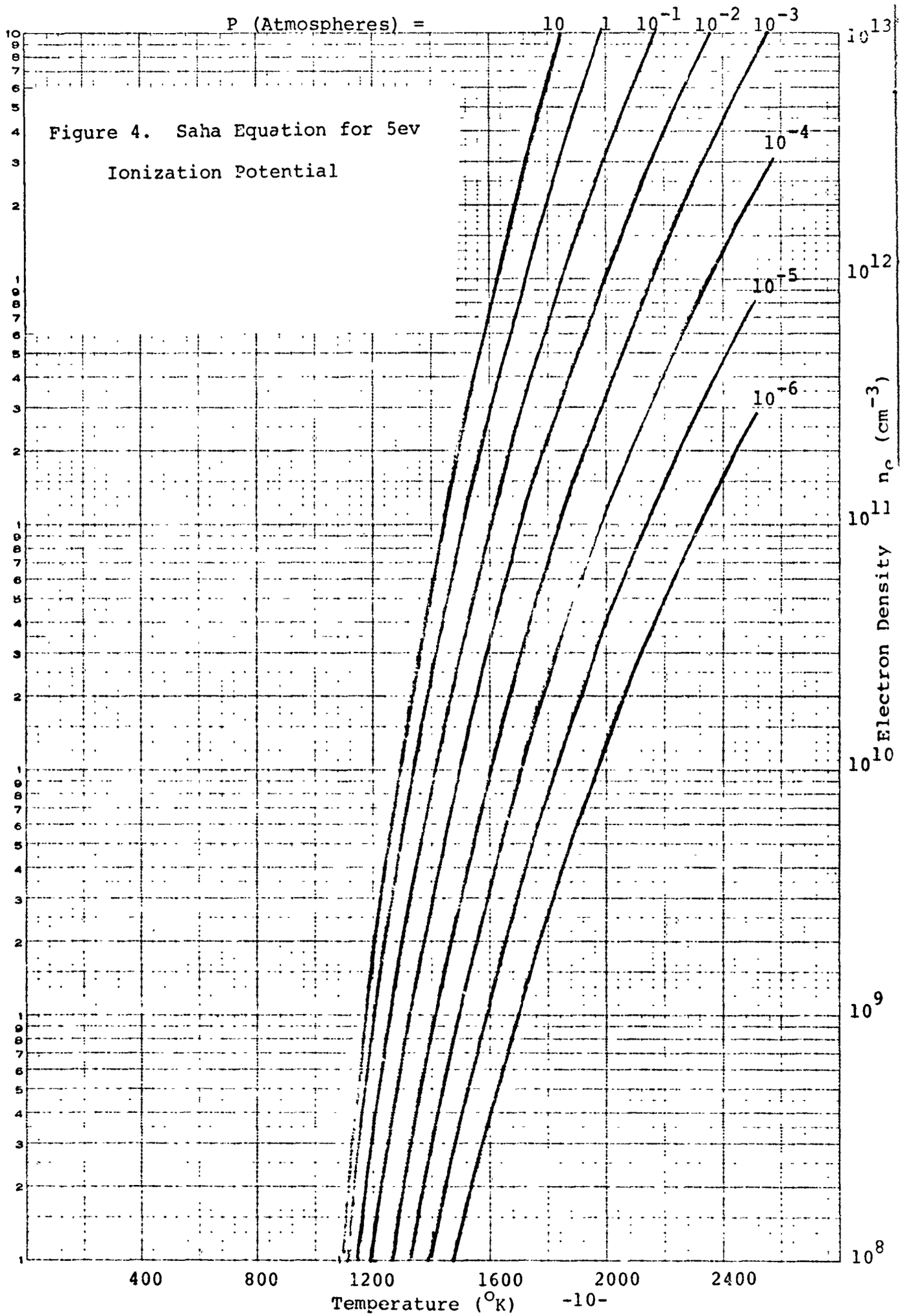

Figure 4. Saha Equation for 5ev Ionization Potential

EUGENE DIETZGEN CO.
MADE IN U.S.A.

NO 340-LS10 DIETZGEN GRAPH PAPER
SEMI-LOGARITHMIC
5 CYCLES X 10 DIVISIONS PER INCH

shown is for a 5ev ionization energy with the statistical weights $\omega_1 = 2$, $\omega_a = 1$, $\omega_e = 2$. Each curve corresponds to a constant pressure condition. The units are in atmospheres.

From that it is clear that purely thermal conditions would require gas temperatures that are too extreme to produce a significant electron density. Reasonable temperatures, however, could provide an adequate initial electron density seeding for the microwave plasma.

4.0 VAPOR PRESSURE

The vapor pressure of magnesium was computed from the data of Kelly (Ref. 24). This was obtained so that an evaluation of the conditions of Frayne's experiment, Ref. 25, could be made. Equation 1 represents the functional form for the pressure P, in atmospheres of the crystal to gas transition.

$$4.1 \quad -R \ln P = \frac{36{,}560}{T} + 2.83 \log T + 6.65 \times 10^{-4} T - \frac{3.39 \times 10^4}{T^2} - 36.74$$

where R is 1.9869 calories/degree Kelvin

T is in degrees kelvin. This is valid for the temperatures up to the melting point, 922° kelvin, for magnesium.

For the liquid to gas transition the relation has the form of equation 2.

$$4.2 \quad -R \ln P = \frac{49600}{T} + 23.0 \ln T - 103.58T.$$

These equations were used to present the data in a graphic form in figure 5. The vapor density may be derived from these values. This is graphed in Figure 6. To the precision of the graphed data, there is little difference in the liquid-gas and solid-gas formulations.

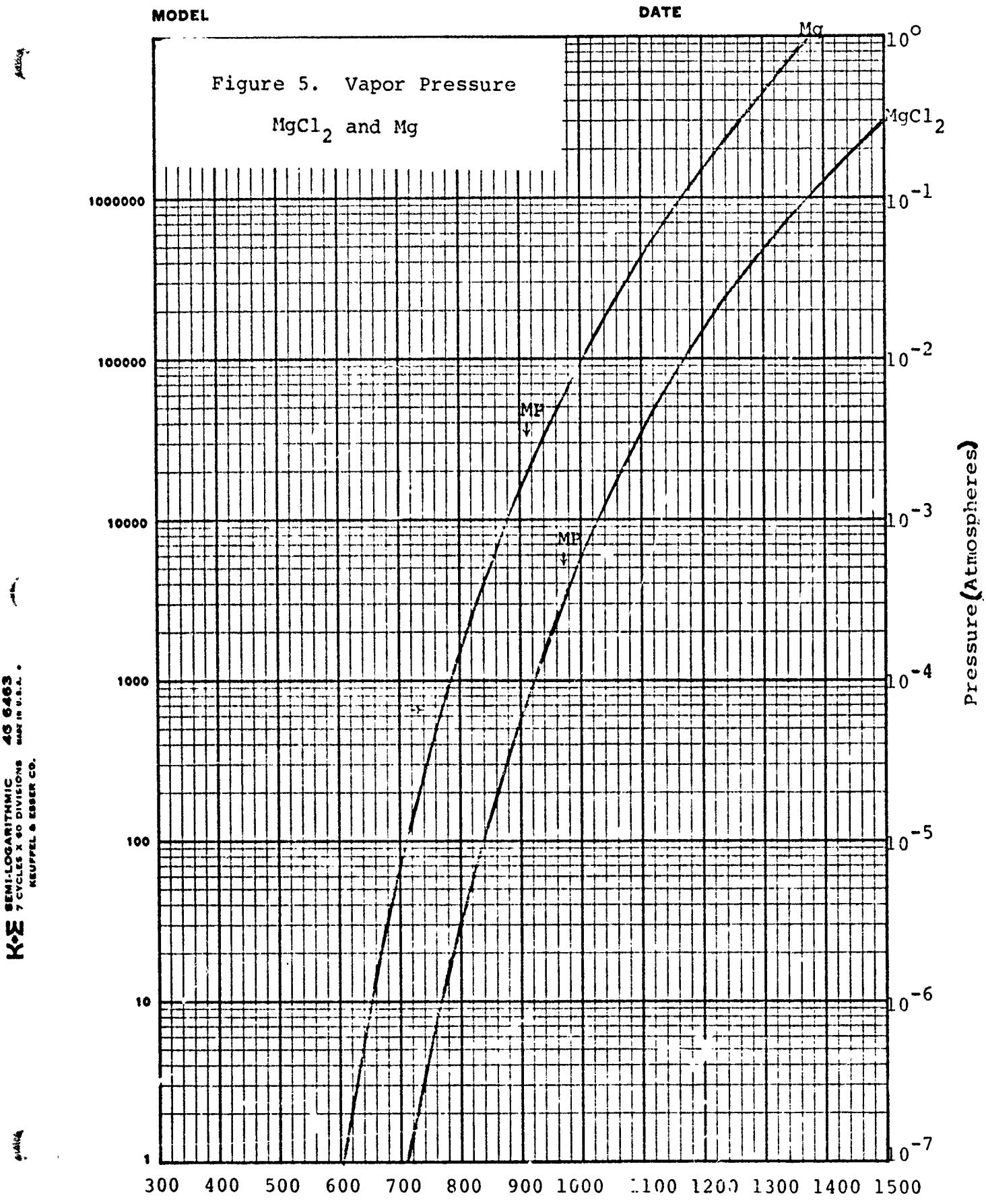
MODEL
DATE
Figure 5. Vapor Pressure
$MgCl_2$ and Mg
Mg
$MgCl_2$
MP
MP
1000000
100000
10000
1000
100
10
1
10^{0}
10^{-1}
10^{-2}
10^{-3}
10^{-4}
10^{-5}
10^{-6}
10^{-7}
Pressure (Atmospheres)
300 400 500 600 700 800 900 1000 1100 1200 1300 1400 1500
Temperature (^{o}K)
K•E SEMI-LOGARITHMIC 46 6463
7 CYCLES X 60 DIVISIONS MADE IN U.S.A.
KEUFFEL & ESSER CO.

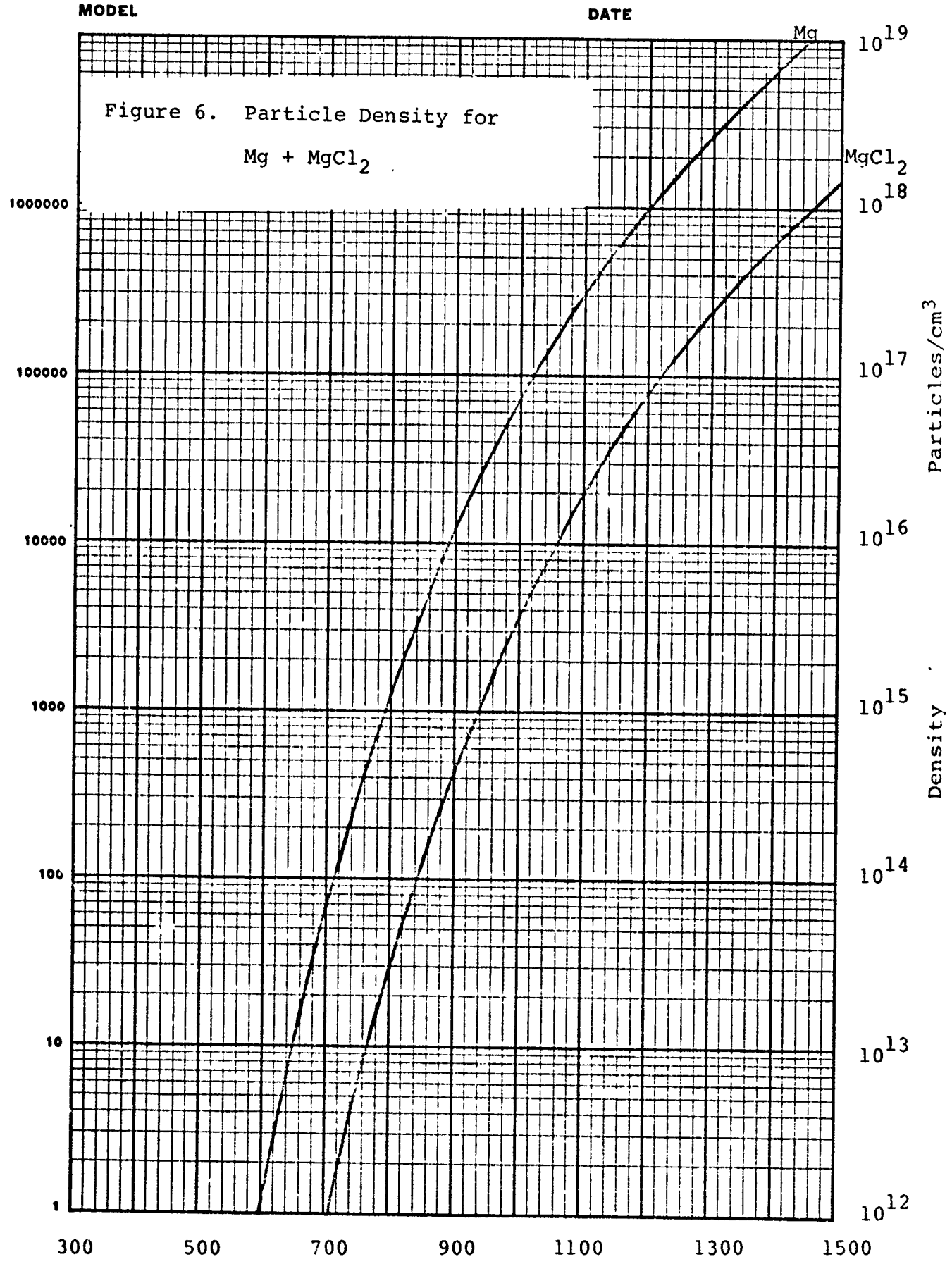

Figure 6. Particle Density for $Mg + MgCl_2$

The difference between the two results is only as low as 600° kelvin. Confirmation is found in later work at the lower temperatures Ref. 26.

The heat of fusion of the magnesium is about 2160 calories/mole. The magnesium halides are the compounds of most interest in the present study. In the case of the magnesium halides the heat of fusion is somewhat greater so that it is to be expected that the disparity between the extrapolation of a measured liquid-gas vapor pressure curve will result in values for the halide which are higher than will be found in experiment. $MgCl_2$ is the only halide vapor pressure curve that is tabulated in the literature available at this establishment. It is due to Kelly Ref. 24 and is included in figure 5 and 6. The magnesium bromide should not depart very much from this curve since the heat of fusion of both $MgBr_2$ and $MgCl_2$ are similar, 8300 to 8100 calories/mole. In addition, the melting points are virtually identical 984° to 985° Kelvin. No data is available on the boiling point of $MgBr_2$ but, in the absence of better data, it may be assumed that the melting temperatures, boiling temperatures and critical temperatures are related through the use of Guldberg's Rule and the principle of corresponding states. Ref. 27, P238. Since the halides are a homologous series one may expect the critical pressures to form a trend based on the molecular weight.

$BaCl_2$, is also a (II-VII) compound, which has a boiling point, 1560°C. This is even higher than $MgCl_2$, 1412°C. With such a high boiling point it would be difficult to expect a vapor pressure in the anhydrous $BaCl_2$ which exceed the $MgCl_2$. It has been observed

by Dr. Bramley that the anhydrous form of $BaCl_2$ under the activation of a 1KW microwave source results in a radiant discharge which includes all the well known band structure and relative intensities of the BaCl molecule. This discharge exhibited a greenish white color and included both the $^2\Sigma \rightarrow {}^2\Sigma$ and $^2\Pi \rightarrow {}^2\Sigma$ spectral band systems. Since her spectrographic equipment range did not extend beyond 0.76 microns it was not possible to ascertain the presence of $^2\Pi \rightarrow X^2\Sigma$ from 0.8421 to 0.0908 microns. Based on her previous postulate that the only difference between the strong emission in the flame excited sodium d lines as compared to the pure microwave excitation of hot sodium chloride was the presence of the water vapor product of the oxyhydrogen torch used. She tentatively used the hydrate form $BaCl_2 \cdot 2H_2O$ in an enclosed chamber in the microwave cavity. The result was a marked change in the intensity distribution of the spectral band system with the overall discharge changing to a brilliant green. A spectral evaluation indicated a virtually complete suppression on a relative basis of the $^2\Sigma \rightarrow {}^2\Sigma$ bands and also the relative suppression of the system of ionized Ba lines. Since the heating of the hydrate barium chloride does not result in the vaporization of the barium chloride at a low temperature but, rather, a simple driving off of the water of crystallization it would be suspected that the introduction of water vapor with the anhydrous $BaCl_2$ would lead to the same results. Dr. Bramley found this to be the case. This established the existance of a quenching mechanism in 1963, that would be beneficial to the populating of metastable state. In the extension of this present study, it is anticipated that the quenching mechanism that appears successfull in the

$BaCl_2 \cdot 2H_2O$ will be found to be effective in the $MgCl_2 \cdot 6H_2O$ charge for the microwave laser cavity.

5.0 SOME ESTIMATES ON THE DIATOMIC SPECIES OF INTEREST

In the process of establishing reactions rates it will be necessary to identify the characteristics of some of the species that will be encountered in the plasma. This section is a partial collection of some of the subsets of the magnesium halides for the convenience of further work.

Bond strengths have been given for the diatomic molecule possibilities in this group in Ref. 28. They are present in table 5.2A in Kilocalories per mole at 25°C. (298.1°Kelvin). The bond lengths for the symmetrical members are also tabulated in table 5.2B as presented in Ref. 27. No data is available to us for the remaining potential pairs. From the values assigned for the atomic and ionic radii, however, Table 5.2C an estimate can be made of the bond lengths which is simply the sum of the positive and negative radii of the components of the diatomic molecule. The magnitude of the error in such a simplistic assumption is illustrated in the comparison table 5.1 for the known cases.

Error in the Bond Length Predictions

Table 5.1

Molecule	Listed Values	Estimated (table 2C)	Disparity
Mg_2	3.197	3.198	-0.001
F_2	1.417	1.418	-0.001
Cl_2	1.988	2.078	-0.090
Br_2	2.290	2.348	-0.058
I_2	2.662	2.698	-0.036

TABLE 5.2a.

BOND STRENGTHS OF THE DIATOMIC SPECIES

(Kilocalories/mole) (25°C)

	Mg	F	Cl	Br	I
Mg	8	105.5	89	75	68
F		37	59.9	55.9	67
Cl			58	52.3	50.5
Br				46.34	42.8
I					36.50

TABLE 5.2b.

Bond Length (Å)

	Mg^{o}	F^{-}	Cl^{-}	Br^{-}	I^{-}
Mg^{o}	3.197	2.15	2.63	2.78	3.02
F^{+}	-	1.417	1.60	1.72	1.83
Cl^{+}	-	1.89	1.988	2.20	2.31
Br^{+}	-	2.04	2.23	2.290	2.46
I^{+}	-	2.28	2.47	2.59	2.662

TABLE 5.2c.

Radii, Atomic and Ionic (Å)

	-1	0	+1	+2	+5	+7
Mg	-	1.598	0.82	0.66	-	-
F	1.33	0.68	-	-	-	0.08
Cl	1.81	0.97	-	-	0.34	0.27
Br	1.96	1.13	-	-	0.47	0.39
I	2.20	1.35	-	-	0.62	0.50

On the assumption that errors not significantly at odds with those presented we assume the remaining values for the other diatomic possibilities in Table 5.2B.

6.0 ESTIMATE OF THE ELECTRON TEMPERATURE

Von Engle and Steenbeck developed a method of estimating the electron temperature in a positive gas column. The analysis is dependent on the assumption that the mean free path of the electrons is much smaller than the diameter of the tube.

Analytically, the equation has the form:

6.1 $$\left(\frac{X}{A}\right)^{\frac{1}{2}} e^{A/X} = BC^2p^2R^2$$ where,

$X = T_e/V_i$ $A = 1.1606 \times 10^4$ degrees kelvin/electron volt

$B = 1.16 \times 10^4$

V_i = ionization potential

p = pressure in mm of mercury

R = tube radius in cm

C = a constant for the particular gas and is derived from the relation

6.2 $$C = \left(a\, V_i^{\frac{1}{2}}/\mu^+ p\right)^{\frac{1}{2}}$$

where $a = S/(V - V_1)$ (ions/cm^3mmHgev), S = differential ionization coefficient (ions/cm^3mmHg). The mobility μ^+ is in cm/sec volt cm. We have presented this function in figure 7.

The pertinent values for some of the gases that can be used are given in table 3. Thus for Argon at a pressure of 1.0mmHg in a 1cm radius tube processes of diffusion to the wall will balance the electron production process at

CpR = 0.034 which results (figure 7), in

$T_e/V_i = 1100$

Therefore for argon $T_e \sim 17{,}335^{\circ}$Kelvin.

TABLE 3.

Gas	Vi (εv)	Metastable State (εv)	C*	C**
He	24.58	19.8	0.0039	3.9×10^{-3}
Ne	21.56	16.62	0.0059	6.5×10^{-3}
A	15.76	11.55	0.053	3.4×10^{-2}
Kr	14.00	9.91	--	5.1×10^{-2}
Xe	12.13	8.32	--	
N_2			0.095	
H_2			0.0135	

* Von Engle and Steenbeck (See P. 240 Cobine, Gaseous Conductors, Dover 1958.)

** Calculated from the newer transport property values (normalized to He).

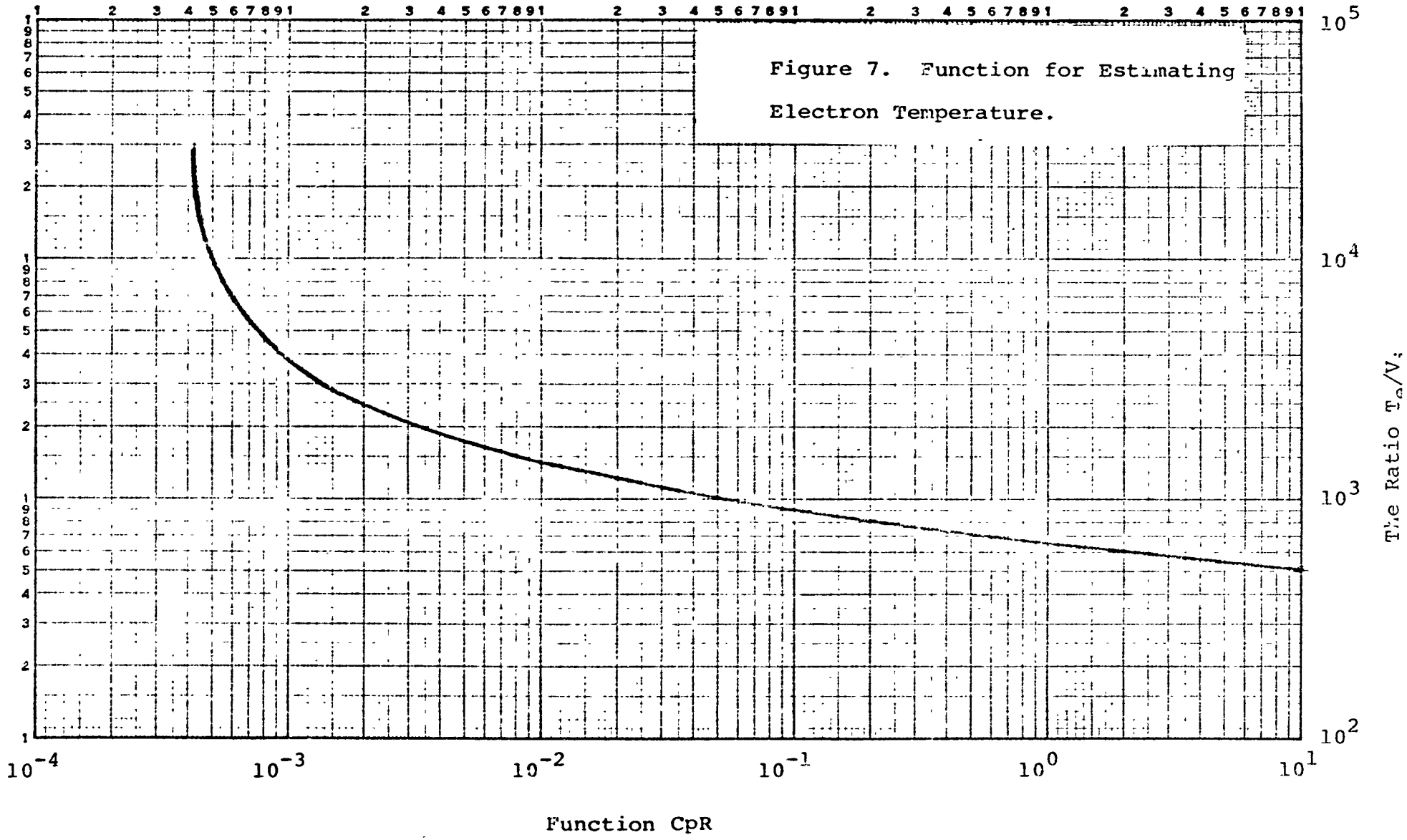

Figure 7. Function for Estimating Electron Temperature.

The constant C is a function of the gas temperature, T_g, through the mobility-pressure product. Therefore, if the mobility μ_o^+, and pressure p_o at the room gas temperature $T_o(^oK)$ are known the mobility μ_g^+ and pressure p_g at the gas temperature $T_g(^oK)$ may be obtained. This leads to the simplified relation

6.3 $$\mu_g^+ p_g = \mu_o^+ p_o \frac{T_g}{T_o} .$$

From the equation 6.2 for C it is clear that if C_o is defined as the value of the constant at room temperature then C at temperature T_g can be written as a function of temperature alone i.e.

6.4 $$C = C_o(T_o/T_g)^{\frac{1}{2}}.$$

The gas temperatures of the order of room temperature the values of C can be used directly. Higher gas temperatures will be encountered at the higher pressures and would require an appropriate decrease in the value of CpR. This quantity reaches its minimum value at about 4.4×10^{-4} when $T_e/V_i = 23{,}000$. A maximum electron temperature for a particular radius tube, at a specific minimum pressure and for a particular material is then predicted on the basis of the relation graphed in Figure 8. These electron temperatures were developed for the noble gases in a 1cm tube for a room temperature gas situation. Higher gas temperatures have little effect on the electron temperature at the higher pressures. If however, the temperature is raised at the lower pressures a marked increase in the electron temperature will be obtained. To illustrate, increasing the gas temperature from 277^oK to 1188^oKelvin (895^oC) decreases C by a factor of 2. This results in helium at 1mm pressure having an electron temperature of $60{,}500^o$Kelvin instead of 41000^oKelvin. The same gas temperature change at 100mm of Hg

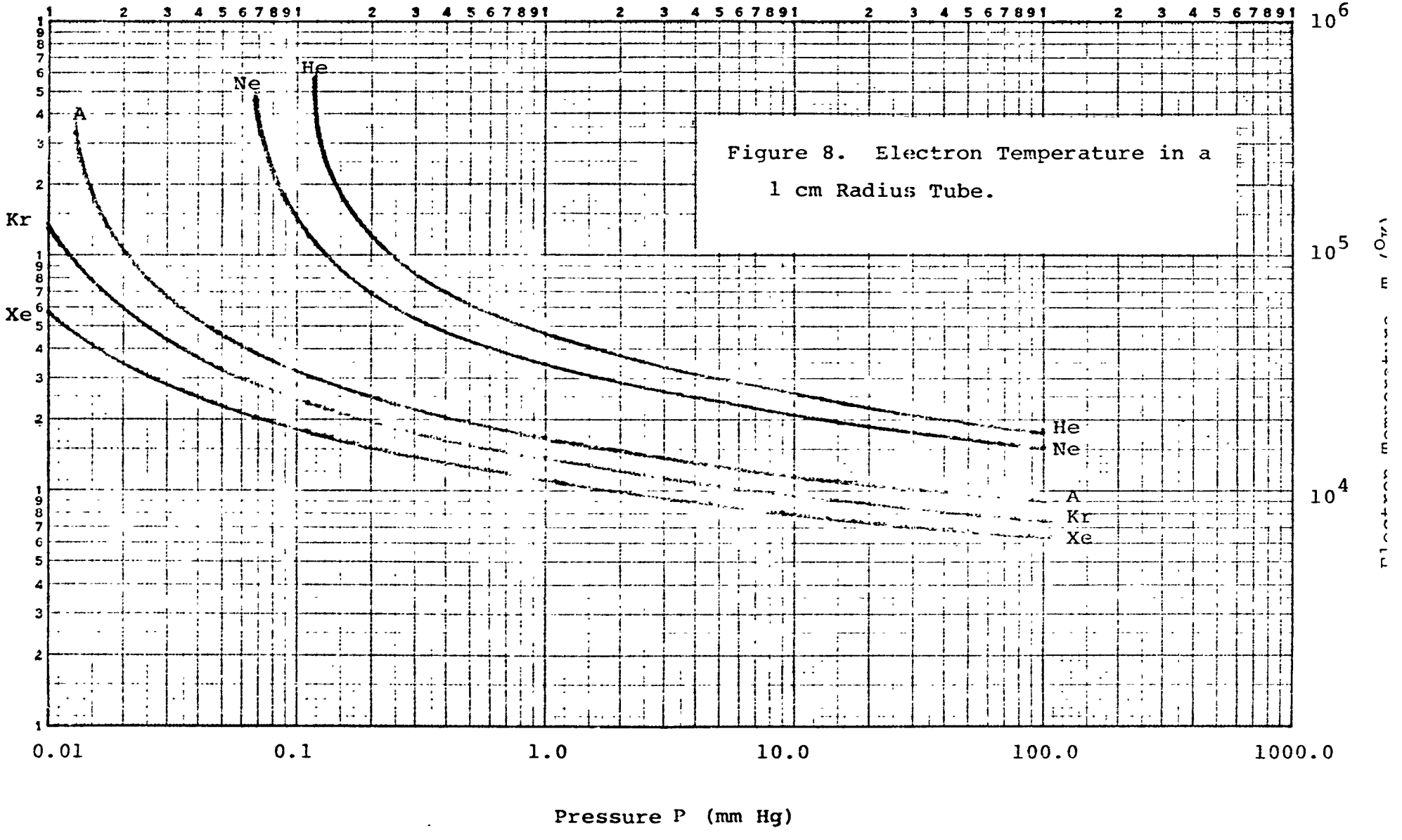

Figure 8. Electron Temperature in a 1 cm Radius Tube.

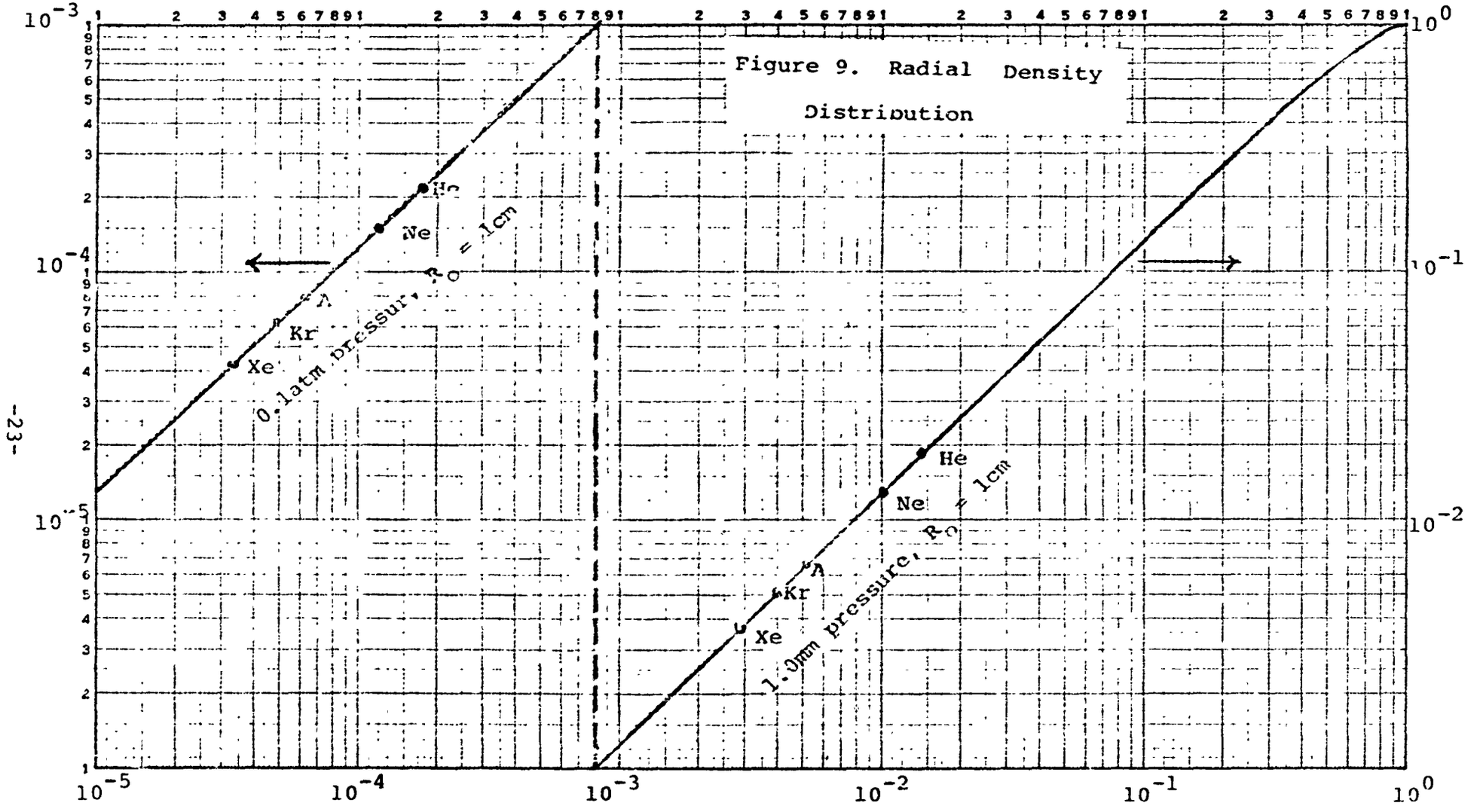

pressure would change the helium electron temperature from 19,000°K to 20,500°K. The pressure of the fill gas is important in establishing the average energy of the electrons with respect to the dissociation level that corresponds to the process $Mg(halide) \rightleftarrows Mg^* + (halide)_2$.

7.0 COMPUTATION OF THE RADIAL DENSITIES

It has been shown that when the electron mean free path is short compared to the tube radius, the radius density distribution will correspond to that of the zeroth order Bessel function J_o.

7.1 $n_r^+ = n_o^+ J_o (2.404r/R.)$. n_o^+ is the number of positive ions per cm^3 on the axis of the quartz plasma tube and n_r^+ is the number of positive ions per cm^3 at the radius r less that the inner radius R of the plasma tube. The positive ions follow this distribution and are shown as a function of δ/R_o where δ(cm) is the distance from the wall of the tube. The equivalent of 1 mean free path from the wall of the tube for the ionic gas atoms for two pressure regimes are shown in Figure 9. Since the conditions determining the diffusion of ions and electrons is ambipolar (Ref. 29, P.243) the concentrations of ions and electrons are equal at all points $n^- = n^+$ the electron density distribution has the same functional form. The refractive index of the plasma is dependent on the charge density. This predicts the gradient of the refractive index that will be encountered by the entering microwave.

8.0 PLASMA RESISTIVITY

The plasma resistivity is also a function of the electron density and the electron temperature. The relationship is a modification of the Lorentz gas approximation.

8.1 $\rho_L = 3.8 \times 10^3 \frac{Z \ln\Lambda}{T^{3/2}}$ ohm cm

A correction is required for Z = 1 which is expected to be the primary situation, Z is the degree of ionization, the change is in the constant and the equation becomes

8.2 $\rho = 6.53 \times 10^3 \ln\Lambda/T^{3/2}$ ohm cm.

The extended studies Ref. 17 to 22 confirm, at least, the magnitude of this correction. Figure 10 presents the region of interest and Appendix 4 gives the program used.

9.0 RESISTIVITY MODELS FOR THE PLASMA

The range of resistivities pertinent to the present problem varied from 10^{-2} to 12×10^{-2} ohm cm for the electron temperatures and densities of interest. It had been expected that a liquid load would be able to represent this range. It was found, however, that at the frequency of the microwave 2.45×10^9 Hz even high molal solutions of sodium chloride still had too high a resistivity, table 9.4.

Table 9.4

Resistivity of Sodium Chloride Solutions, ohm cm, at Microwave Frequencies

Frequency \ Molality	.1	.3	.5
3×10^8 Hz	101	35	22
3×10^9 Hz	33	19.9	14.3
10^{10} Hz	5.9	5.72	5.6

ohm cm

Spectoscopic Graphite electrodes were found to be .001 ohm cm which is a bit too low. The #3 pencil "lead" was found to be 0.062 ohm cm, right at the center of the range, and the H pencil "lead" was found to be 0.030 ohm cm. Both of these materials

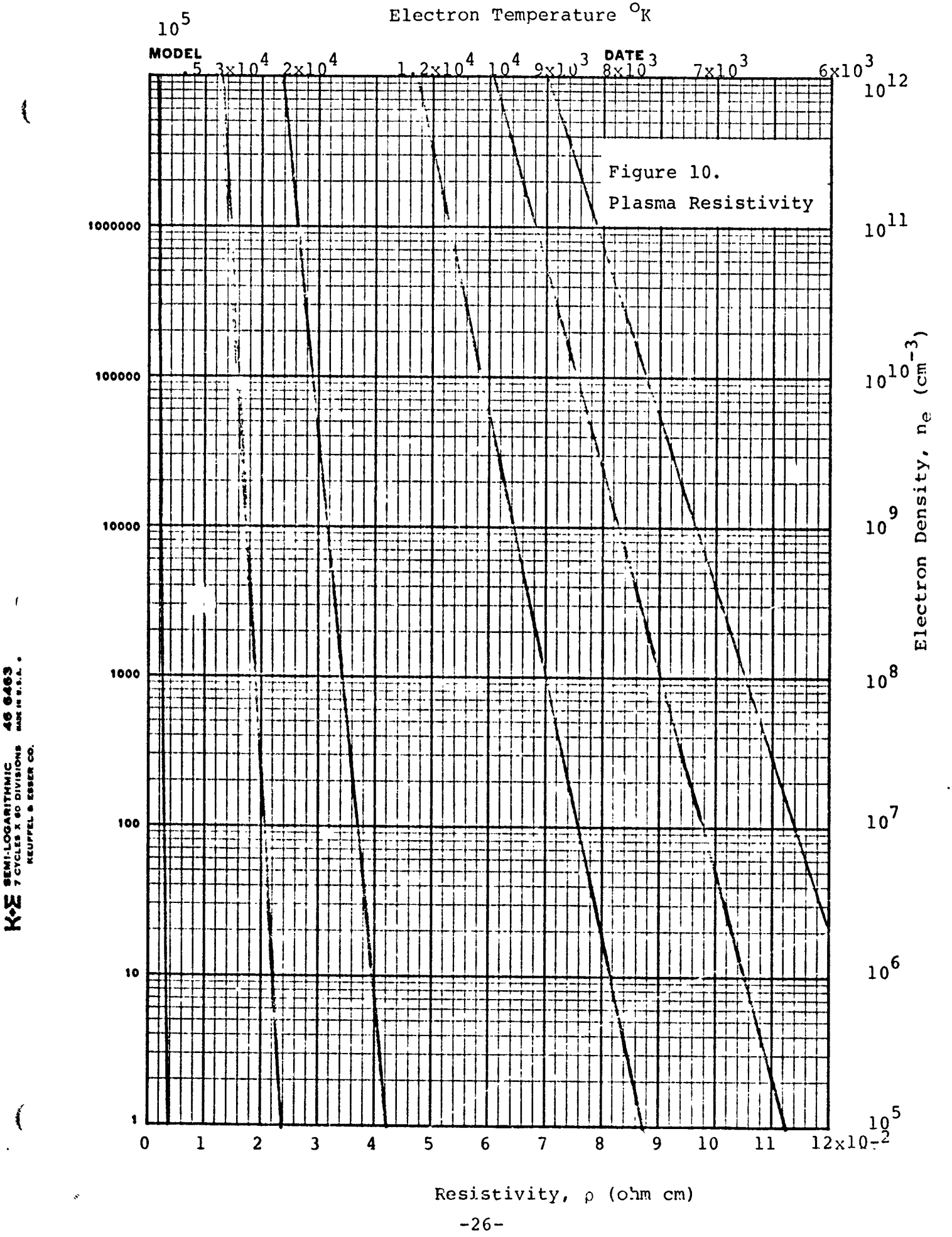

Figure 10.
Plasma Resistivity

maintain their integrity at high temperatures and correspond to realistic values in the range of interest. These were used as test loads in the cavity.

10.0 SKIN DEPTH

The opacity of the plasma tube to the microwave is a function of the physical thickness δ of the plasma and the frequency ν_o of the applied microwaves. If the applied frequency is much less than the collision frequency ν_c the relation

10.1 $\delta_o = (\rho/\pi/\nu_o\mu_o)^{\frac{1}{2}} = 5.033 \times 10^3 (\rho/\nu_o)^{\frac{1}{2}}$ cm where μ_o is the permeability of free space, $4\pi \times 10^{-5}$ hy/cm, see Ref. 31. The value of δ_o is that depth of the resistive medium at which the attenuating portion of the propagation constant reduces the field intensity to e^{-1} of its initial value. The applied frequency is 2.45×10^9 Hz so that δ_o based on these premises is

10.2 $\delta_o = 0.102 \times (\rho)^{\frac{1}{2}}$ cm, ρ resistivity (ohm cm)

The resistivity range anticipated will lie between 10^{-2} and 2×10^{-1} ohm cm which predicts values of $\delta_o = 10^{-2}$ to 4.6×10^{-2} cm for the usual skin effect values. When the phase velocity becomes imaginary, as it will when ν_o is less than the plasma frequency ν_p, the amplitude will decrease by e^{-1} in the depth δ_i

$$10.3 \quad \delta_i = \frac{c}{2\pi \nu_p} / (1 - (\nu_o/\nu_p)^2)^{\frac{1}{2}} \text{cm}.$$

Since the plasma frequency may be written as a function of the electron density n_e, Section 13, this becomes,

10.4 $\delta_i = 5.323 \times 10^5/n_\varepsilon^{\frac{1}{2}} (1 - 7.46 \times 10^{10}/n_\varepsilon)^{\frac{1}{2}}$.

Figure 11 represents these two skin depth values at the frequency that is being applied. The larger value of δ is to be taken. No magnetic field is considered in this case. You will note that the skin depth, under these circumstances, becomes a function of the radial dimension of the plasma. This is due to the radial variation in the electron density n_e.

11.0 EXPECTED VALUES OF Q

The values of Q for the TE_{11n} and TM_{01n} modes were calculated from the known relation given in Appendix 3.

n is defined as the number of ½ wavelengths along the axis of the cavity. The result, for a 10.82cm diameter cavity with a cavity resistivty of $\rho = 7 \times 10^{-6}$ ohm cm corresponding to the brass cylinder chosen, are shown in figure 12 for the TE_{11n} and in figure 13 for $TM_{01}n$. In these figures the value of Q is shown as a function of the ratio of cavity length to diameter with n as the parameter associated with each of the nine solid curves. Several specific free space wave lengths are overlayed as dashed curves. The anticipated wave length is 12.28 cm. In order that the variation with frequency might be shown, figure 14 was developed with n and frequency as parameters and Q and L/D again as coordinates.

The values predicted for the Q of such a brass cylinder should have been of the order of 18,500 for the TM_{016} mode and about 22500 for the TE_{119} mode. The results of measurements for the empty cavity are shown in table 11.5.

Figure 11. Skin Depth at 2.45 Kilomegahertz.

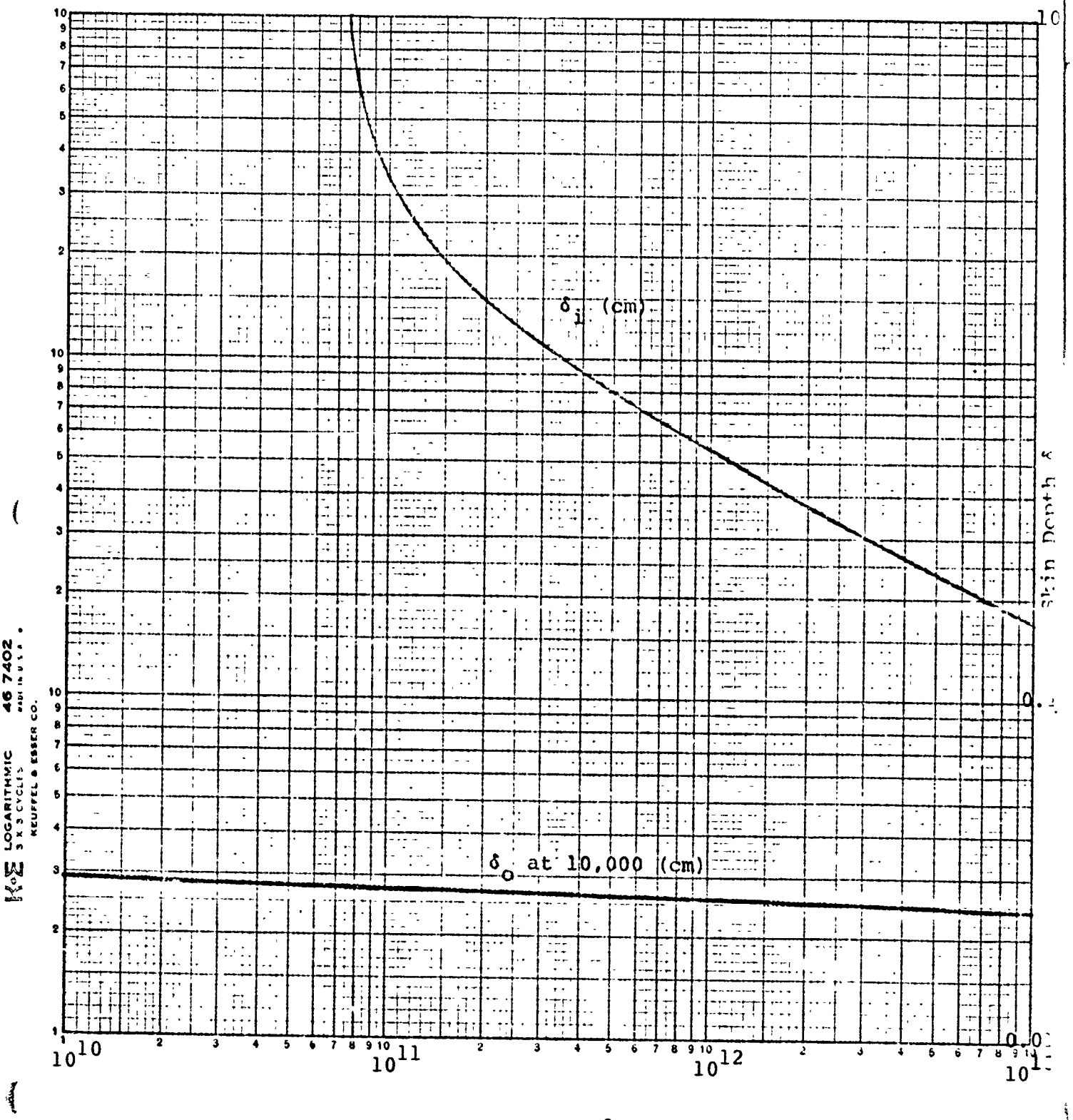

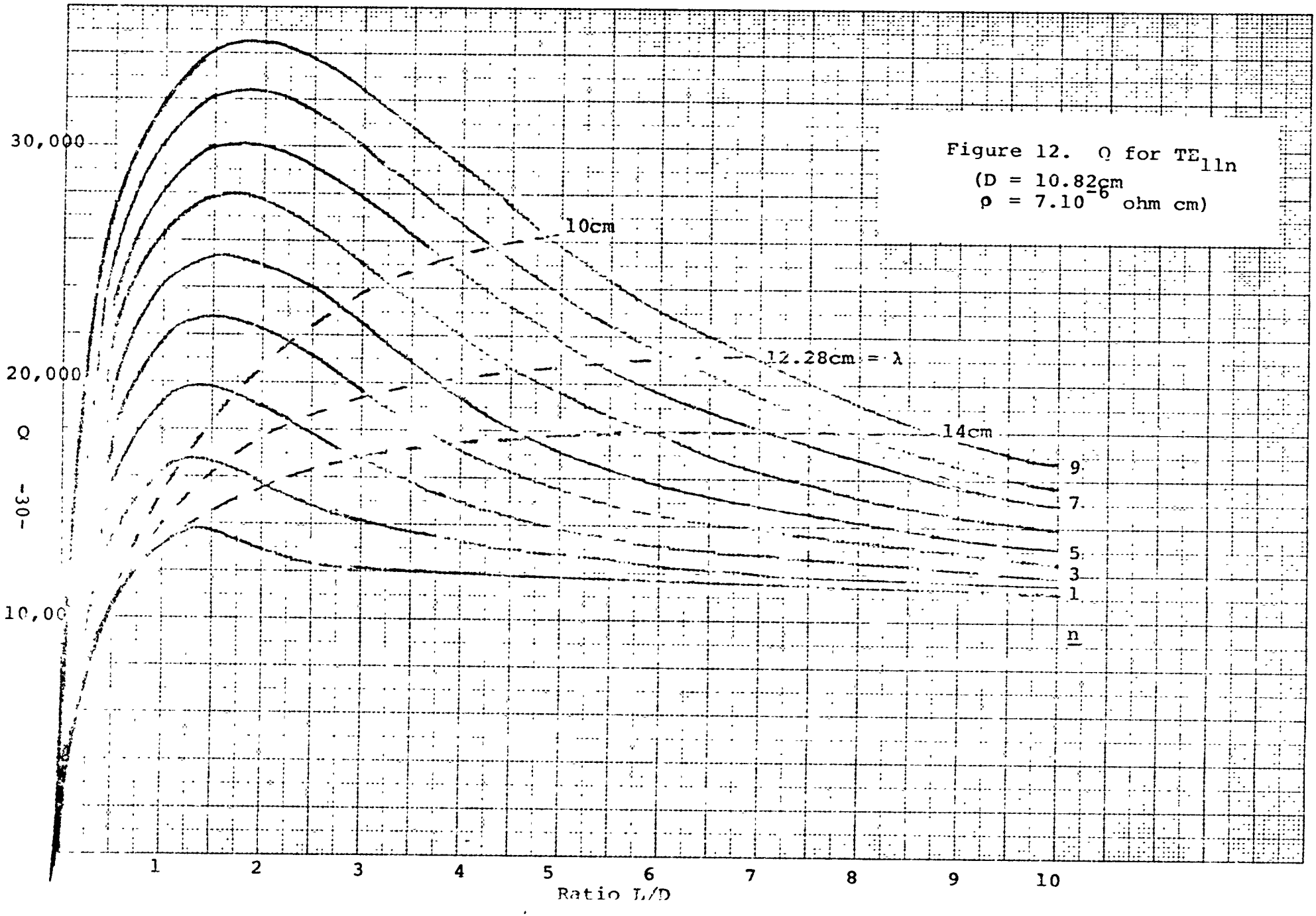

Figure 12. Q for TE_{11n}
(D = 10.82cm
$\rho = 7.10^{-6}$ ohm cm)

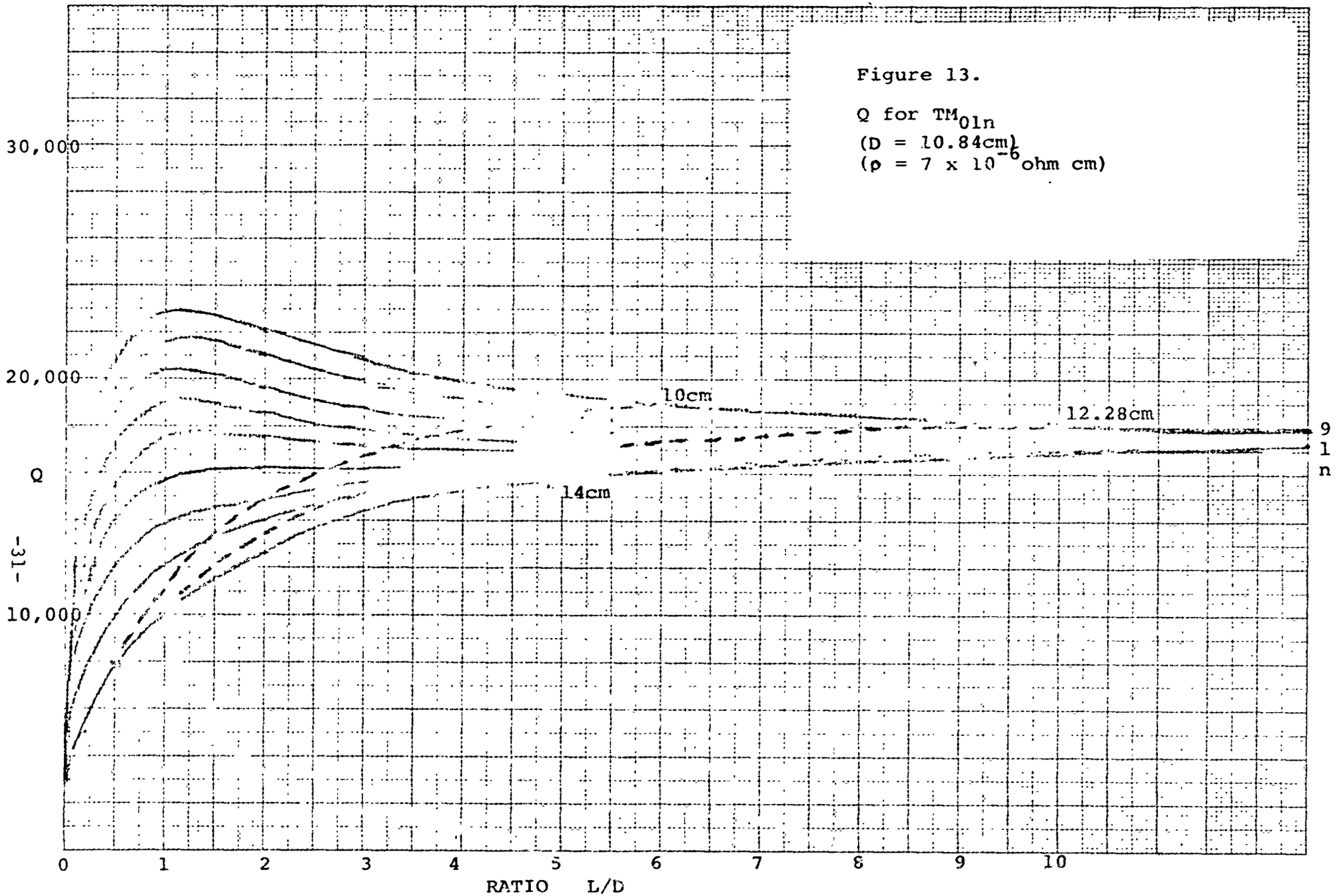

Figure 13.

Q for TM_{01n}
(D = 10.84cm)
($\rho = 7 \times 10^{-6}$ ohm cm)

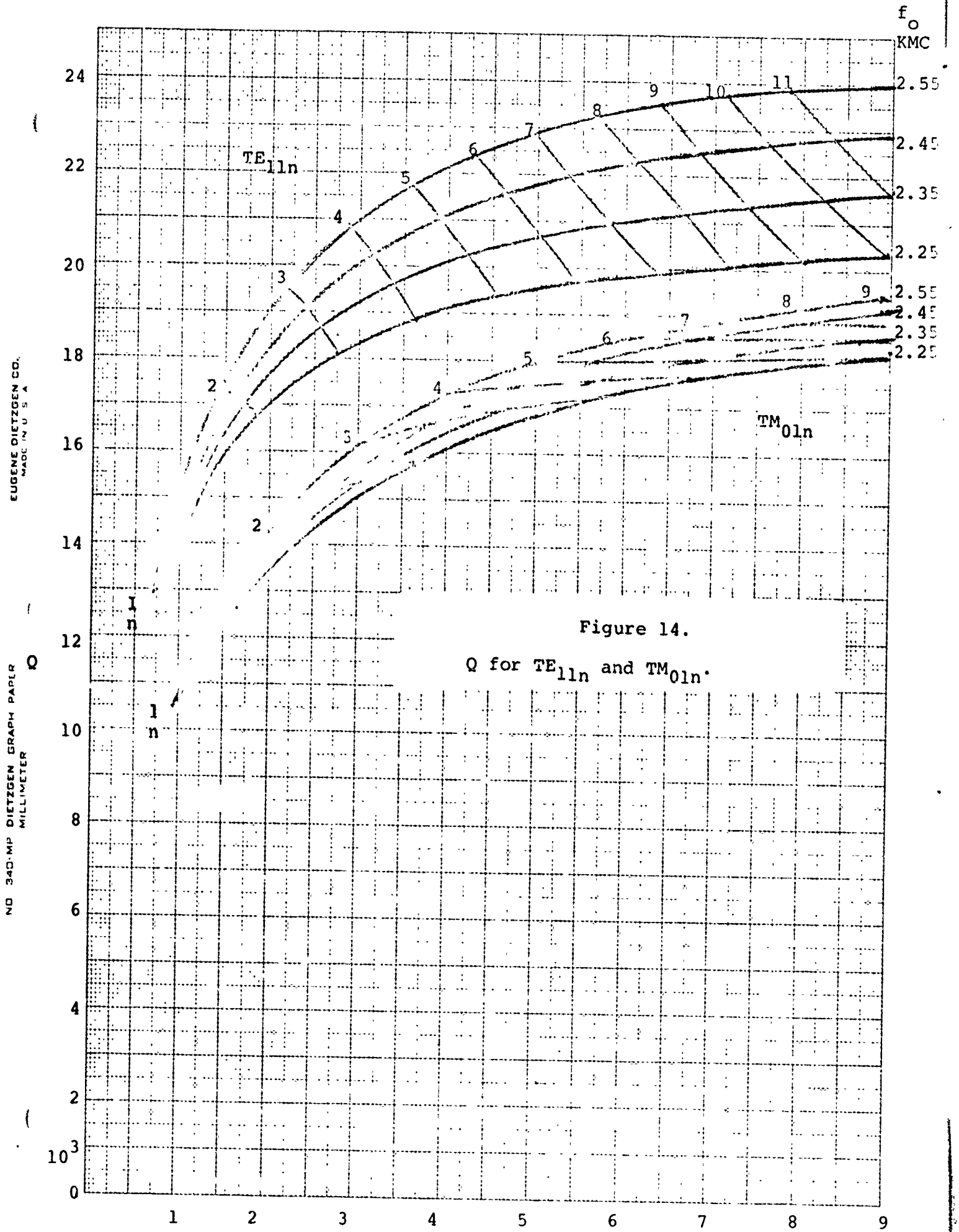

Figure 14.

Q for TE_{11n} and TM_{01n}.

Table 11.5

	Predicted	Measured	Measured (after alterations)
TM_{016}	18,500	18,460	not measured
TE_{119}	22,500	12,370	8,010

The source of the losses in the cavity, as measured earlier, is most probably in the irregular surface offered by the threaded section required for the tuning piston. This could be reduced considerably by the extension of the piston in the form of a cup. Such a cup is merely a tubular extension of the edge of the piston in the cavity so that the irregular surface due to the threads are eliminated from the cavity. The alternative is to reduce the length of the existing cavity by attaching an extension to the tuning pistons that presents a new piston surface which remains beyond the threaded section. The cavity was altered by placing apertures on one end for introducing the microwaves. The additional structure at this end is probably contributing to the additional reduction in the Q. The apertures used for the coaxial probes will also contribute to the reduction in Q.

12.0 FIELD INTENSITY DISTRIBUTION IN THE SYMMETRICAL TM_{01n} MODE

The three equations:

12.1 $E_z = 0.8195\ J_o\ (0.4208r)\ \cos\ (0.2942z)\ E_o$, the axial field intensity at the axial point z

12.2 $E_r = 0.2411\ J_1\ (0.4208r)\ \sin\ (0.2942z)\ E_o$, the radial field intensity at the radial point r and axial point z

12.3 $E = (E_z^2 + E_r^2)^{\frac{1}{2}}$ the magnitude of the full field intensity are

valid for 2.45×10^9 Hz. The tube dimensions were 5.715cm in radius in the TM_{01n} mode with n/L = 0.0936.

For the mode values n, the tube lengths L are,

n	L
6 half periods	64.07cm, 25.22 inches
7 half periods	74.75cm, 29.42 inches

corresponding to this basic configuration. The values of J_o and J_1 are the usual Bessel functions and the field intensities E are normalized to the applied field E_o. In this case E_o must be considered the actual field generated by the magnetron at the entrance to the cavity multiplied by the Q of the cavity. Figure 15 shows the distribution of the field intensity as a function of the fraction of the tube radius at 1cm intervals along the z axis from the point of peak axial intensity. In the same cavity regions the direction of the electric vector has also been determined. Figure 16 presents this information graphically as a function of the fractions of the cavity radius with the z axis distances (in cm) as a parameter. The angle ϕ is 90 degrees when the electric vector lies parallel to the axis of the cavity, $E_r = 0$. Decreasing the diameter of the cavity increases the inguide wavelength so that the distribution shown extends to more and more of the total length of the cavity. It may be shown for this frequency that a reduction in the radius to R = 1.845 inches, 4.68cm, from the present value should result in the distribution shown stretched out by a factor of 14.7 to 1 so that the present 5.334cm quarter wave point would occur at 78.46cm. Experimental verification can be performed by inserting a suitable copper sleeve and placing a smaller diameter extension on the tuning piston. The solutions

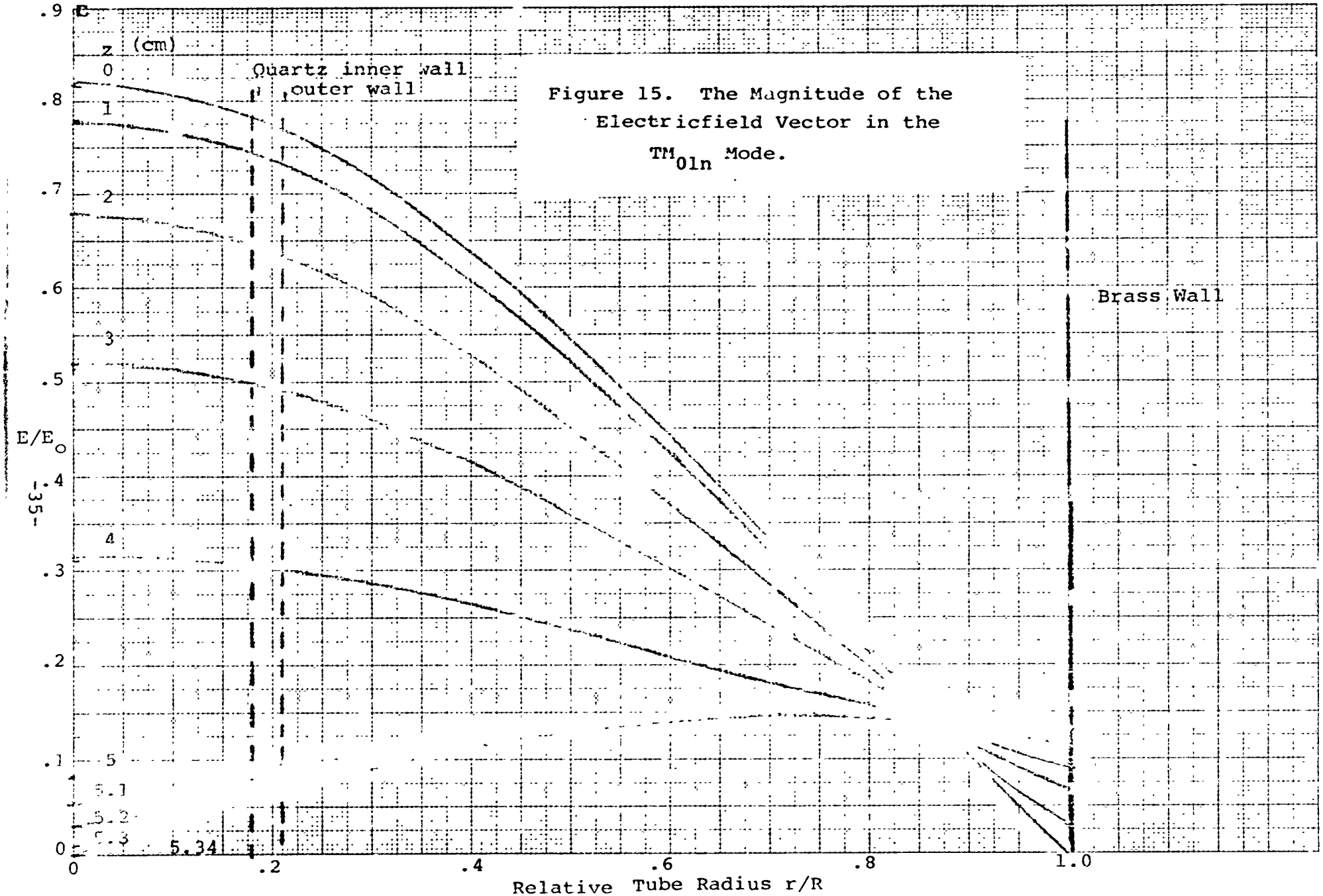

Figure 15. The Magnitude of the Electricfield Vector in the TM_{01n} Mode.

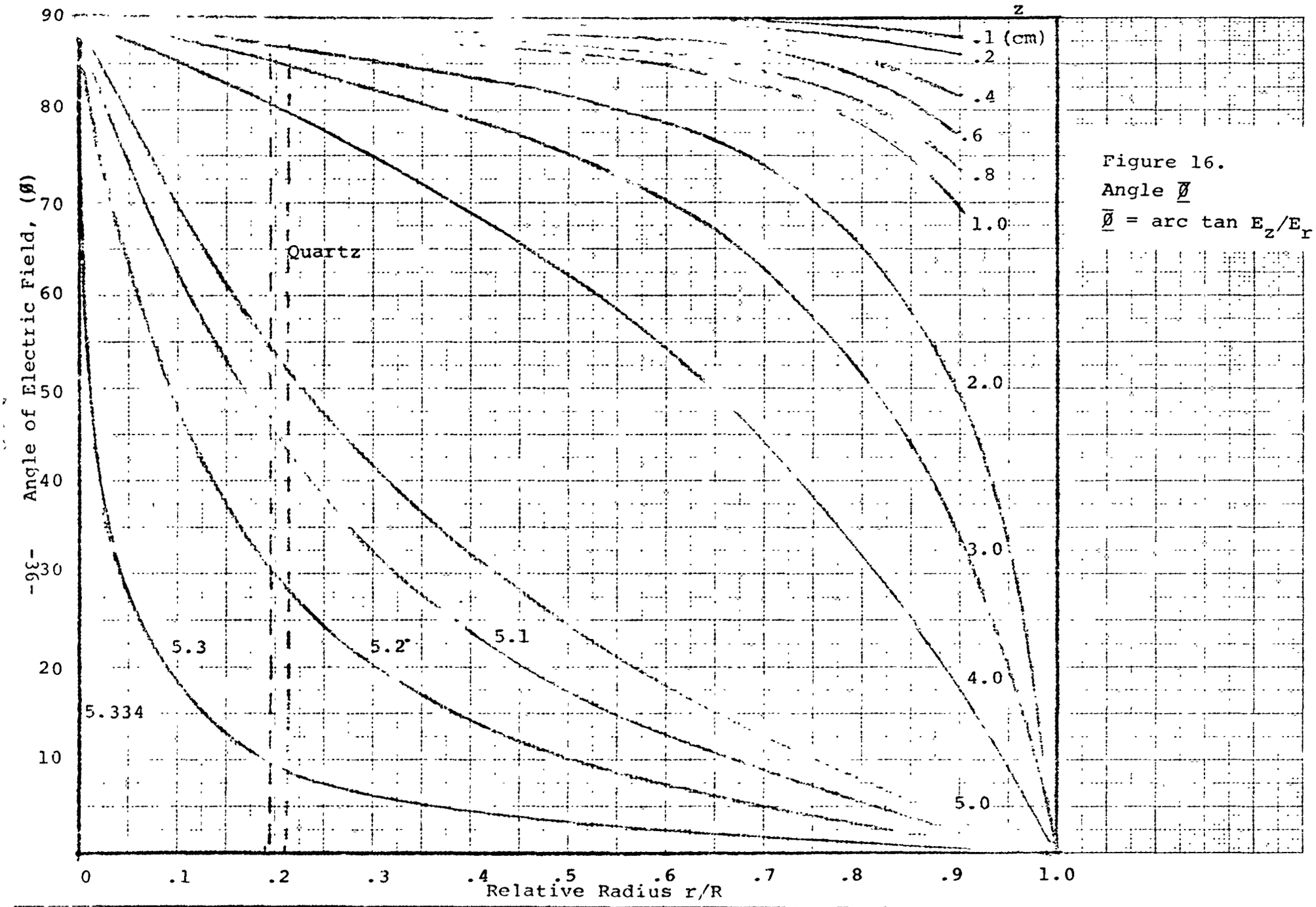

Figure 16.
Angle $\overline{\emptyset}$
$\overline{\emptyset}$ = arc tan E_z/E_r

and placing a smaller diameter extension on the tuning piston. The solutions for the TE_{11n} mode may be obtained in the same manner. Our notation corresponds to that found in Ref. 6 P.299. At the lower pressures the plasma tube a relatively small value of Q will result in breakdown in this cavity at these field intensities. See Section 16 for the case of the travelling wave.

13.0 FREQUENCIES OF THE PLASMA

The basic resonances encountered in a plasma will include the following:

The Electronic Plasma Frequency

13.1 $$\nu_{pe} = \frac{\omega_{pe}}{2\pi} = \left(\frac{n_e e^2}{\pi m_e}\right)^{\frac{1}{2}} = 8.97 \times 10^3 \, n_e^{\frac{1}{2}} \text{ Hz}$$

e = electronic charge (seu)

m_e = electronic mass (gms)

m_i = ionic mass (gms)

The Ionics Plasma Frequency

13.2 $$\nu_{pi} = \left(\frac{n_i e^2}{\pi m_i}\right)^{\frac{1}{2}} \text{ hertz} = 2.09 \times 10^2 \, (n_i)^{\frac{1}{2}} \text{ Hz}$$

n_i = ions/cm^3

The Collision Frequency

The collision frequency is a function of the diffusion coefficient and can be estimated from the time required to deflect a particle through a 90^o in a kinetic collision. The methods of analysis are developed in Ref. 4 with the results that

13.3 $$\nu_{coll} = \frac{17.94\, n_o e^4 Z^4 \ln\Delta}{m_e^{1/2} (3kT)^{3/2}} = \frac{.9877\, n_o Z^4 \ln\Delta}{M_e^{1/2} T^{3/2}}$$ Z = 1 for electrons

$M_e = 1/1823$ in atomic mass units

where the shielding coefficient is:

13.4 $$\Delta = \frac{3}{2Z_i e^3} \left(\frac{(kT)^3}{\pi n_e} \right)^{1/2}$$, z is the number of charges carried by the particle, n_o is the total number of particles per cm^3 in the cavity and k is the Boltzmann constant.

Cyclotron Frequency

When there is a magnetic field present a frequency occurs which is a function of the strength of that field and the charge to mass ratio of the particles, thus:

13.5 $$\nu_c = \frac{\omega_c}{2\pi} = \frac{ZeB}{2\pi mc}$$ Hz for electrons, this reduces to

13.6 $$\nu_{ce} = 2.829 \times 10^6 \text{ B Hz.}$$

for ions, this reduces to

13.7 $$\nu_{ci} = 1.54 \times 10^3 \frac{ZB}{M} \text{ Hz.}$$

Acoustic Frequencies

In addition, there will be chamber acoustic frequencies which will be a function of the chamber length L and the quartz plasma chamber diameter d for a simple tubular chambers. To illustrate the frequency

13.8 $$\nu_{aL} = \frac{V_{acoustic}}{2L} = \left(\frac{Z\gamma_e kT_e + \gamma_i kT_i}{4m_i L^2} \right)^{1/2}$$ Hz would correspond to the longitudinal modes only.

Clearly the plasma frequency and collision frequency can be of the same order as the driving frequency by a judicious choice of temperature, pressure, and species. Attaining 10^{11} electrons/cm^3

electron density could give an S band plasma frequency while about 1.4×10^{19} particles per cm^3 at room temperature results in a S band collision frequency. To attain a cyclotron frequency of this order, a field of about 1000 gauss is required.

Other potential acoustic frequencies for the radial modes could come into play most prominantly in conjunction with the pulse repetition frequency associated with a pulsed microwave source. A hydrodynamic cylindrical shock wave generator could be the result with all the peculiarities associated therewith. Ref. 5. Detailed specifications for some of the frequencies are included in a developing literature which includes references 10 to 16 for the simple cylindrically symmetrical cavities.

14.0 REFRACTIVE INDEX OF THIN PLASMAS

The propagation of electromagnetic waves in a plasma is characterized by the dielectric constant of the medium. In the absence of both a significant attenuation and an applied magnetic field, the plasma exhibits a real index of refraction μ. This refractive index is a function of a ratio of the plasma frequency ω_p to the frequency ω of the incident electromagnetic wave. As long as the ratio is less than 1 this refractive index is real and less than 1. The refractive index is not a function of the angle of incidence on the plasma under these circumstances, there is an angle of incidence that is equivalent to the Brewster's angle in optics. At this angle there is a minimum surface reflectivity. The Brewster angle for this condition is

14.1 $\theta_B = \tan^{-1}\mu.$

The result of an index of refraction, μ, less than 1 for the

plasma means that there is a critical angle, θ_{cr}, beyond which total reflection occurs. This is encountered when the electromagnetic wave proceeds, through the interface between freespace and the plasma, from freespace side of the interface. This angle has the value

14.2 $\theta_{cr} = \sin^{-1} 1/\mu$.

If the value of the frequency ratio ω_p/ω exceeds unity the refractive index becomes imaginary and it is not possible to use a simple linearly polarized wave and obtain a minimum reflection since tan θ_B is imaginary.

The value for the frequency ratio that results in this refractive index μ

14.3 $\mu = (1 - (\omega_p/\omega)^2)^{\frac{1}{2}}$ is obtained from the plasma frequency which is a function of the electronic charge, mass and density of charge. In a plasma composed of positive charges of mass, m_i, and n_e, negative charges of mass m_e one obtains a plasma frequency ratio

14.4 $$\frac{(\omega_{p^+}^2 + \omega_{p^-}^2)}{\omega^2} = \left[\frac{n_e e^2}{\varepsilon_o m_e} + \frac{Z n_i e^2}{\varepsilon_o m_i}\right] / \omega^2 = \left(\frac{\omega_p}{\omega}\right)^2$$

The condition of electrical neutrality requries $Z_{ni} = n_e$ therefore:

14.5 $$(\omega_p/\omega)^2 = \frac{n_e e^2}{\varepsilon_o m_e \omega^2} \left[\frac{M + 1}{M}\right] \quad \text{where } M = \frac{m_i}{m_e}$$

and ε_o is the permitting of free space.

The functional relation between the electron density and the refractive index for this simple plasma is:

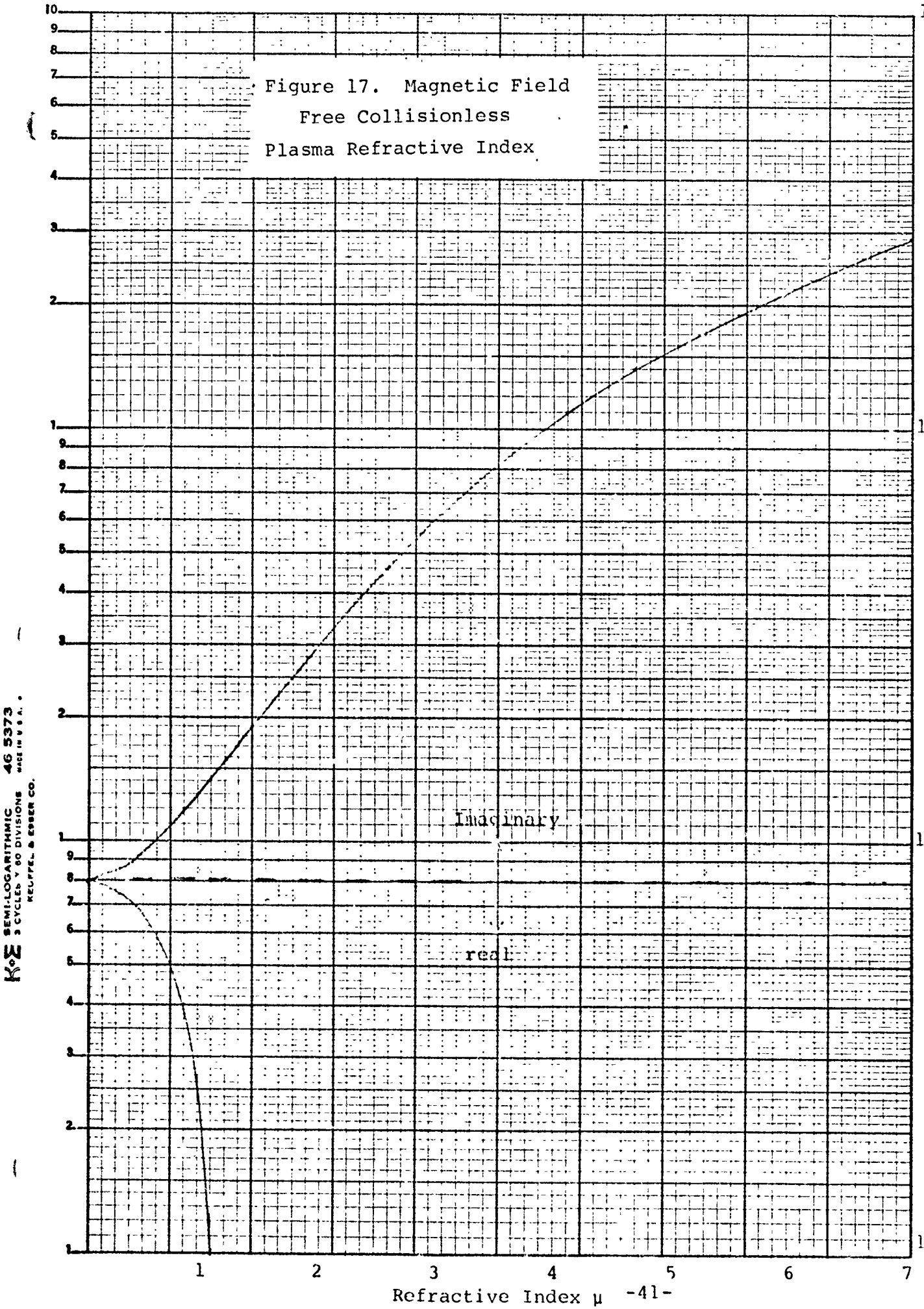
Figure 17. Magnetic Field Free Collisionless Plasma Refractive Index
Imaginary
real
Refractive Index μ
Ionized Particle Density (cm^{-3})
10^{13}
10^{12}
10^{11}
10^{10}
1
2
3
4
5
6
7
K&E SEMI-LOGARITHMIC 46 5373
3 CYCLES X 60 DIVISIONS
KEUFFEL & ESSER CO.

Figure 18. Refractive Index of a Thin Plasma 7 x 10^{10} electrons/cm^3

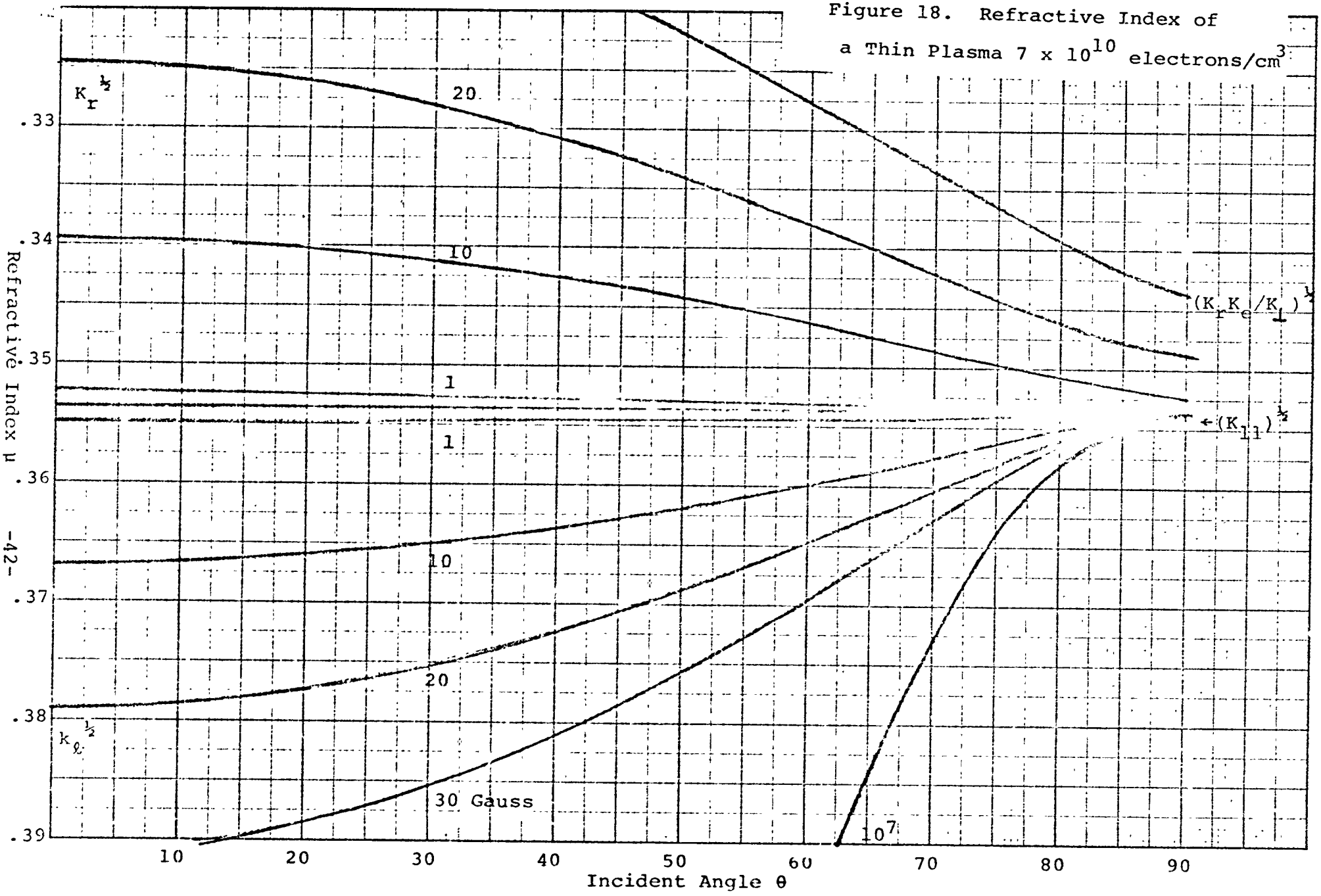

$$14.7 \quad \mu = \left[1 - \frac{n_e e^2}{\varepsilon_o m \omega^2} \left(\frac{M + 1}{M} \right) \right]^{\frac{1}{2}}$$

When S Band microwaves, 2.54×10^9 hertz, are used, figure 17 becomes the graphic representation for this equation. It shows both the real and the imaginary values for the appropriate electron densities. The application of a DC magnetic field may be shown to modify the refractive index radically (Ref. 23). See Section 15. The application of these appropriate equations result in extensive modifications of the plasma characteristics for the various forms of polarized incident waves. Some refractive indices are shown in figure 18 for a selected electron density and for several selected intensities of a constant applied magnetic field.

There are four limiting indices two of which occur at normal incidence and two of which occur at grazing incidence these are:

14.7 $\mu_r = k_r^{\frac{1}{2}}$ for right circular polarized waves

$\mu_l = k_\ell^{\frac{1}{2}}$ for left circular polarized waves

at the incidance of angle $\theta = 0$ degrees

14.8 $\mu_{\parallel} = (k_{\parallel})^{\frac{1}{2}}$ linear parallel polarization

$\mu_{\perp} = \frac{k_r k_l}{k_{\perp}}^{\frac{1}{2}}$ linear perpendicular polarization.

At an incidence angle of $\theta = 90$ degrees. The effect of the various magnetic fields is shown parametrically.

If transport theory is introducted, Ref. 23 Chapter 5, the plasma becomes alive with additional potential effects which are a

function of the electron energy. Representative cases for a 2000 Gauss DC field are shown in figure 19 to 22 where each group is for a specific electron density.

15.0 REFLECTIVITY OF A THIN PLASMA

The concept of a skin depth in the "thin plasma" refers to the wavelength created in the plasma by the frequency of a driving microwave source. For this region the free space wavelength of the microwave source is less than the wavelength in the plasma. The implication is that a less dense "dielectric" material is being entered from a more dense medium and Fresnel relations from an index of refraction are valid. This comes from the following basic concepts.

If one investigates the solution of Maxwell's equations for a plane wave (Ref. 31, P.271, etseq) there is obtained a simple solution for the field intensity perpendicular to the direction of propagation of the form

15.1 $E_\xi = E_{o\xi}\cos(\omega t - \alpha\zeta - \theta_1)$

if the plane wave is going in one direction only and the conductivity of the medium is zero. This field is periodic in both space and time and $\omega = 2\pi f$ where f is the frequency. The period along the time axis is $2\pi/\omega = T$. The period along the space axis is the wavelength which is $2\pi/\alpha$ where α is the real part of the propagation constant $k = \alpha + i\beta$, $\beta = \beta(\rho) = 0$.

The argument $\phi_1 = \omega t - \alpha\zeta - \theta$, of this periodic function is defined as the phase and θ_1 is the phase angle. If the plane ζ = constant at time t = 0 the question is how must it be displaced along the ζ axis in order that it remain invariant for a change in t. Since

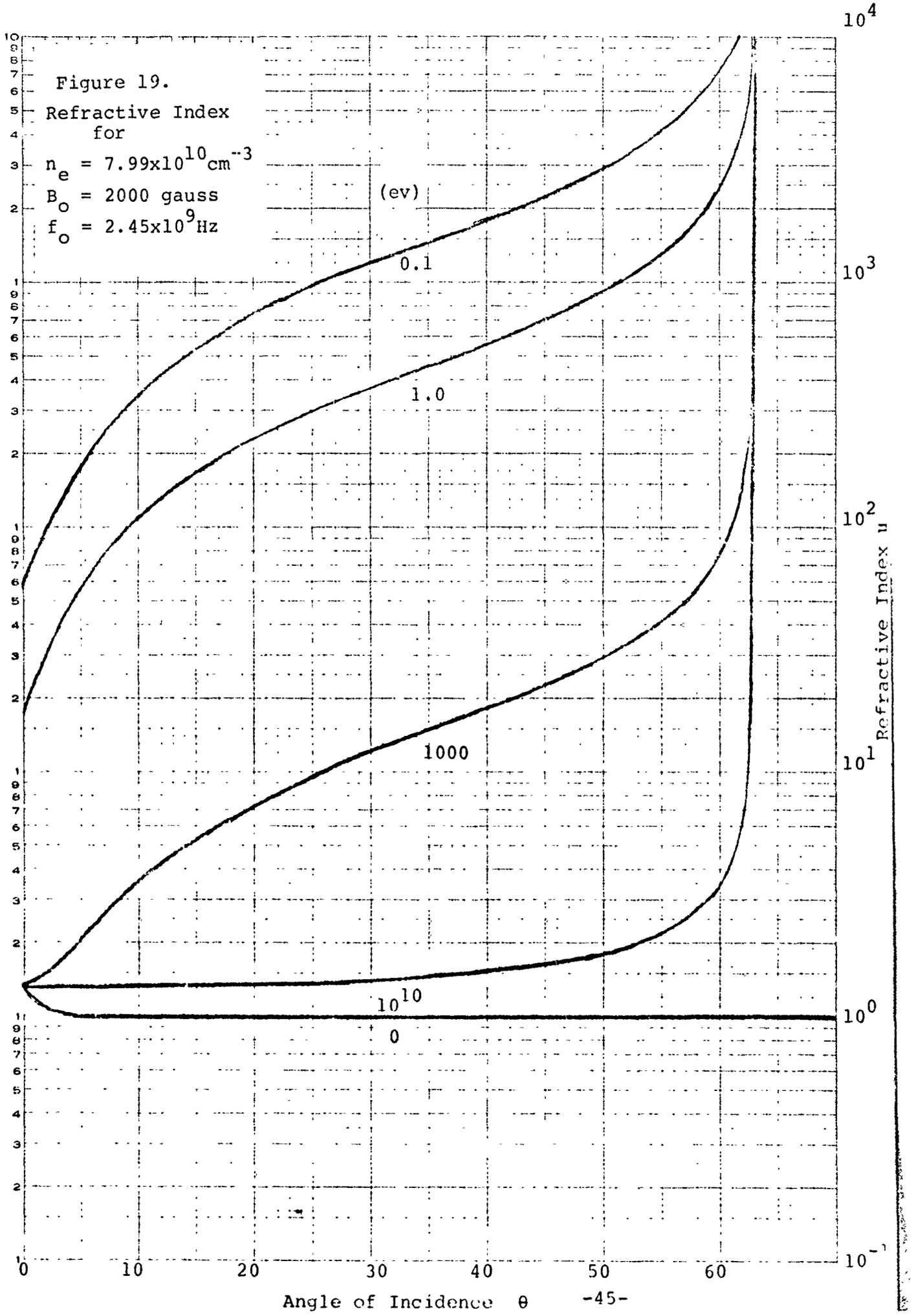
Figure 19.
Refractive Index
for
$n_e = 7.99 \times 10^{10} cm^{-3}$
$B_o = 2000$ gauss
$f_o = 2.45 \times 10^9 Hz$
(ev)
0.1
1.0
1000
10^{10}
0
10^4
10^3
10^2
10^1
10^0
10^{-1}
Refractive Index u
0
10
20
30
40
50
60
Angle of Incidence θ
EUGENE DIETZGEN CO.
MADE IN U.S.A.
NO. 340-LS10 DIETZGEN GRAPH PAPER
SEMI-LOGARITHMIC
5 CYCLES X 10 DIVISIONS PER INCH

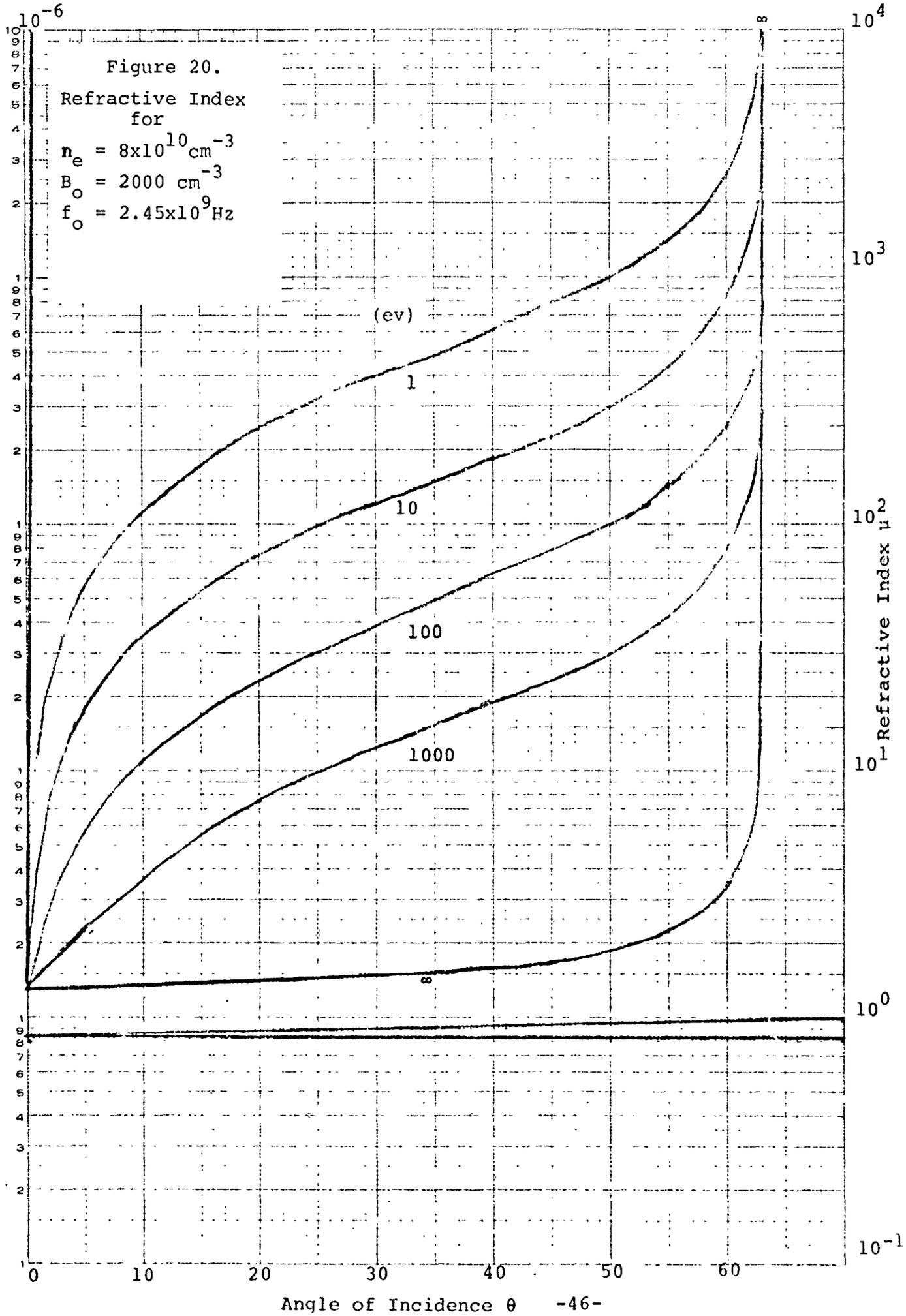

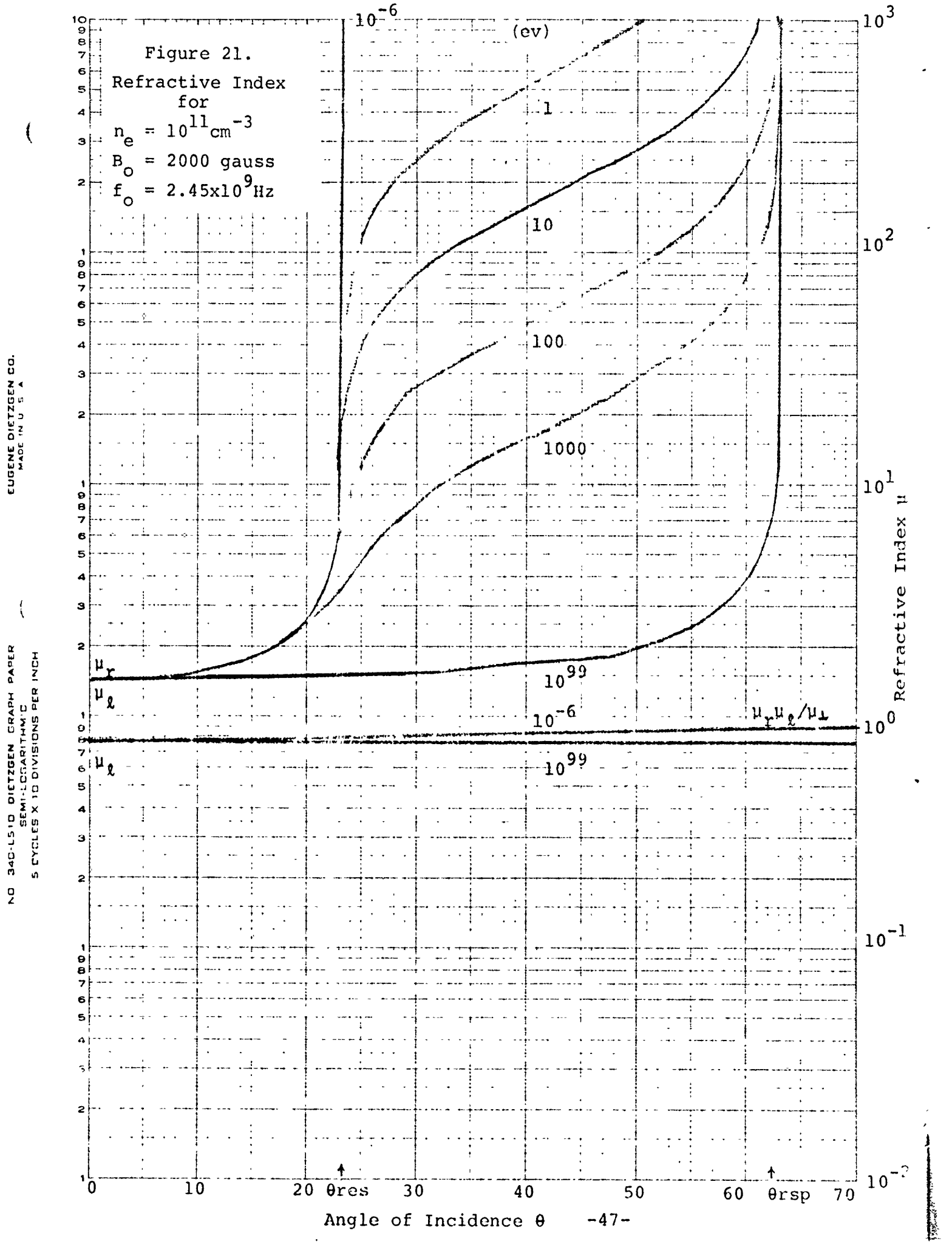

EUGENE DIETZGEN CO.
MADE IN U.S.A.

NO 340-L510 DIETZGEN GRAPH PAPER
SEMI-LOGARITHMIC
5 CYCLES X 10 DIVISIONS PER INCH

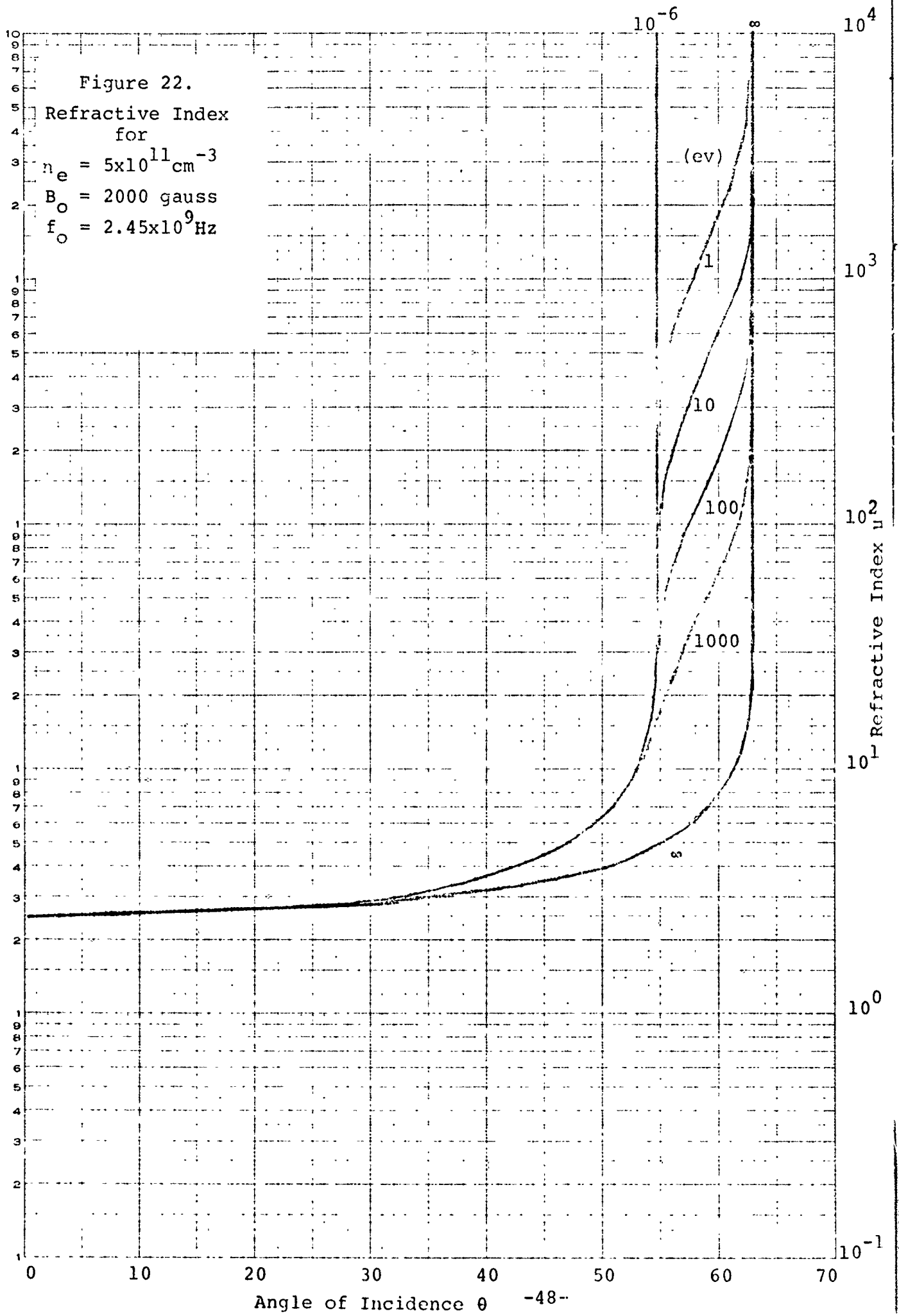

15.2 $\phi_1 = \omega t - \alpha\zeta - \theta_1$ constant then the derivation

15.3 $d\phi_1 = \omega dt - \alpha d\zeta = 0$ and the velocity along the axis

$$V = d\zeta/dt = \omega/\alpha$$

but for a nonconducting medium it is found that

15.4 $$\alpha = (\mu_1\varepsilon_1)^{\frac{1}{2}}\omega$$

The phase velocity is then simply equal to

15.5 $$V = \frac{1}{(\mu_1\varepsilon_1)^{\frac{1}{2}}} .$$

If the velocity in free space is

15.6 $$C = \frac{1}{(\mu_o\varepsilon_o)^{\frac{1}{2}}}$$

the refractive index is

15.7 $$\mu = \frac{C}{V} = \frac{(\mu_1\varepsilon_1)^{\frac{1}{2}}}{\mu_o\varepsilon_o}$$

A cylinder of "thin" plasma may be considered as a waveguide section.

The normal incidence of an electromagnetic wave on such a thin plasma will therefore result in a reflection at the interface, which is a function of the refractive index, μ. This latter may be written in terms of a function of the ratio of the wavelength inside the plasma λ_p wavelength in free space λ_o that is incident on the plasma i.e.:

15.8 $$\mu^2 - 1 = \left(\frac{\lambda_o}{\lambda_p}\right)^2 \left(1 + \left(\frac{Z}{M}\,\frac{n_i}{n_e}\,\frac{m_e}{m_i}\right)\right)$$

To this approximation, the refractive index is

15.9 $$\mu = \left\{1 - \left[\left(\frac{\lambda_o}{\lambda_{pe}}\right)^2 + \left(\frac{\lambda_o}{\lambda_{pi}}\right)^2\right]\right\}^{\frac{1}{2}} .$$

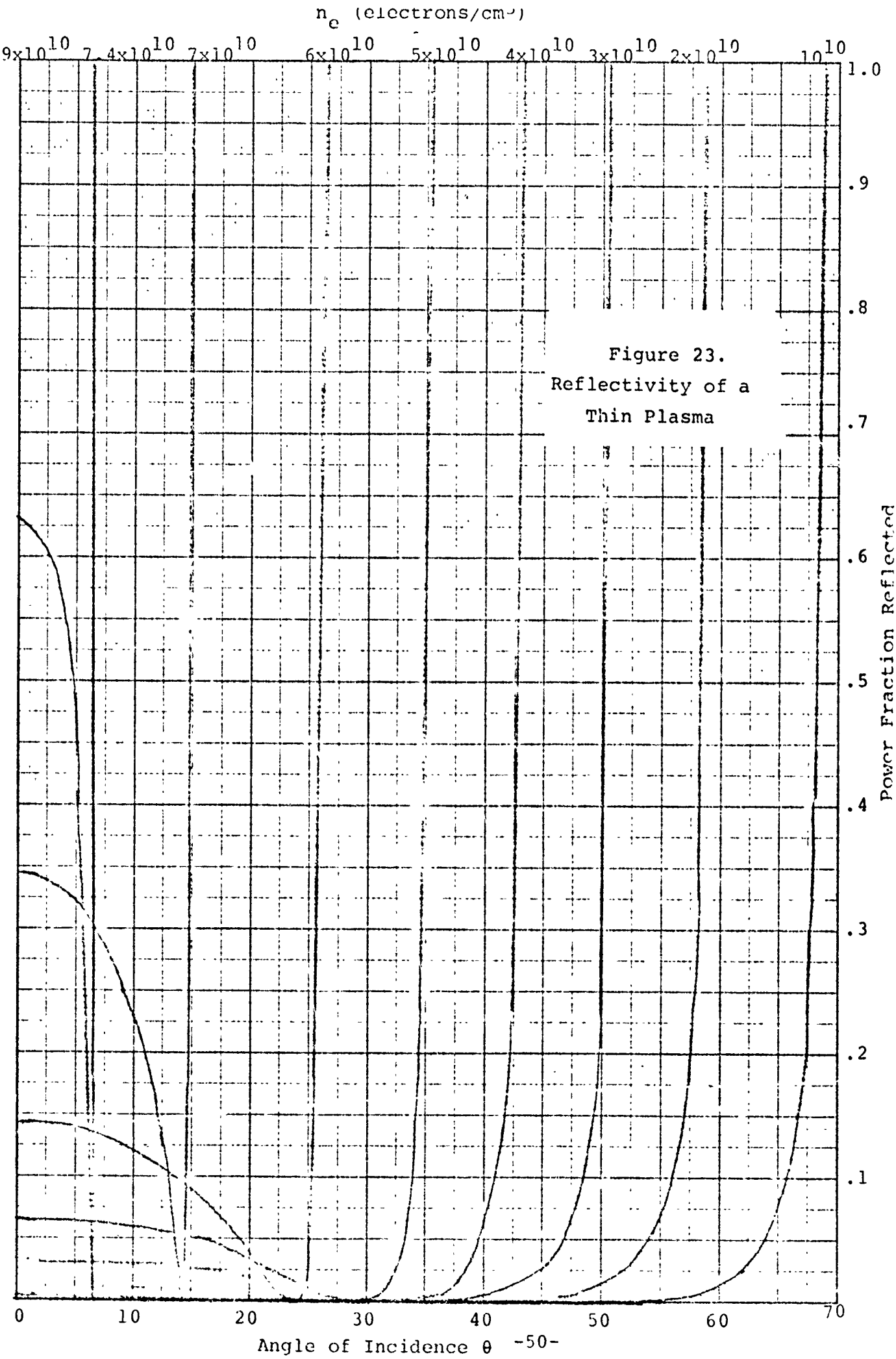

Figure 23.
Reflectivity of a
Thin Plasma

where λ_{pe} is the wavelength in the plasma if the plasma were composed of electrons alone and λ_{pi} is the wavelength in the plasma if the plasma were composed of ions alone.

In such a plasma the unique angle that results in smallest amplitude reflected wave is Brewster's angle. This angle is obtained for that linearly polarized EM wave that has its E component lying in the plane of incidence at the boundary between the two media. At Brewster's angle the sum of the angle of incidence θ and the angle of refraction r, is 90^{o}, therefore $\tan \theta = \mu$ from Snell's law.

To illustrate consider a case of "thin" plasma with no magnetic field and a negligible collision frequency. When a 12.2 cm S band microwave is incident thereon, the value of the refractive index, μ is $\mu = (1 - 1.33 \times 10^{-11} n_e)^{\frac{1}{2}}$. The reflectivity R, at normal incidence, is $R = \left(\frac{\mu-1}{\mu+1}\right)^2$.

In the absence of significant absorption, then, the reflectivity may be specified as a function of the electron density, figure 23. The curves are shown as a function of the angle of incidence on the plasma. Each of the curves corresponds to a single value of electron density when a microwave having a freespace wavelength of 12.2 cm is impinging. The interpretation, up to, $n_e = 7.49 \times 10^{10}$ electron/cm^3 for S band is that there is, always an angle of incidence for the parallel polarization of the EM wave at which no reflection occurs.

Because the phase velocity is greater than the velocity of light in the medium confining the plasma it is not possible to confine this applied EM wave within this form of plasma. If, however, the collision frequency remains negligible it is possible by applying

a dc magnetic field to make the phase velocity less than the velocity of light. The refractive indices are still real and have the values.

15.10 $\mu = \left[1 - 8.96 \times 10^{-14} n_e \lambda^2 (1 \pm \lambda/\lambda_{co})^{-1}\right]^{\frac{1}{2}}$

15.11 $\mu = \left[1 - 8.96 \times 10^{-14} n_e \lambda^2 (1 \pm 5.136 \times 10^{-8} \frac{m_i}{M} ZB\lambda)^{-1}\right]^{\frac{1}{2}}$.

Therefore, for a singly ionized plasma Z = 1 with the electron population n_e, $M = m_e$, the S band wavelength, $\lambda = 12.2$ the index of refraction reduces to

15.12 $\mu = (1 - 1.33 \times 10^{-11} n_e (1 \pm 1.15 \times 10^{-3} B\ (\text{Gauss})^{-1})^{\frac{1}{2}}$.

There is, therefore, always a real refractive index of one of the incident circularly polarized wave when the negative sign is chosen and the magnetic field exceed the value $B > 1.95 \times 10^7 \frac{M}{m_i Z\lambda}$ Gauss.

Again for electrons, $B > 1.05 \times 10^4/\lambda$ Gauss. Where λ is in cm. You will note that when 5×10^5Hz is involved λ is of the order of 6×10^4cm and $B > 0.18$ Gauss would be representative. As an example the earth's magnetic field is at least 0.25 Gauss at the ionized layers of the atmosphere, the index of refraction is greater than 1 reguardless of the electron density only provided that the collision frequency is << than 5×10^5Hz. This condition is met in the D, E, F regions of the ionoshpere and was one of the first tests of the theory.

The clear implication is that a circularly polarized microwave can be guided in a plasma with a static magnetic field. This index can be varied by changing the field intensity thereby permitting the use of a single frequency. The electron density and electron velocities are then controlled by the pressure of the

plasma. This establishes the fact that controls are now available for tailoring the excitation mechanisms for particular population inversions.

16.0 CALCULATION OF THE PEAK FIELD INTENSITY AS A FUNCTION OF THE POWER INPUT FOR A TRAVELLING WAVE

The peak field intensity of a travelling wave in a circular waveguide has been computed for a specific power flow. (See Moreno, Microwave transmission data, Dover 1948, P.124,125) the cases are:

For TE_{11} mode

16.1 $$E = \left(\frac{503}{a^2} \left(\frac{\lambda_g}{\lambda} \right) P \right)^{\frac{1}{2}} \text{ volts/cm.}$$

for the existing geometry $a = 5.715$ cm

$\lambda = 12.24$ cm

$\lambda_c = 19.50$ cm

$\lambda_g = 15.71$ cm

P = Power (watts)

16.2 $$E = 4.447\ P^{\frac{1}{2}} \text{ volts/cm}$$

This occurs on axis.

The case of the TM_{01} involves two situations. The first results when $a/\lambda < 0.761$. In this case the maximum field intensity occurs on axis. The equation

16.3 $$E = \left(130 \frac{\lambda^2}{a^4} \left(\frac{\lambda_g}{\lambda} \right) P \right)^{\frac{1}{2}} \text{ volts/cm.}$$

For this mode the geometry changes the values of $\lambda_c = 14.93$ cm and $\lambda_g = 21/35$cm.

16.4 $$E = 5.64\ P^{\frac{1}{2}} \text{ volts/cm.}$$

at P = 1kw $E_{TE} = 145$V/cm and $E_{TM} = 178$ V/cm.

serious lack of data for the remaining II-VII compounds. It is suggested that an investigation of this paucity of data and some more extended thermo chemical calculations are in order. Section 5 lists some of the preliminary data that will be required to extend this type of study.

2b. The electron temperature estimation in Section 6 based on the Von Engle - Steenbeck method has been applied to those noble gases for which a legitimate value the constant C could be postulated. Similiar estimates should be made for other of the vapors and gases that could offer a buffer potential. The H_2O vapor that has been so effective in the $BaCl_2$ experiments in particular should be evaluated in more detail.

2c. Section 7 developes the radial density distribution encountered in a wall confined plasma. Such a distribution will be much less liable to exhibit a strong reflection when the steep portion of the gradient is of the order of a ¼ wavelength than when the gradient is sharp enough to be considered to be a discontinuity. Advantage should be taken of this characteristic. The relation to the skin depth which is treated in section 10 should be amplified.

2d. The field intensity distribution in the TM_{01n} mode has been shown in Section 12. The unique character of the magnitude of the field intensity at r/R_o = .87 staying virtually constant at about .18 of E_o may be useful. At this distance only the direction of the vector field is changing. The TE_{11n} mode should also be investigated.

2e. The most interesting aspect of sections 14 and 15 is the truly tremendous range of potential values for the refractive index when the magnetic field is introduced and the extraordinary effects introduced by increasing the initial energy of the electrons. It will be the developement of this work that will lead to the ultimate in the final designs.

18.0 RECOMMENDATIONS

1. Future Cavity Modifications

It is recommended that future cavities be constructed with flanges at both ends. Sealing shall be both for vacuum and for microwave integrity. The use of a hard vacuum in the cavity around the quartz tube will eliminate the convective losses and insure that the cavity surface will remain oxide free. This could reduce the total cavity loss to a few watts while permitting the quartz tube wall to operate at more temperatures that are more than 1000^{o}C. A thinner tube quartz wall would reduce the total emission by the quartz wall. The freedom from oxygen will allow an interior coating of silver in the cavity which will insure; a, the increase in Q; b, the reduction in effective emissivity; and c, the reduction in the loss of visible and ultra violet radiant power from the plasma itself. The end plates of the cavity should contain the screw thread for the tuning pistons. These shold be on both sides of the cavity. The controls for both the fill and vacuum equipment of the laser tube and for the auxiliary vacuum envelope shall be on one of the end plates. The tuning pistons should be designed with a flange quarter wave choke. The losses introduced by a well made tuning piston of this sort will be less than 0.001 db per piston. The feed through for cavity excitation should be a coaxial line with micrometer tuning on each of the four input probes.

Since the differential pressure between the cavity and the laser tube is small a simple O ring seal may be considered between the quartz tube and the end plates of the cavity. This allows the

Brewster windows to be attached to the metallic extension of the plasma tube. Because of the unique character of the laser beam these windows and the closing laser mirrors may be situated at a considerable distance form the active region. The length of this "Buffer gas region" can reduce the potential for window contamenation enough so that only the mildest of aerodynamic windows is required. It might be possible to use the pulse frequency of the magnetron to make the plasma itself act as a piston for operating the aerodynamic window.

The cavity volume is sufficiently large to allow the insertion of various structures with geometries that correspond to both cylindrical and spherical coordinates. Such loose structures as slow wave lines and consecutive cavities may also be examined.

A long solenoid should be wrapped around the cavity capable of producing axial magnetic intensities up to 10,000 oersteds for short periods and 1,000 oersteds on a d.c. basis.

2. Extensions in the Analytic Work

The analytic work, to this point, must be considered as preliminary because of the wealth of conditions that may be imposed on the plasma and the varied responses that can be expected. Much of the future analytic work will be dictated by the results of the experimental testing program. Some points, however, should be expanded upon among these are:

2a. Section 4 identifies the vapor pressure and densities obtained on the basis of present data this is somewhat lower than the values used by Frayne from the International Critical Tables. There is a

19.0 SUMMARY

This report presents the basic material that was used to develop the cavity design. A partial reference list is included concerning only those aspects that are fundamental to the problem.

From this, we have refined our understanding of the interface conditions between the plasma, the plasma envelope, and the waveguide. Factors such as the latter, however, must not dictate the cavity design because such high sensitivity would not permit stable operation. The design has been based on the ability to adapt to all reasonable modifications such an experimental system might encounter. To this end the structure is a large diameter cavity containing a number of longitudinal half wave periods. Both standing waves and travelling waves can be introduced. Linearly, lavio and dextro rotary circularly polarized waves can be introduced. The cavity size is sufficiently large to permit insertion of various potential configurations such as involve the increase in the, in-guide, wavelength, loosly coupled consecutive ½ wave cavities, slow wave structures and conical cavities. The reflectivity of the interior of the microwave cavity is sufficiently high to reduce the radiative transfer between the microwave cavity wall and the plasma envelope. This permits the quartz envelope to operate at a high temperature even though the brass cavity is at less than 100°C. A reexamination of the available vapor pressure data on magnesium and the magnesium halides shows a need for additional experimental work in this field particularly at the lower temperatures. Reasonable electron temp-

eratures have been predicted for the noble gases as buffers. The radial electron density has been estimated as a function of the core electron density. The resistivity of the plasma has been obtained as a function of the electron density and temperature. The quartz tube diameter is equal to the skin depth at 1.3×10^{11} electrons/cm^3 on the assumption of a constant electron density. The theoretical cavity Q was not obtained although the TM_{016} mode was close. The alterations in the method of cavity excitation caused a decrease in the Q to 8000 in the worst case. The magnitude and direction of the field intensity were established in the resonant cavity modes. The peak field intensity was obtained for the travelling wave mode. The expected plasma frequencies were obtained and estimates of the effects of these frequencies and electron densities and energies on the refractive index of the plasma have been indicated. The effect of introducing a longitudinal magnetic field has also been indicated. The external character of the cavity has been maintained clear so that such longitudinal magnetic fields might be readily applied. The laser mirror mounting was constructed independently of the overall cavity and mounted on an invar rod. Temperature variations in the cavity will not affect the size to the laser cavity. An all quartz tube was designed to allow the Brewster windows to operate at a higher temperature than the Quartz envelope. This is to reduce the potential for condensation on the window surfaces. The microwaves are introduced either by the apertures at the end of the cavity or by the coaxial couplings in the cavity walls. Suitable isolation of the magnetron is obtained by good microwave practice.

20.0 REFERENCES

1. Data for Plasmas in LTE, Drawin Felenbak, (Page 49 etseq) Granthus Villars Paris, 1965.

2. Spectra of Diatomic Molecules, Herzberg, (page 466 etseq) D. Van Nostrand Company, 1950.

3. Molecular Spectra and Molecular Structure II Herzberg (Page 501 etseq) D. Van Nostrand Company, 1945.

4. Physics of Fully Ionized Gases, Spitzer, (Page 120 etseq) Interscience Second Ed., 1962.

5. Waveguide Handbook, Marcuvitz, McGraw Hill, 1951.

6. Principles of Microwave Circuits, Montgomery, McGraw Hill, 1948.

7. Fehsenfeld, RSIV36, 294, 1965.

8. Bossisio, Journal of Microwave Power 7 (4) 1972.

9. McTaggert, Journal of Microwave Power 5 (4), 1970.

10. Dattner, Phys. Rev. Letters, P. 205 V10, 1963.

11. Shohet & Moskowitz, JAP, P. 1756 V36, 1965.

12. Agdur, Enander, JAP, P. 575 V33, 1962.

13. Kent, Heintz, JAP, P. 1741 V39, 1968.

14. Mallovarpu, Asussen Haley, IEEE Trans Plasma Science, 1978.

15. Asmussen, Mallavarpu, Hammer, P. 109, Proc. IEEE V62, 1974.

16. Fredericks, Asmussen, P. 508, Appl Phys. Letters, V19, 1971.

17. Chapman & Cowling Mathematic Theory of Nonuniform Gases, Cambridge, 1953.

18. Cowling, P. 453 Proceed. Royal Soc. A183, 1945.

19. Landsoff P. 904 Phys. Rev. V76, 1949.

20. P. 442, Phys. Rev. Vol. 82, 195[illegible].

21. Cohen Spitzer, Routly, P. 230 Phys. Rev. V80, 1950.

22. Spitzer & Harp, P. 977, Phys. Rev. V89, 1953.

23. Waves in Anisotropic Plasmas, Allis, etal MIT Press, 1963, Chapter 5.

REFERENCES

24. Contributions to the Data on Theoretical Metallurgy Bulletin 601 Bureau of Mines, PP66 & 67 Kelley.

25. Phys. Rev. Vol 34 15 August 1929. P690-596, John G. Frayne.

26. Vapor Pressure of Mg Between 223 and 385°C, Gilbreath NASA TND 2723 (1965).

27. Molecular Theory of Gases and Liquids, Hirschfelder, Curtiss Bird, P238, Wiley 1954.

28. Handbook of Chemistry & Physics, Chemical Rubber Publishing.

29. Gaseous Conductors, Cobine P238, McGraw-Hill 1947.

30. Heat Transfer, Vol. 1, Dakob, P.538 etseq., Wiley 1949.

31. Electromagnetic Theory, Stratton P.504, McGraw-Hill, 1941.

APPENDIX I

OPERATING INSTRUCTIONS AND TEST DATA

S-Band Cylindrical Cavity

for Laser Excitation

Operating Instructions
and
Test Data

November 13, 1980

ITT AVIONICS DIVISION
390 Washington Avenue, Nutley, N.J. 07110

CONTENTS

I. INTRODUCTION

The equipment described herein was developed by ITT Avionics for the U.S. Army, Ft. Belvoir, Va. under Contract No. DAAK 70-79-C-0171. It consists of a high power S-band source, which is coupled to a cylindrical cavity in which the microwave energy is used to excite a plasma for laser experimentation. This report contains a brief description of the equipment (Section II), Operating Instructions (Section III) and a summary of test data (Section IV).

II. GENERAL DESCRIPTION

A. RF Source

The RF Source is a completely enclosed High Power Microwave generator capable of providing 1200 watts of CW RF power at 2450 MHz. The source consists of a magnetron tube, power supply, blower, and associated protection and interlock circuits. This source, when used with its external circulator/load is fully protected against all possible load mismatches.

B. Cylindrical Cavity

The purpose of the cylindrical cavity is to receive energy from the high-power S-band source, and to couple the energy into a plasma tube centered within the cavity. A sketch of the cavity is given in Figure 1. The outer conductor is made of brass tubing, 4.5 inches ID. The useable electrical length of the cavity is 32 inches and the overall length is about 40 inches. A sliding short is provided on one end of the cavity so that the electrical length can be varied; electrical contact is provided by a simple threaded joint, covered with conductive grease.

The openings in the end walls of the cavity are one inch in diameter, providing a clear optical aperture of one inch. The one inch diameter extension tube on each end, acts as a cutoff waveguide, to highly attenuate the microwave signal, and thus prevent leakage from the open ends. The three inch length provides an attenuation of greater than 100 dB.

The cavity can be operated in several different modes in order to evaluate, and ultimately to maximize the coupling efficiency to the plasma. The cylindrical waveguide modes which can be propagated within the cavity are the TE-11 and TM-01 modes. In each case,

the cavity can be configured to operate in a resonant condition (unterminated) or a travelling wave condition, with the output terminated.

It should be noted that, depending on the nature of the plasma, the center tube containing the plasma may appear more or less conductive, in which case the cavity can propagate in the TEM mode essentially as a coaxial line. The field configuration in this case, is virtually the same as the TM-01 mode, but the propagation velocity will be different.

A listing of the possible propagation modes, considering the cavity as either a cylindrical waveguide or a coaxial line, together with the guide wavelengths, is given below:

Mode	Guide Wavelength (inches) (freq. = 2450 MHz)
TE-11, circular wg	6.2
TM-01, circular wg	8.3
TEM, coaxial	4.8
TE-11, coaxial	5.6 (approx.)

Since the guide wavelength of each of the modes is different, the length of the cavity must be adjusted for resonance in each case. The guide wavelength will also vary depending on the nature of the plasma. Therefore, in order to assure a resonant condition for any possible plasma state, the range of adjustment is equal to one-half guide wavelength in the TM-01 mode ($\approx$ 4.2 inches).

C. Test Setup

A block diagram of the feed network for coupling the RF energy from the source to the cavity is shown in Figures 2 and 3. The objective was to provide maximum flexibility for laboratory experimentation, utilizing components selected for simplicity and low cost, with size and weight of secondary importance.

A waveguide feed network, shown in Figure 2, is used for the resonant cavity mode of operation, and can also be used for the travelling wave mode for excitation of the TM-01 mode or a single (linearly-polarized) TE-11 mode (Figure 3a).

The coaxial feed network, shown in Figure 3b is used only for the travelling wave mode, and can be used to excite the TM-01 mode or crossed TE-11 modes for circular polarization.

For both feed networks, the output of the high power source is coupled to a circulator/load combination which isolates the source from any reflections from the cavity. The circulator is followed by a dual directional coupler used to measure both incident and reflected power. The coupler is followed by a triple stub tuner used to match the impedance looking into the cavity, in the resonant mode. The signal is then coupled to either the sum port or the difference port of a Magic-Tee Hybrid, for either in-phase or anti-phase excitation of the cavity, corresponding to excitation of the TM-01 and TE-11 modes respectively. Flexible waveguides carry the power from the hybrid to the cavity when the waveguide feed is used.

With the coaxial feed network, waveguide-to-coax transitions are connected to the hybrid and these are in turn connected through semi-rigid coaxial cable to coaxial probes mounted in the cavity walls. With the coaxial feed, the cavity must be terminated on the opposite end; this is accomplished by four separate probes connected to high power loads by semi-rigid coaxial lines.

To excite the circular polarization mode, two coaxial hybrids are connected to the outputs of the Magic-Tee hybrid to form four outputs. These are connected to four input probes in the cavity wall, by coaxial lines, to provide quadrature phase excitation of crossed TE-11 modes.

A photo of the cavity and waveguide feed is given in Figure 4.

III. OPERATION

A. RF Source

The RF Source is connected as shown in Figure 2. The source should never be operated without a circulator/load connected to its output, since severe damage to the magnetron tube can occur due to high VSWR. The source front panel consists of the following controls with its associated functions: (See photo in Figure 5.)

Power On/Off	Turns on AC power and also provides 25 amps of circuit protection
Power, Pilot Light (amber)	Indicates presence of AC power
Ready, Pilot Light (amber)	Indicates 60 second delay after AC power is turned on - RF power can now be activated

RF On, Pilot Light (red)	Indicates RF power is active
Over Temp, Pilot Light (red)	Indicates a high temperature condition exists in the magnetron tube when RF On, Start button is depressed. RF cannot be activated under this high temperature condition. If RF is active when a high temperature condition occurs, the RF power will automatically be turned off.
Water Shut-Off, Pilot Light (red)	Indicates water flow to circulator is not adequate for proper cooling when RF On, Start button is depressed. RF cannot be activated under this condition. If the RF is active when low water flow condition occurs, the RF power will automatically be turned off.
Start Button	Start button activates RF power, only if no high temperature condition exists and water flow rates are adequate.
Stop Button	Stop button turns off RF power
Water Flow Control Connector	Connects the circulator water flow sensor to the RF source

The circulator is water-cooled and protected via a water flow sensor inter-lock. A flow rate of at least 0.5 gal/min is required to properly cool the circulator. Should the flow rate drop below 0.5 gal/min the RF power output will be interrupted. Indication of this fault will be shown by the (red) water Shut-Off Pilot Light when the RF is reactivated by RF On, Start Button. The waveguide circulator load should always be operated with an air flow in order to prevent overheating of the load.

A block diagram of the RF source is shown in Figure 6, and a parts list is given in Figures 7a, b, c. The status of the magnetron tube can be checked by breaking the connection at TPI and placing a 0-1 DC ampmeter and 0-5 KV DC voltmeter at this point. Typical readings are as shown on the schematic diagram.

B. Cylindrical Cavity

The cylindrical cavity can be configured for operation with either a waveguide feed or a coaxial feed network. The operating procedure for each is described below.

1. Waveguide Feed

For waveguide excitation, the cavity end-plate with integral waveguide flanges is used. This end-plate is attached to the end cavity by screws; the apertures in the plate provide the coupling to the cavity.

For the resonant cavity mode, all of the coaxial probes are removed, and the openings in the cavity walls are covered with the small plates provided. For the travelling wave mode, the four probe covers near the waveguide feed are left on, but the covers on the opposite end are removed and replaced by the coaxial probes, for connection to the external high power loads.

The position of the sliding short circuit is adjusted, by rotating the extender tube on the output end. In the resonant cavity mode, the short circuit position is adjusted for resonance, as discussed in Part C below; for the travelling wave mode, the short is set to a position of 1-3/4 inches on the scale provided which provides the best match for the coaxial probes.

2. Coaxial Feed

For coaxial excitation, the endplate with the waveguide flanges is removed and replaced with the solid, flat endplate. Depending on the desired mode of excitation, either two or four coaxial probes are used on the input end. For excitation of either the TM-01 mode, or a single (linearly polarized) TE-11 mode, only two probes are used, displaced 180° from each other. For excitation of crossed TE-11 modes, all four input probes are used. It should be noted that for coaxial excitation, regardless of the mode being excited, all four terminating probes must be used with their associated loads attached. Failure to terminate the cavity, when using coaxial excitation, can result in voltage breakdown at the probes and/or overheating of the coaxial feed lines.

C. Test Setup and Tuning Procedure

The test setup and tuning procedure are discussed with reference to Figures 2 and 3 described earlier. The portion of the setup from the source to the Magic-Tee Hybrid, is the same, regardless of whether waveguide or coaxial excitation is to be used. The circulator and its load, the dual directional coupler, the triple-stub tuner and the hybrid are all fabricated in WR-284 waveguide, and are assembled in the conventional way.

1. Waveguide Feed - Resonant

Excitation of a particular propagation mode in the cavity is determined by the particular hybrid ports to which the source is connected as follows:

TM-01	Sum Port driven Difference port terminated
TE-11	Difference port driven Sum port terminated

In either case, the colinear ports of the hybrid are connected to the cavity input ports by means of the flexible waveguide.

The procedure for tuning the network for optimum coupling in the resonant mode, is as follows:

(1) Connect power meters to the forward and reflected power ports of the dual directional coupler, and to the directional coupler in the load port of the hybrid.

(2) Turn the middle screw of the triple stub tuner to insert the stub all the way in.

(3) Turn the power on, and observe the incident and reflected power; the reflected power will typically be almost equal to the incident.

(4) Move the sliding short circuit (by turning the extender tube as described above), and watch for a reduction in reflected power. Set the short circuit to the position for minimum reflection.

(5) Readjust the triple stub tuner, first the center stub and then the others, to minimize the reflected power.

With the short circuit and the tuner properly adjusted, the reflected power and the power out of the isolated port of the hybrid should each be 20% of the incident, or less.

If either the reflected power or the isolated port power can not be adjusted to be less than 20%, then the cavity may be tuned to a spurious mode. In this case, readjust the sliding short circuit to search for another resonance, i.e. a dip in reflected power, and repeat steps (4) and (5).

The resonant condition is quite critical because of the high Q of the cavity, especially when unloaded. Also, when a plasma is present in the cavity, the resonant condition will vary with the condition of the plasma, and so the sliding short and the stub tuner will probably require re-tuning after the plasma is excited.

2. Waveguide Feed - Travelling Wave

The procedure for tuning the setup in the travelling wave mode is as follows:

(1) Connect high power terminations to all four output coaxial probes

(2) Set the sliding short to 1-3/4 inches on the scale.

(3) Adjust the tuner so that all three probes are all the way out.

(4) Turn the power on and observe the incident, reflected and isolated power. If the reflected and isolated power are below 20%, no additional tuning is required.

(5) If the reflected power is too high, the tuner can be adjusted to minimize the reflected power.

3. Coaxial Feed

The coaxial feed network may be used in any of the travelling wave modes. However, since the TM-01 and the single TE-11 mode can be excited with the waveguide feed, use of the coaxial feed is recommended only for excitation of the circularly polarized mode, i.e. crossed TE-11 modes in quadrature phase.

For the circularly polarized mode, the waveguide-to-coax adaptors are connected to the colinear ports of the Magic-Tee hybrids. Two coaxial hybrids are in turn connected to the adaptors; the adaptors feed the sum ports, and the difference ports are terminated as shown in Figure 3. One pair of coaxial cables are connected from one hybrid to two of the coaxial probes (opposite each other). The other hybrid is connected to the other two coaxial probes, using a pair of cables which have been cut for 90° shorter length at 2450 MHz.

(1) With the setup configured as described above, and with all four output probes terminated, adjust the tuner so that all three stubs are all the way out.

(2) Turn on the power and observe the incident and reflected power.

(3) The circuit should be self-calibrated in this case. The tuner should not be adjusted from its maximum out position in this case, since this would create a risk of breakdown or overheating of the coaxial feed network.

IV. TEST DATA

A variety of low-power and high-power measurements were made to characterize the performance of the cavity in the various modes. The low-power measurements included swept frequency plots, of input reflection for the resonant condition, and of input reflection and transmission for the travelling wave case. Transmission is measured from the input to each of the output probes (individually); since there are four probes, -6 dB is equivalent to complete transmission. A listing of the test data is given below:

High power measurements were made with the RF high power source at a single frequency of 2450 MHz.

Sheet No.	Parameter Measured	Cavity Configuration
4-1	Reflection	TE-11, Resonant, Empty
4-2	Reflection	TE-11, Resonant, w Pyrex tube
4-3	Reflection	TM-01, Resonant, Empty
4-4	Reflection	TM-01, Resonant, w Pyrex tube
4-5	Reflection	(same as 4-4, expanded scale)
4-6	Transmission	TE-11, Travelling Wave, Empty
4-7	Reflection	TE-11, Travelling Wave, Empty
4-8	Transmission	TM-01, Travelling Wave, Empty
4-9	Reflection	TM-01, Travelling Wave, Empty
4-10	Summary of high power measurements	

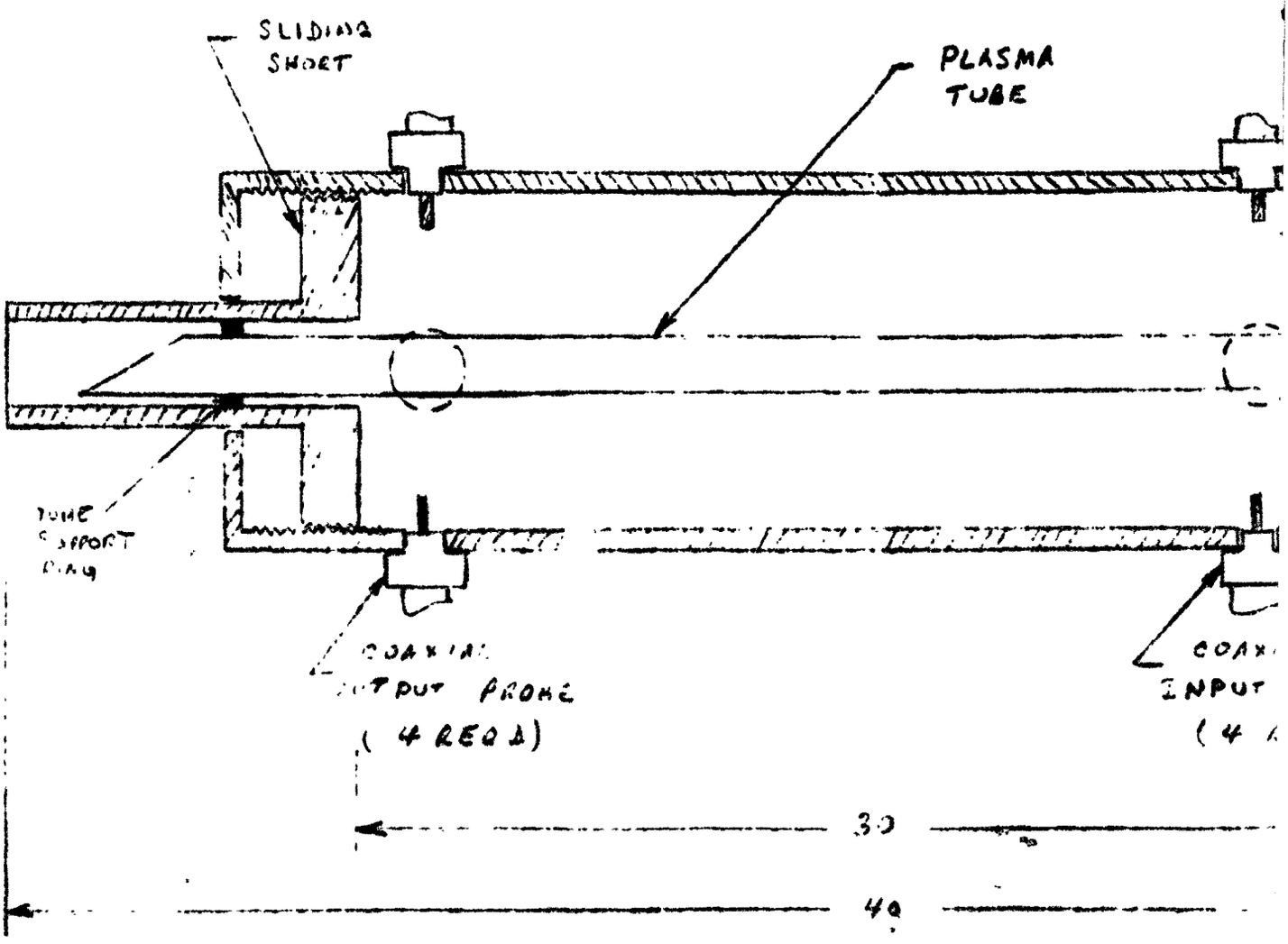
SLIDING SHORT
PLASMA TUBE
TUNE SUPPORT ROD
COAXIAL OUTPUT PROBE
(4 REQ'D)
COAX INPUT
30
40

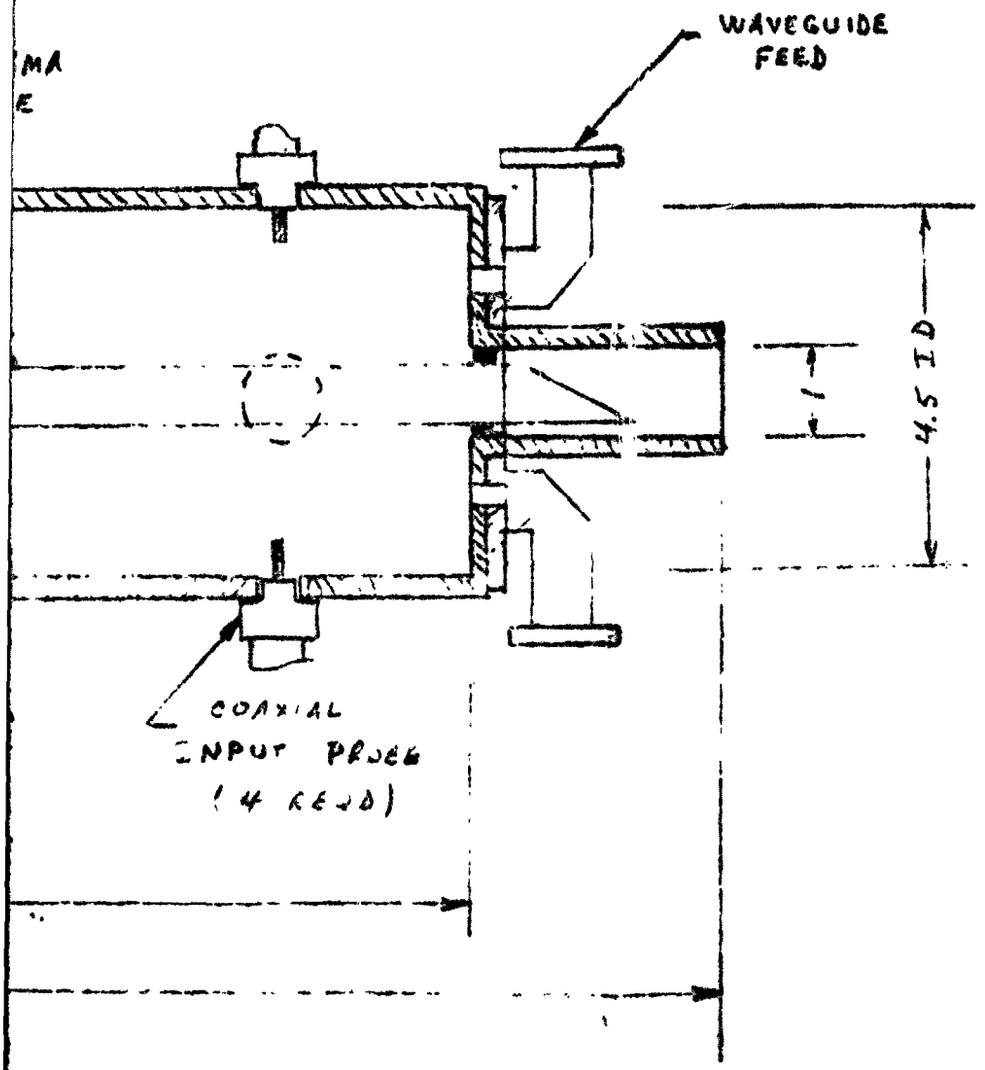

FIG. 1 - SKETCH OF CYLINDRICAL CAVITY

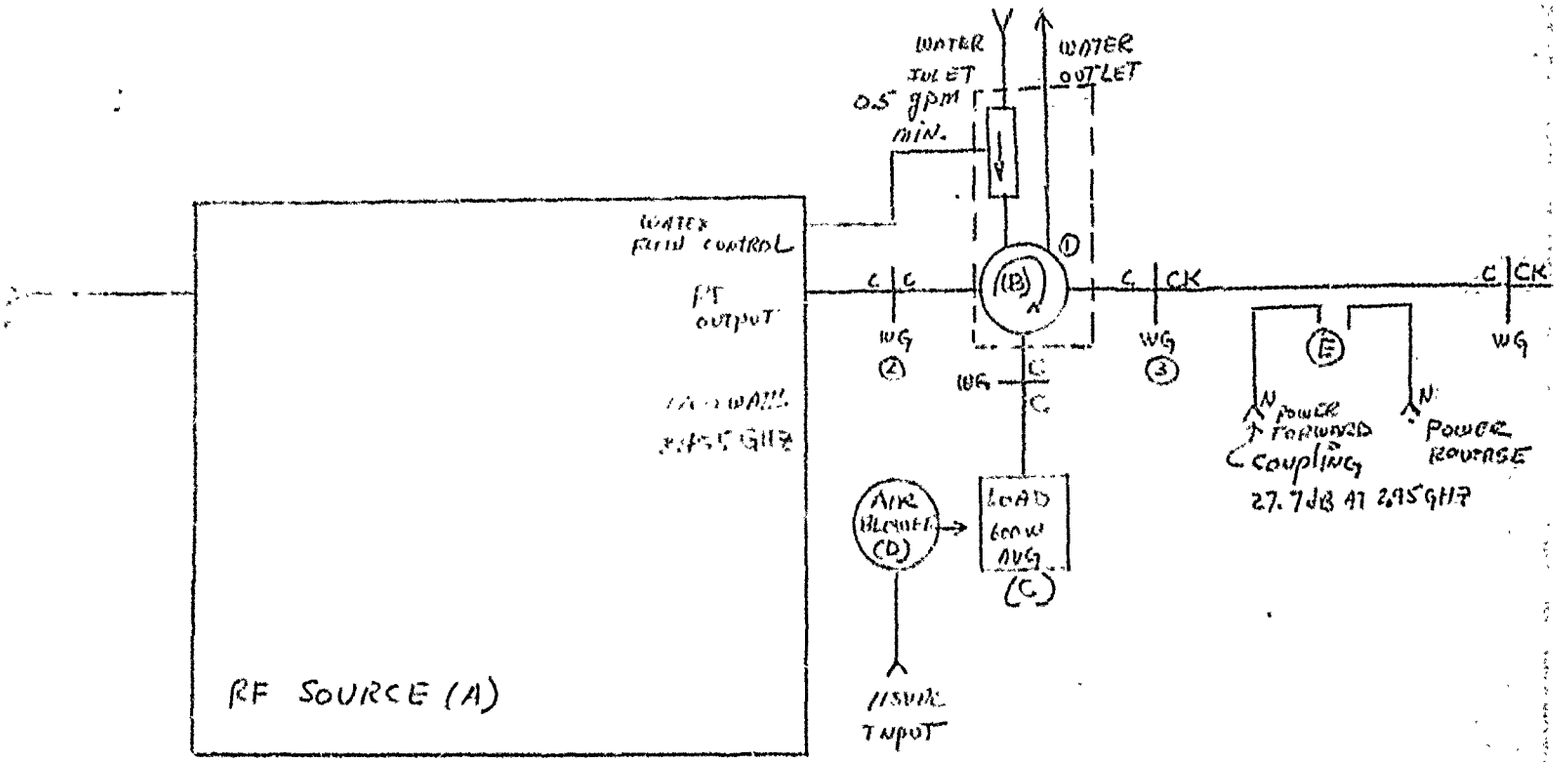

System Parts List

	A	RF Source	ITT Built
	B	Circulator, waveguide + water flow sensor	Merrimac # FCW/1521, Pressure Con
	C	Load, waveguide 600 watt	ARF Products # ID 903
	D	Air Blower	Customer Supplied
	E	Directional Coupler (sidewall waveguide)	ITT Supplied
	F	Twist, waveguide	ITT Supplied
	G	Triple Stub Tuner, waveguide	Gerling Moore # 4037
	H	4-port Hybrid Tee, waveguide	Struthers # M352S
	I	Transition, WR284 to EIA 1 5/8"	Gerling Moore # 4028
	J	Transition, EIA 1 5/8 to Type N	Andrew # 2261A
	K	Directional Coupler, coaxial	Mecca # 715-30-4
	L	Cable Assembly, 7/8"	Andrew # 25817-5
	M	Load Coaxial, 600 watt	Bird # 8401
1	N	Waveguide Flexible (two)	Gerling Moore # 4017
	O	S-band Cavity	ITT Built

REVISIO

ZONE	LTR	DESCRIPTION

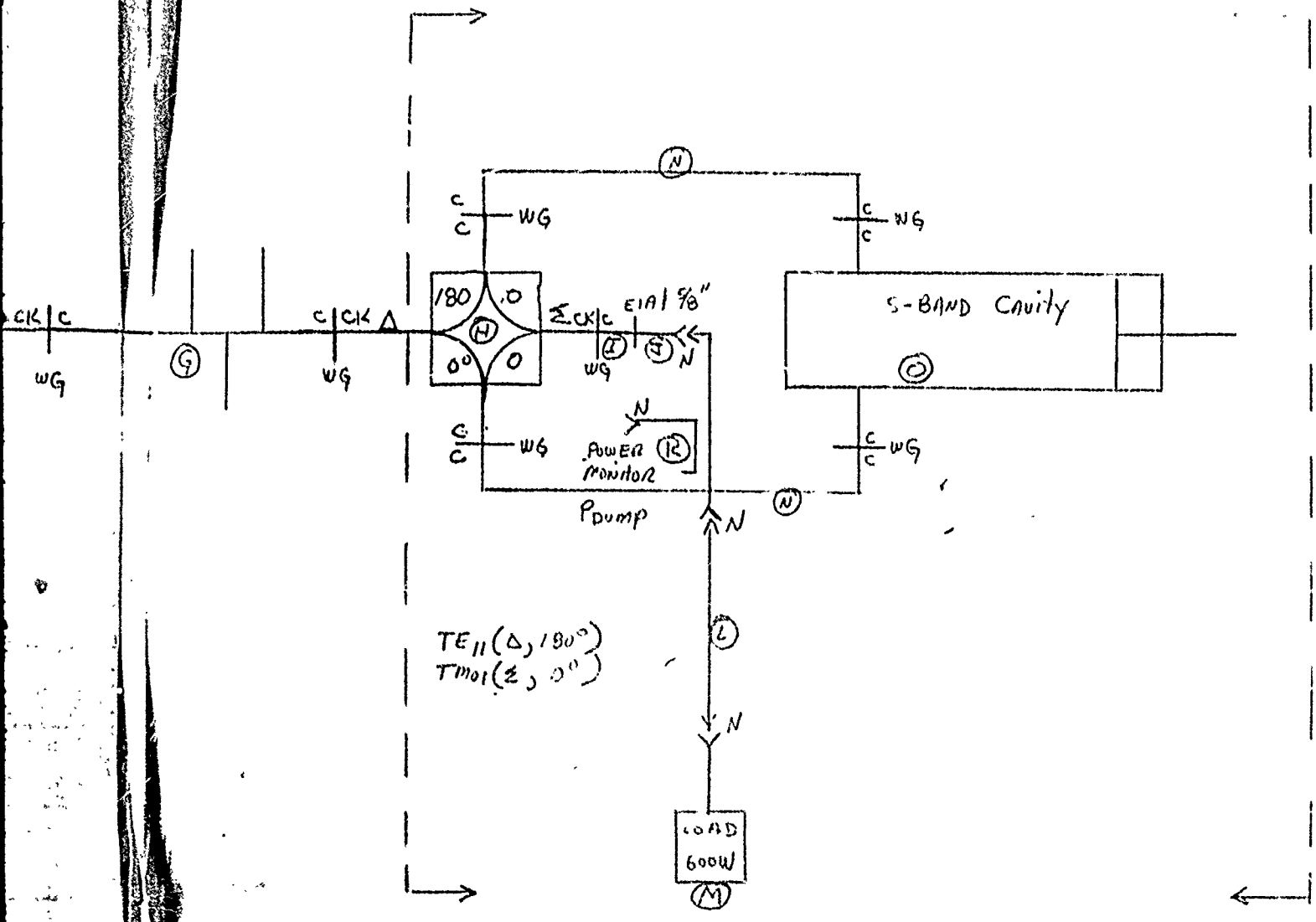

F103

oupling = 27 ... AT 2.45 GHz

1

REVISIONS		
DESCRIPTION	DATE	APPROVED

Cavity
TE11 Modes
TM01

3

SYSTEM PARTS LIST

SIG			
	A	RF SOURCE	ITT BUILT
	B	CIRCULATOR, WAVEGUIDE + WATER FLOW SENSOR	MERRIMAC # FCW/521, PRESSURE CONTR
	C	LOAD, WAVEGUIDE 600WATT	ARF PRODUCTS # ID403
	D	AIR BLOWER	CUSTOMER SUPPLIED
	E	DIRECTIONAL COUPLER (SIDEWALL WAVEGUIDE)	ITT SUPPLIED
	F	TWIST, WAVE GUIDE	ITT SUPPLIED
	G	TRIPLE STUB TUNER, WAVEGUIDE	GERLING MOORE # 4037
	H	4-PORT HYBRID TEE, WAVEGUIDE	STRUTHERS # M3525
	I	TRANSITION, UP284 TO ETA 1⅝"	GERLING MOORE # 4028
	J	TRANSITION, ETA 1⅝ to TYPE N	ANDREW # 226IA
	K	DIRECTIONAL COUPLER, COAXIAL	MECCA # 715-10-4
	L	CABLE ASSEMBLY, 7/8'	ANDREW # 25817-5'
	M	LOAD COAXIAL, 600WATT	BIRD # 8401
	N	WAVEGUIDE FLEXIBLE (TWO)	GERLING MOORE # 4017
	O	GROUND CAVITY	ITT BUILT

ENGINEERING CHECK LIST

ARRANGEMENTS	☐ LOCATE IN GRID. FREEHAND SKETCHING PREFERRED. LOCATE SYMBOLS FUNCTIONALLY AROUND EACH STAGE. ARRANGE STAGES IN LAYERS FROM LEFT-TO-RIGHT OR NEAR LAYERS FROM TOP-TO-BOTTOM.	REF DESIG	☐ IDENTIFY EACH SYMBOL BY REFERENCE DESIGNATION PER USA STD Y32.16. FOR DETAIL SEE ESM. ASSIGN REF. DESIG NUMBERS CONSECUTIVELY FROM LEFT TO RIGHT IN FUNCTIONAL SEQUENCE.
SIGNAL FLOW	☐ DATA INPUTS AT LEFT, OUTPUTS AT RIGHT (PREFERRED) OR INPUTS AT TOP, OUTPUTS AT BOTTOM, OR ANY COMBINATION OF THE TWO ABOVE.	PARTS IDENT	☐ SPECIFY RESISTANCE, CAPACITANCE AND INDUCTANCE VALUES. USE THE FORM OF FEWEST CIPHERS. SCHEMATIC IDENTITIES MUST AGREE WITH ELECTRICAL PARTS LIST
SYMBOLS 2	☐ USE LOGIC SYMBOLS PER USA STD Y32.14 FOR DETAIL, SEE ENGINEERING STANDARDS MANUAL. USE LOGIC SYMBOLS PER USA STD Y32.14 FOR DETAIL SEE ENGINEERING STANDARDS MANU	OTHER INFO	☐ ASSIGN FUNCTIONAL IDENTIFICATION TO PARTS, STAGES AND CIRCUITS. INDICATE MECHANICAL LINKAGE, POT ADJUSTMENT AND OPERATING CONTROLS. INDICATE SHIELDING, PAIRING AND CRITICAL GROUND. OUTLINE TERMINAL BOARDS AND SUB ASSEMBLIES.

DF 1025-87710M

A

3

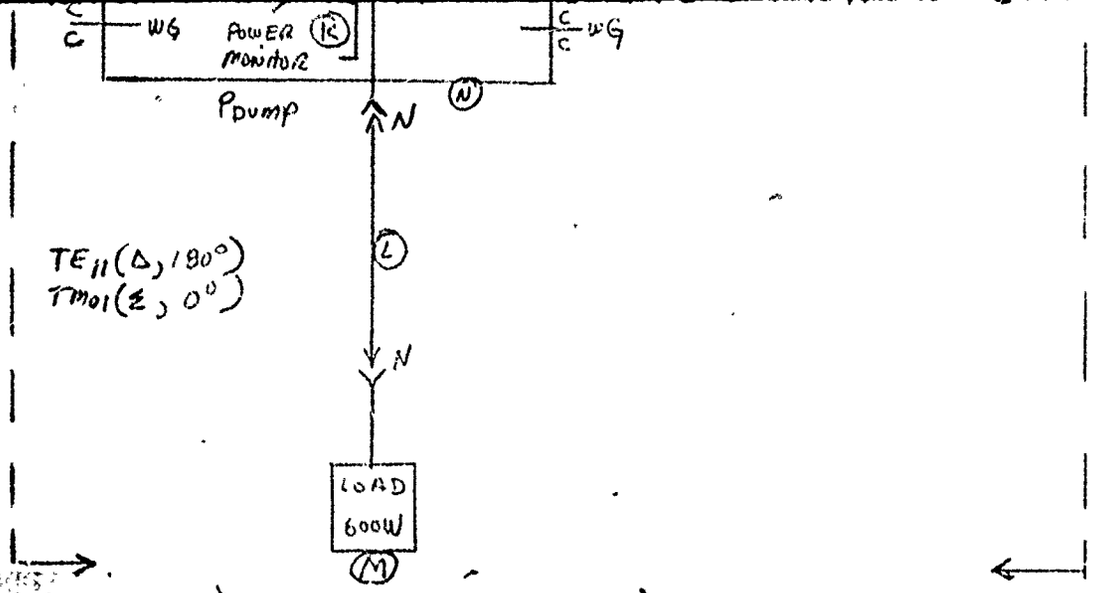

g = 2 [illegible] AT 2.45 GHz

coup [illegible] 0 dB AT 2.45 GHz
coup [illegible] .2 dB AT 2.45 GHz

NOTES (1) observe Circulator [illegible]
(2) WG C [illegible]
(3) WG CK [illegible]

PREM	INSTRUCTIONS	NOTES: 1. PARTIAL REFERENCE DESIGNATIONS ARE SHOWN: FOR COMPLETE DESIGNATION PREFIX WITH UNIT NUMBER AND SUB-ASSEMBLY DESIGNATIONS. 2. UNLESS OTHERWISE SPECIFIED: ALL RESISTANCE VALUES ARE IN ALL CAPACITANCE VALUES ARE IN ALL DIODES ARE ALL TRANSISTORS ARE ALL INTEGRATED CKTS ARE	PREPARED IN ACCORDANCE WITH MIL STD 100	CONTRACT DAAK 70-79-C-	0171 ITT AVIONICS DIVISION
				APPROVALS SIGNATURE & DATE	
				DRAWN	
				CHECKED	
				MECH	
				ELECT	
				STDS	
				E OF M	
			GROUP / SIZE / NEXT ASSY / USED ON	APPLICATION	
				ITEM	SIZE C / CODE IDENT NO 28527
					SCALE / CATEGORY

WG

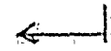

NOTES ① OBSERVE CIRCULATOR POLARITY

② WG C WAVEGUIDE COUPLER

③ WG CK WAVEGUIDE COUPLER

RED IN ACCORDANCE MIL-STD 100	CONTRACT DAAK 70-79-C-	0171 ITT AVIONICS DIVISION	NUTLEY, NEW JERSEY
	APPROVALS SIGNATURE & DATE		
	DRAWN	TEST SET-UP	
	CHECKED		
	MECH		
	ELECT	FIG. 2	
ASSY USED ON	STDS		
APPLICATION	E OF M		
	ITTAV / ITTAV SOURCE	SIZE C / CODE IDENT NO 28527	
	OTHER	SCALE / CATEGORY / SHEET / REV	

SYSTEM PARTS LIST

REF DESIG		
H	4-PORT HYBRID TEE, WAVE GUIDE	STRUTHERS # M3525
I	TRANSITION, WR284 to EIA 1 5/8"	GERLING MOORE # 4028
J	TRANSITION, EIA 1 5/8 TO TYPE N	ANDREW # 22618
K	DIRECTIONAL COUPLER, COAXIAL (TWO)	MICCA # 715-30-4 C/CK
L	CABLE ASSEMBLY, 7/8"	ANDREW # 25817-5 WG
M	LOAD, COAXIAL, 600 WATT	BIRD # 8401
N	WAVE GUIDE FLEXIBLE (TWO)	GERLING MOORE # 4017
O	S-BAND CAVITY	ITT BUILT
P	CABLE ASSEMBLY, 1/2" (FOUR)	ANDREW # 39760-3
Q	LOAD, COAXIAL, 250 WATT (FOUR)	BIRD # 8141

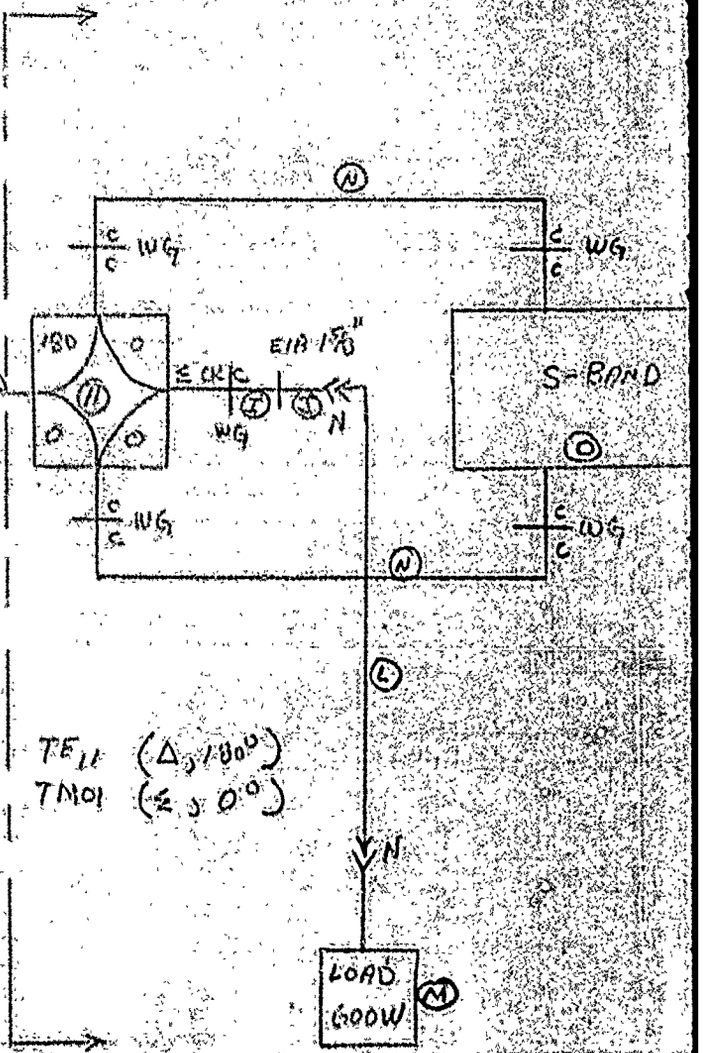

SYSTEM PARTS LIST

REF DESIG		
H	4-PORT HYBRID TEE, WAVE GUIDE	STRUTHERS # M3525
I	TRANSITION, WR284 to EIA 1 5/8" (TWO)	GERLING MOORE # 4028
J	TRANSITION, EIA 1 5/8" to TYPE N (TWO)	ANDREW # 22618
K	DIRECTIONAL COUPLER, COAXIAL (TWO)	MICCA # 715-30-4 C/CK
L	CABLE ASSEMBLY, 7/8	ANDREW # 25817-5 WG
M	LOAD, COAXIAL, 600 WATT (TWO)	BIRD # 8401
N	NOT USED	
O	S-BAND CAVITY	ITT BUILT
P	CABLE ASSEMBLY, 1/2" (FOUR)	ANDREW # 39760-3

NOTE: OBSERVE CABLE S/N. FOR PROPER PHASE POLARITY

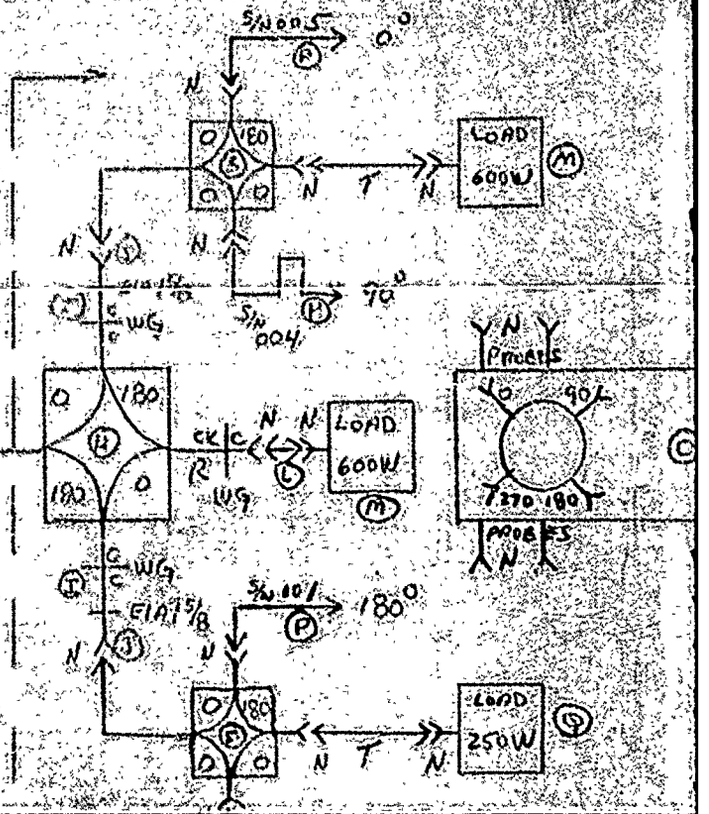

2 1

ORM

REVISIONS		
ZONE	LTR	DESCRIPTION

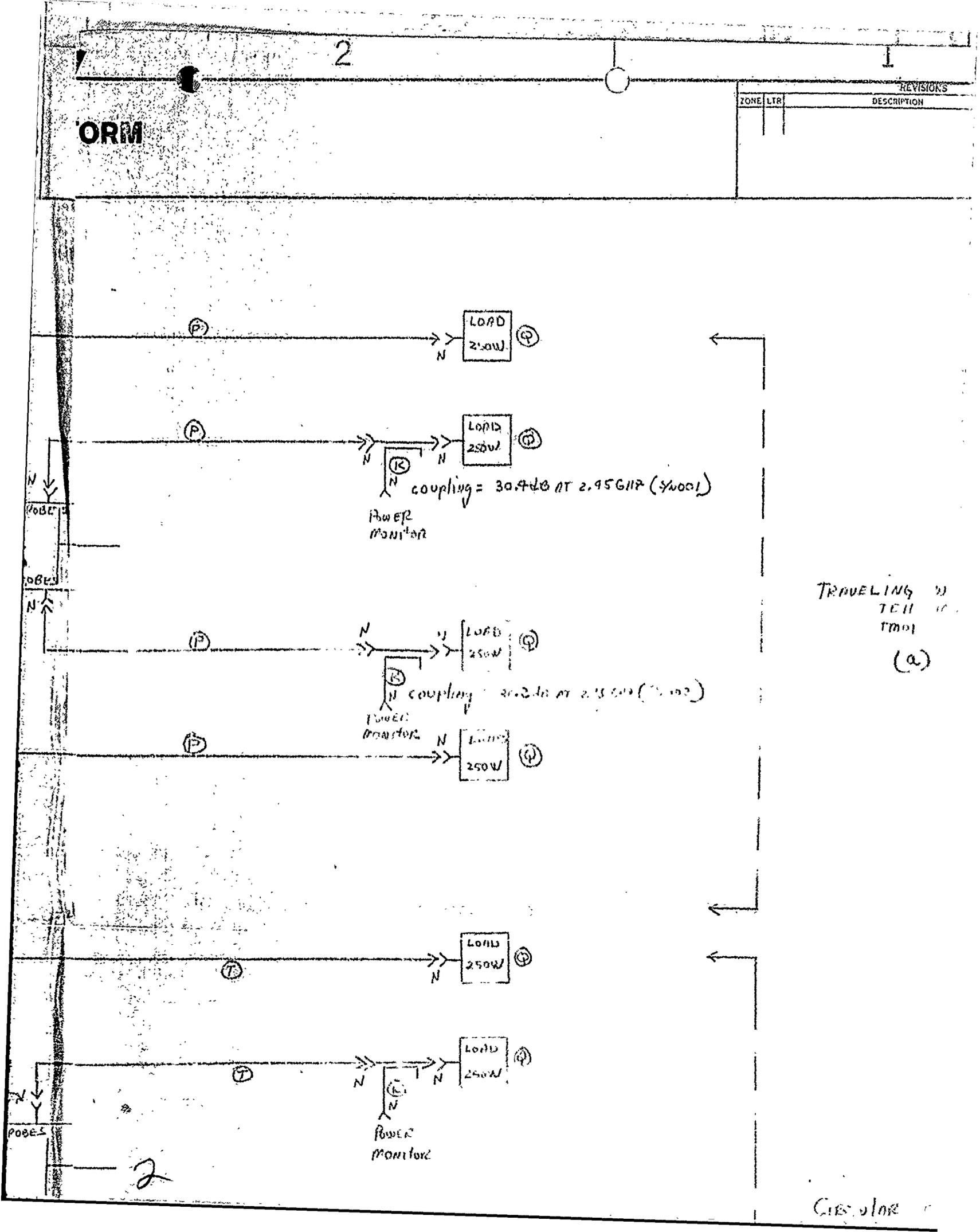

REVISIONS				
ZONE	LTR	DESCRIPTION	DATE	APPRO.

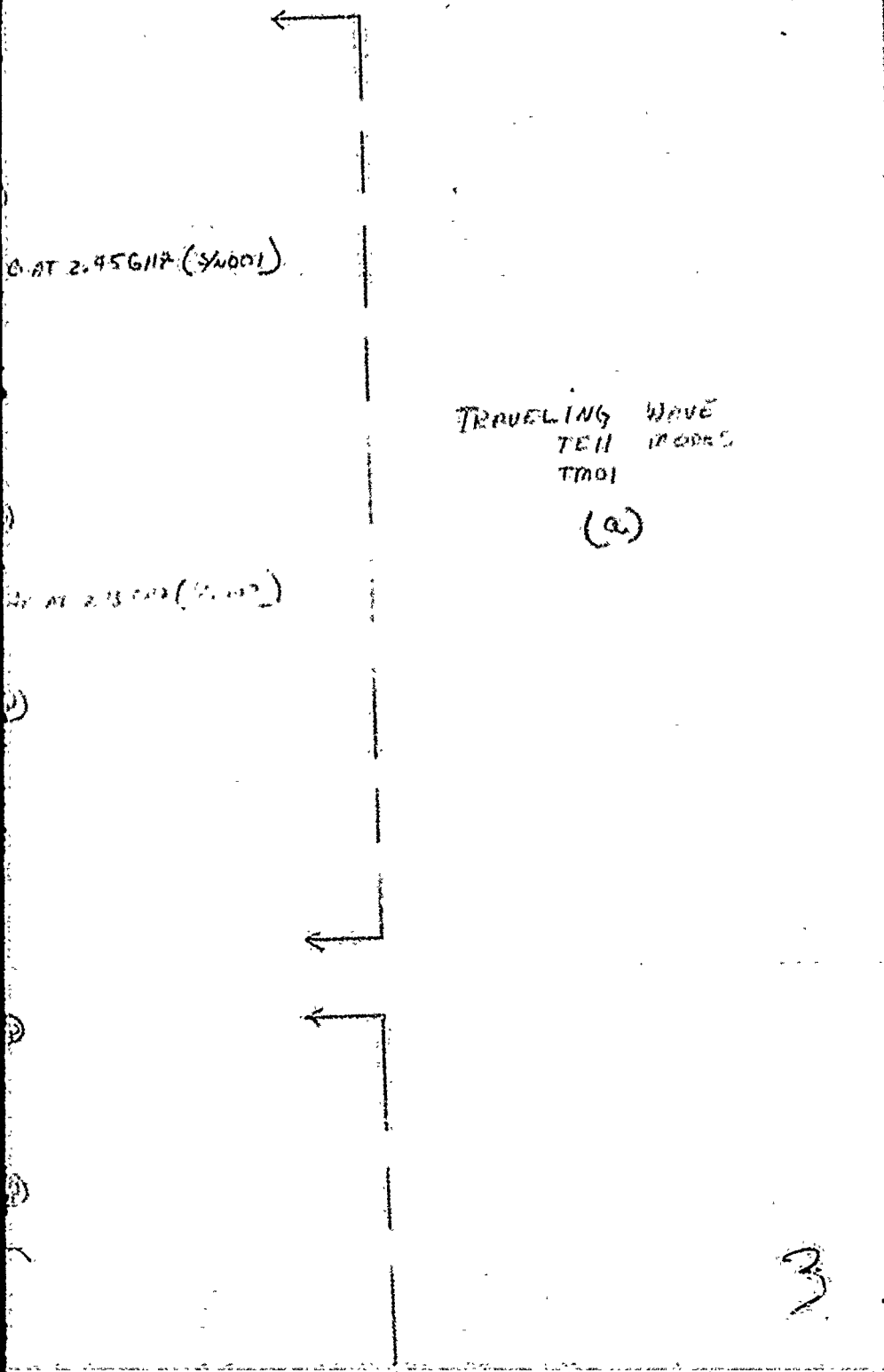

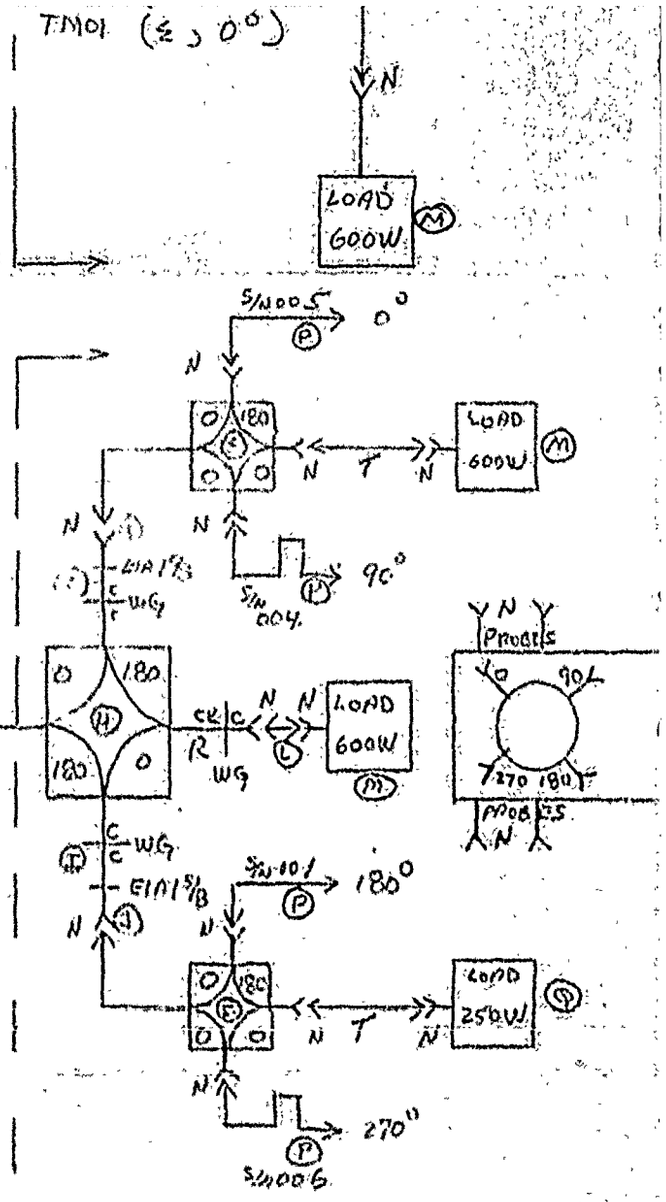

- [illegible] HYBRID TEE, WAVEGUIDE — STRUTHERS #M3C2S
- TRANSITION, WR284 to EIA 1⅝" (TWO) — GERLING #[illegible] 4028
- TRANSITION, EIA 1⅝" to TYPE N (TWO) — ANDREW #226IA
- DIRECTIONAL COUPLER, COAXIAL (TWO) — MECCA #715-30-4 C
- CABLE ASSEMBLY, ⅞ — ANDREW #25817-5
- LOAD, COAXIAL, 600 WATT (TWO) — BIRD #8401
- NOT USED
- S-BAND CAVITY — ITT BUILT
- CABLE ASSEMBLY, ½" (FOUR) — ANDREW #39760-3
- [illegible] ORDER CABLE S/N FOR PROPER PHASE POLARITY

1

- [illegible], COAXIAL, 250 WATT (FIVE) — BIRD #8141
- TRANSITION WR284 to TYPE N — WAVELINE #201-NF
- [illegible] HYBRID TEE, COAXIAL (TWO) — MECCA #61-476D1
- [illegible], COAXIAL (SIX) — [illegible] TEE (A, 100)

ENGINEERING CHECK LIST

SKETCHING	☐ LOCATE ON GRID. FREEHAND SKETCHING PREFERRED. LOCATE CIRCUIT SYMBOLS FUNCTIONALLY AROUND EACH STAGE. CONNECT STAGES IN LAYERS FROM LEFT-TO-RIGHT ARRANGE TWO OR MORE LAYERS FROM TOP-TO-BOTTOM.	REF DESIG	☐ IDENTIFY EACH SYMBOL BY REFERENCE DESIGNATION PER USA STD Y32.16. FOR DETAIL SEE ESM. ASSIGN REF. DESIG NUMBERS CONSECUTIVELY FROM LEFT TO RIGHT IN FUNCTIONAL SEQUENCE.
SIGNAL FLOW	☐ LOCATE INPUTS AT LEFT, OUTPUTS AT RIGHT (PREFERRED), OR INPUTS AT TOP, OUTPUTS AT BOTTOM; OR ANY COMBINATION OF THE TWO ABOVE.	PARTS IDENT	☐ SPECIFY RESISTANCE, CAPACITANCE AND INDUCTANCE VALUES. USE THE FORM OF FEWEST CIPHERS. SCHEMATIC IDENTITIES MUST AGREE WITH ELECTRICAL PARTS LIST
SYMBOLS	☐ USE CIRCUIT SYMBOLS PER USA STD Y32.2 FOR DETAIL, SEE ENGINEERING STANDARDS MANUAL. USE LOGIC SYMBOLS PER USA STD Y37.13 FOR DETAIL, SEE ENGINEERING STANDARDS MANUAL.	OTHER INFO	☐ ASSIGN FUNCTIONAL IDENTIFICATION TO PARTS, STAGES AND CIRCUITS. INDICATE MECHANICAL LINKAGE, POT ADJUSTMENT AND OPERATING CONTROLS. INDICATE SHIELDING, PAGRING AND CRITICAL GROUND. OUTLINE TERMINAL BOARDS AND SUB ASSEMBLIES.

4

3

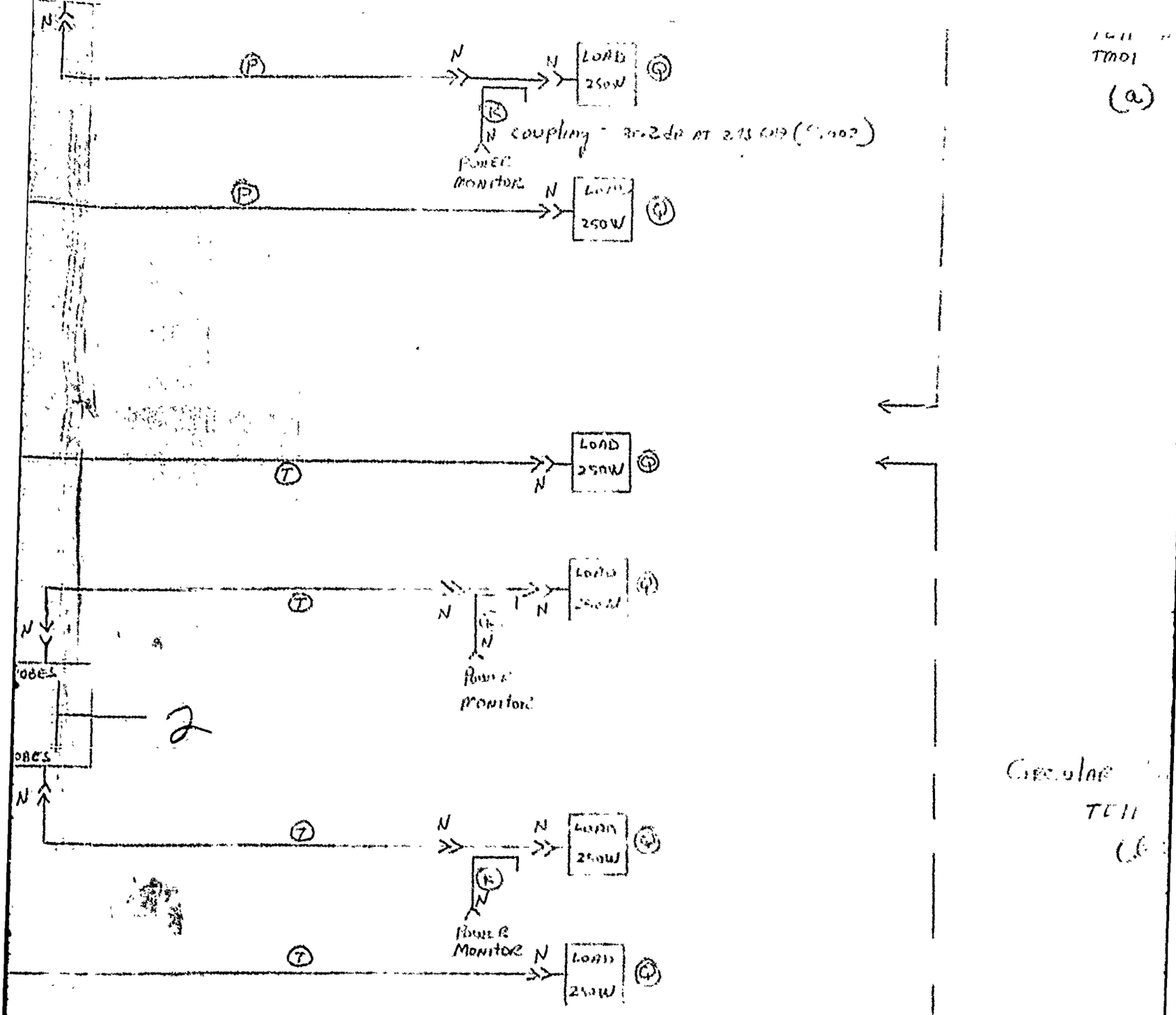

TM01

(a)

Circulate

TC11

(C

Notes

Wq C

Wq C

OPERATOR INSTRUCTIONS

5

NOTES:

1. PARTIAL REFERENCE DESIGNATIONS ARE SHOWN; FOR COMPLETE DESIGNATION PREFIX WITH UNIT NUMBER AND SUB-ASSEMBLY DESIGNATIONS.
2. UNLESS OTHERWISE SPECIFIED:
   ALL RESISTANCE VALUES ARE IN
   ALL CAPACITANCE VALUES ARE IN
   ALL DIODES ARE
   ALL TRANSISTORS ARE
   ALL INTEGRATED CKTS ARE

PREPARED IN ACCORDANCE WITH MIL STD 100

APPLICATION

CONTRACT DAAK70-77-C-0[illegible]

APPROVALS SIGNATURE & DATE

DRAWN

CHECKED

MECH

ELECT

STDS

E OF M

ITAV

OTHER

ITT AVI Div

7

SIZE C

CODE IDENT NO 28527

SCALE

1

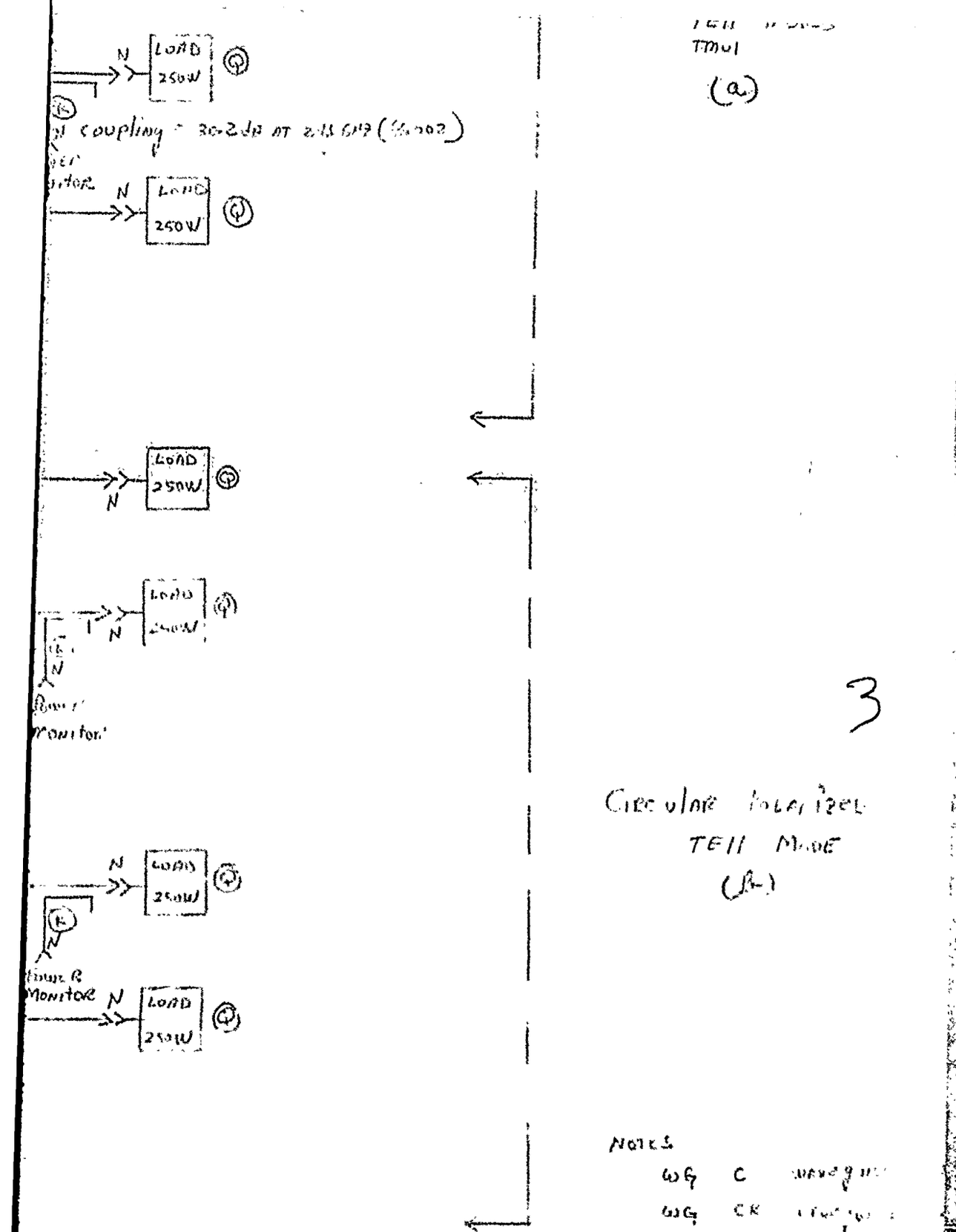

NOTES

WG C

WG CR

PREPARED IN ACCORDANCE WITH MIL STD-100	CONTRACT DAAK 70-77 C-0[illegible]	ITT AVIONICS DIVISION	NUTLEY NEW JERSEY
NEXT ASSY / USED ON	APPROVALS SIGNATURE & DATE		
APPLICATION	DRAWN		
	CHECKED		
	MECH		
	ELECT		
	STDS		
	E OF M		
ITTAV / ITTAV SOURCE		SIZE C	CODE IDENT NO 28527
OTHER		SCALE	CATEGORY / SHEET

NCE DESIGNATIONS ARE
PLETE DESIGNATION
IT NUMBER AND SUB-
NATIONS.
SE SPECIFIED:
VALUES ARE IN
E VALUES ARE IN
RS ARE
CKTS ARE

Fig 2, 3, 6

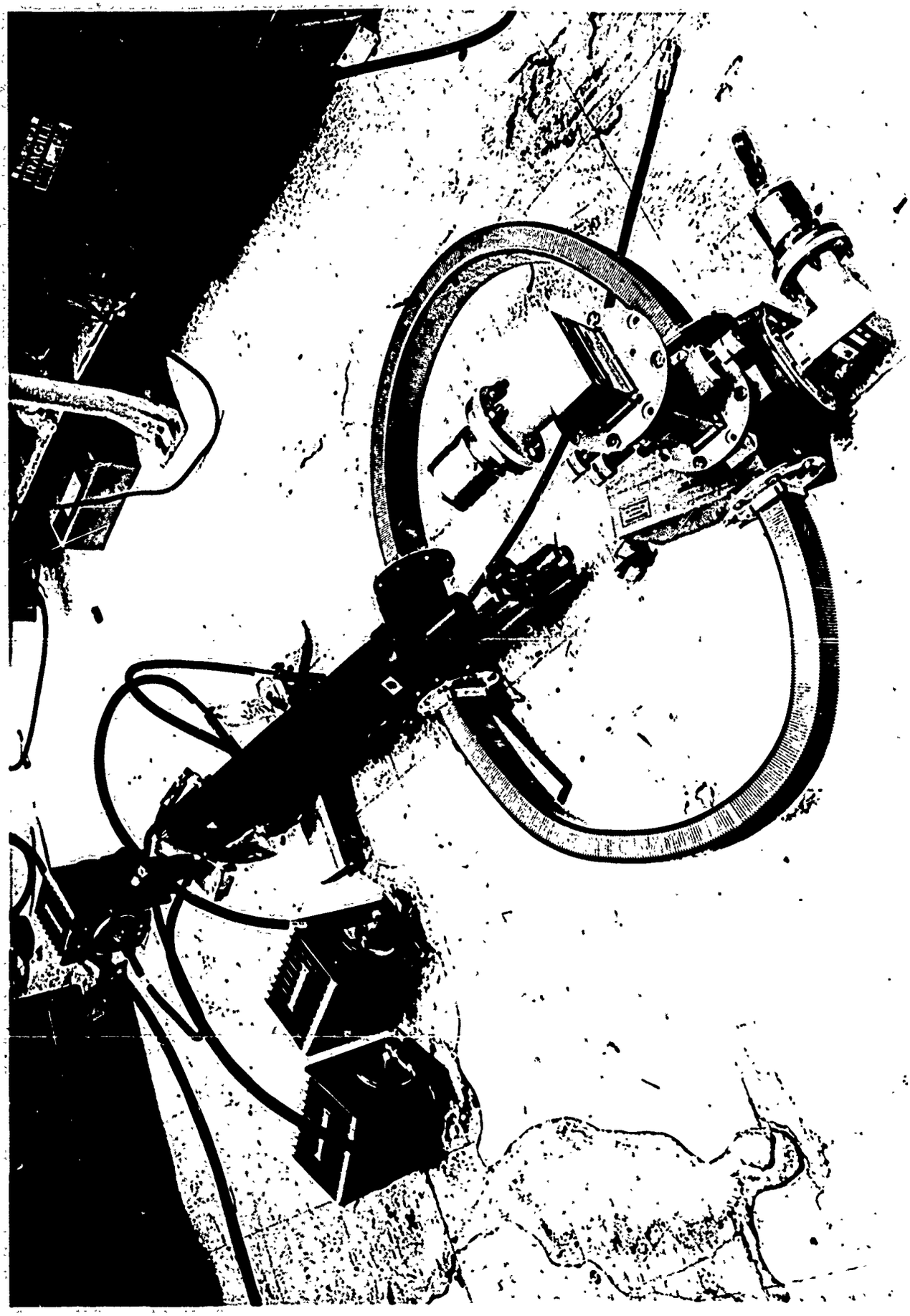

FIG 4 PHOTO OF CAVITY

TTT

76297

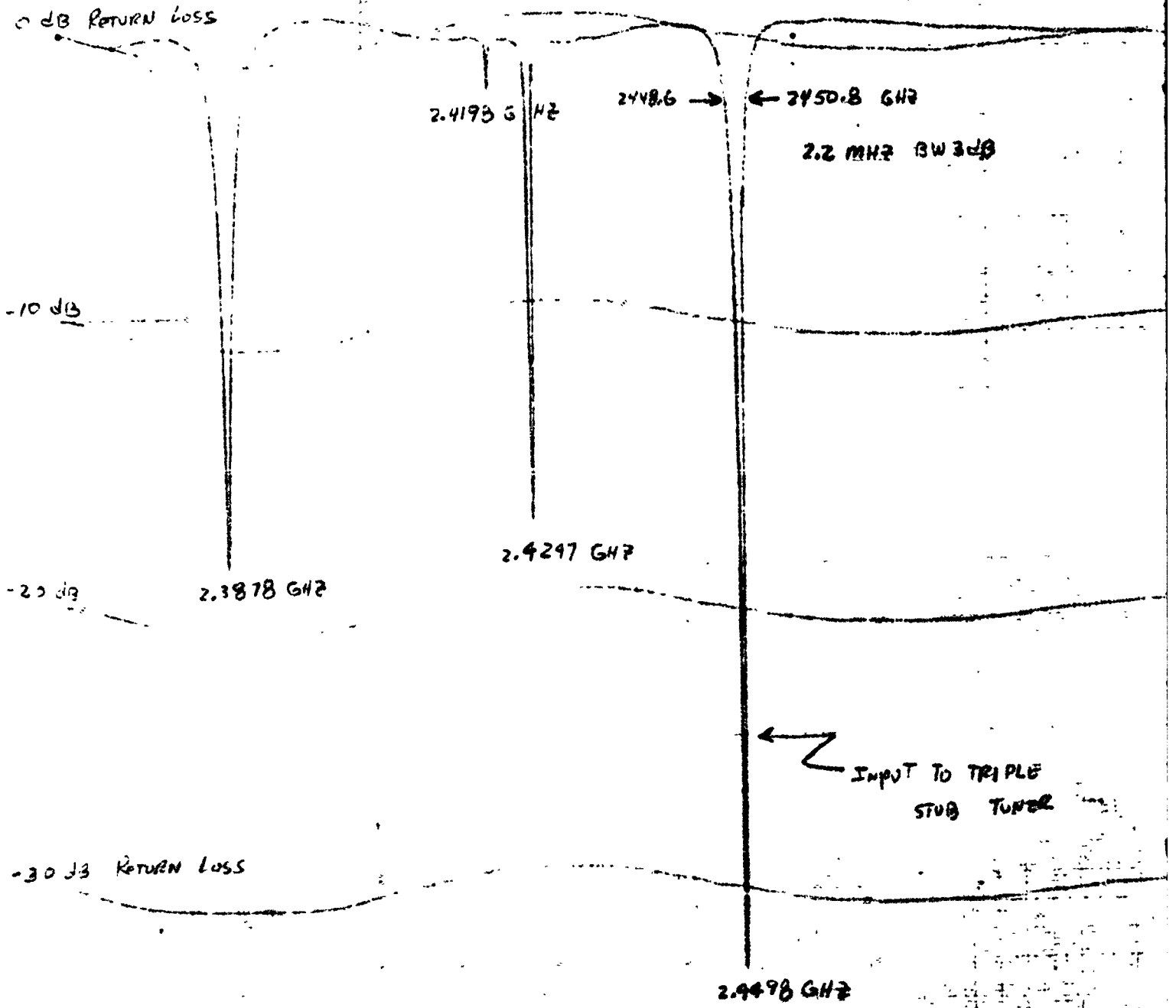
0 dB RETURN LOSS
2.4193 GHz
2448.6
2450.8 GHz
2.2 MHz BW 3dB
-10 dB
2.4297 GHz
-20 dB
2.3878 GHz
INPUT TO TRIPLE STUB TUNER
-30 dB RETURN LOSS
2.4498 GHz

GE 9 10/11/80

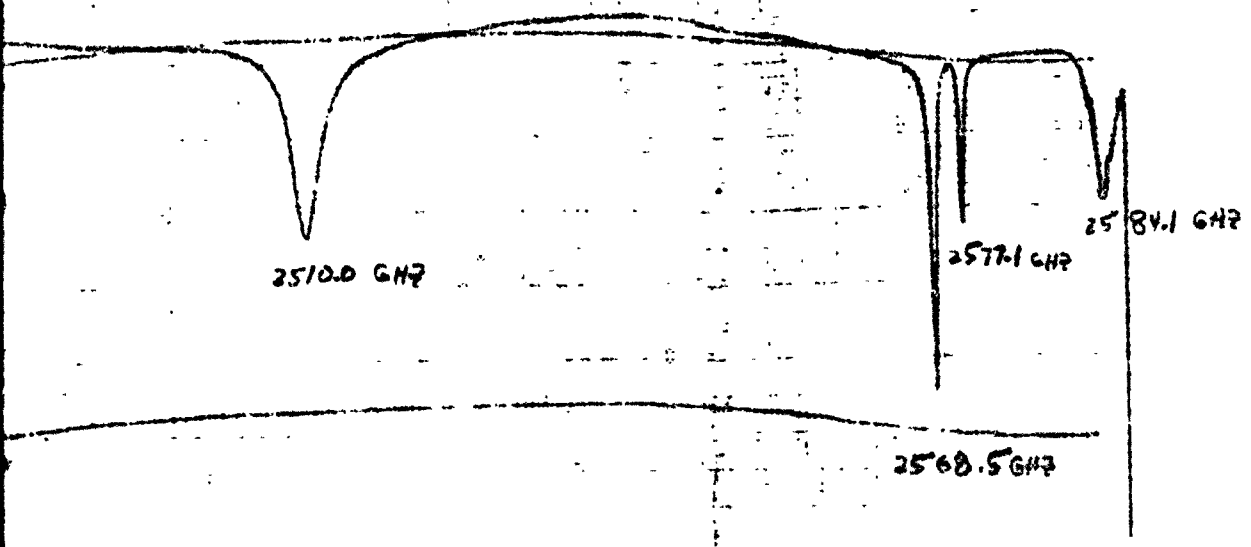

PLE
UNER

RETURN LOSS
MODE TE11 Cavity (Δ MODE)
INPUT WAVEGUIDE

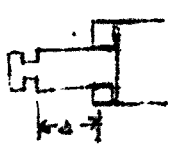

SHORT d = 3¾"
CAVITY CONTENTS AIR
POWER LEVEL 10mW

FIG 4-1

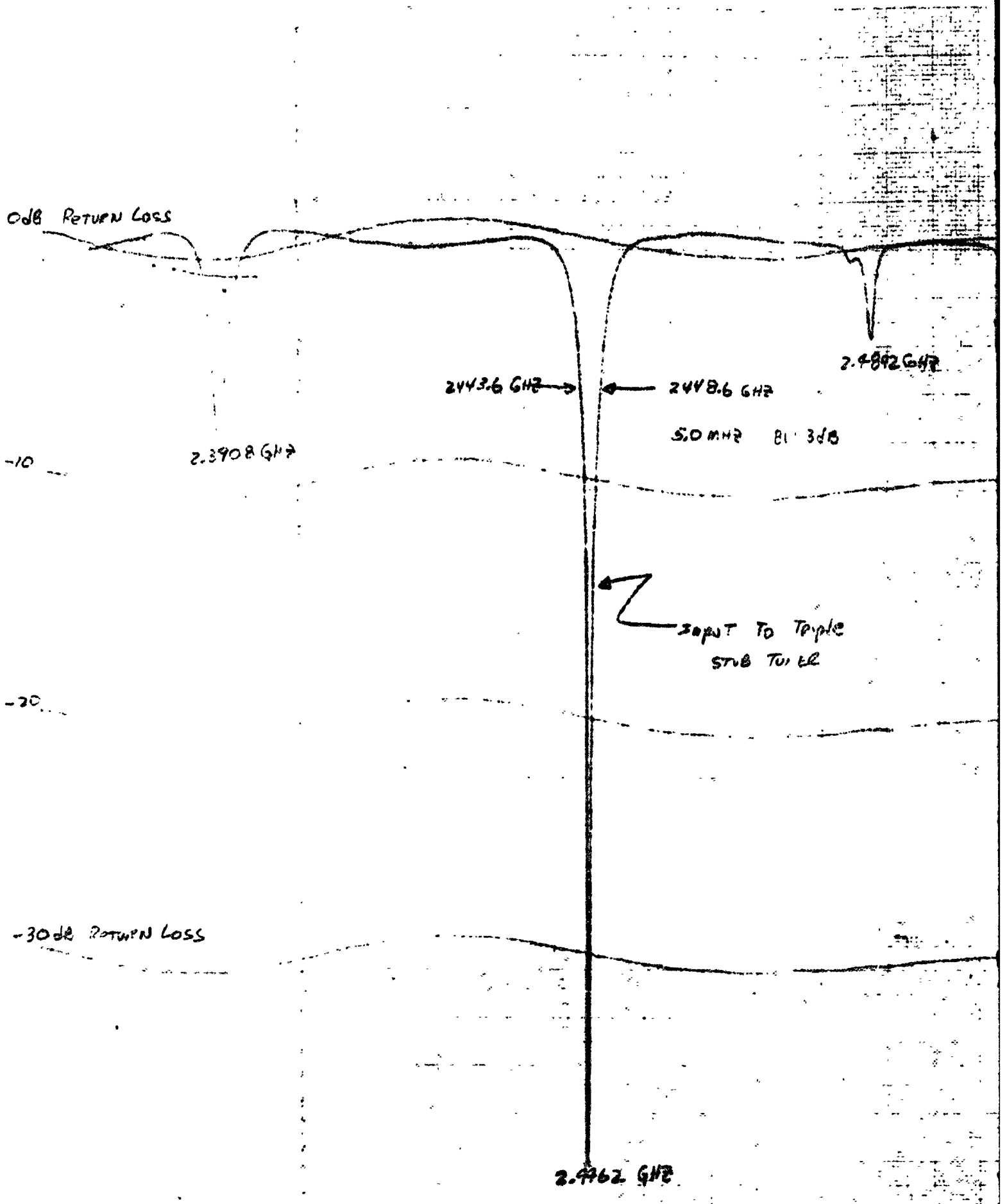
0dB Return Loss
2.4892 GHz
2443.6 GHz
2448.6 GHz
5.0 MHz BW 3dB
-10
2.3908 GHz
Input To Triple
Stub Tuner
-20
-30dB Return Loss
2.4462 GHz

GEG . 10/17/80

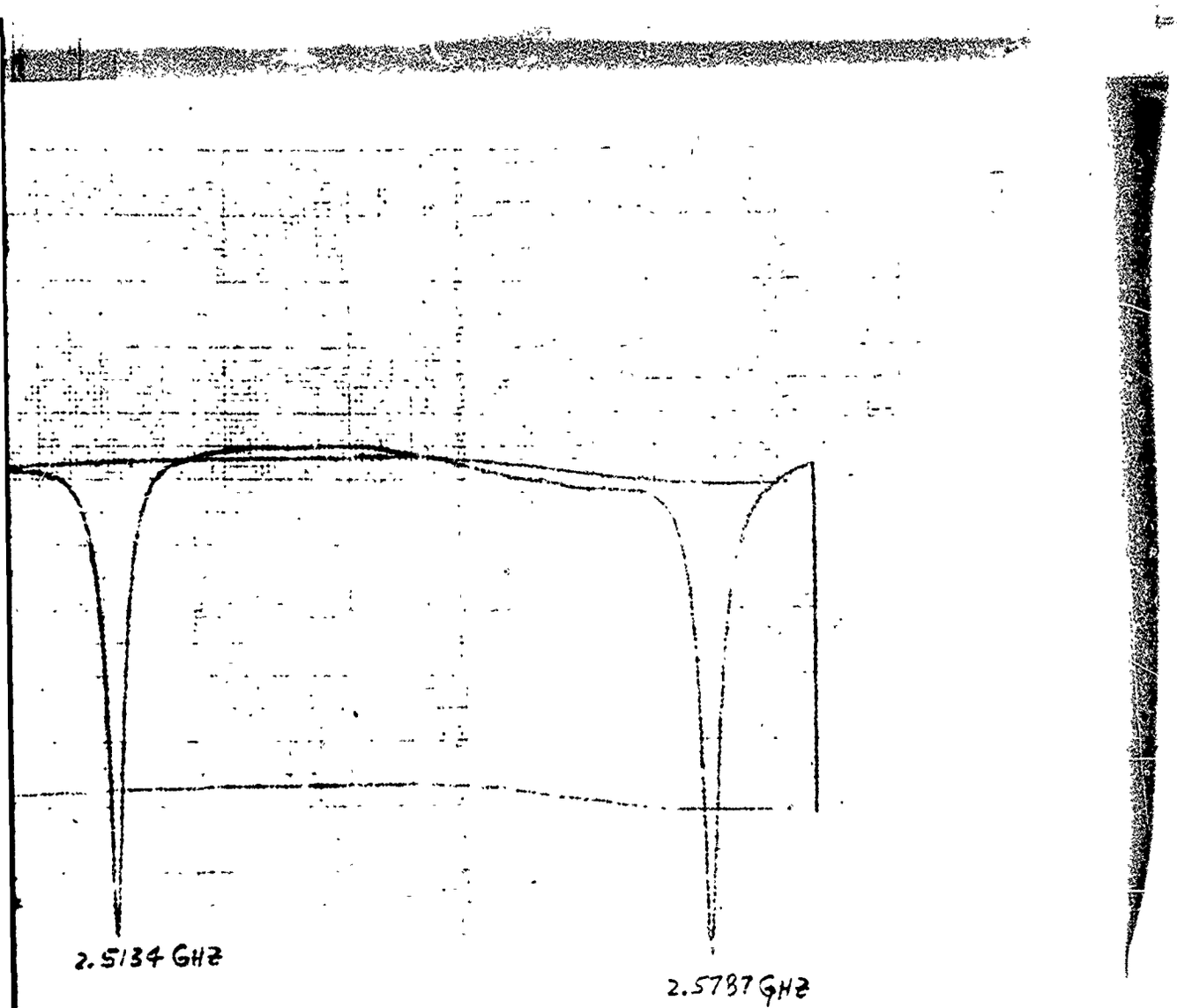

Return Loss
Mode TE11 Cavity (Amodel)
Input Waveguide
Short 3¼"
Cavity Contents Pyrex
Power Level 10 mW

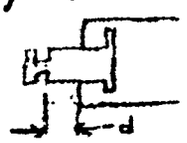

FIG 4-2

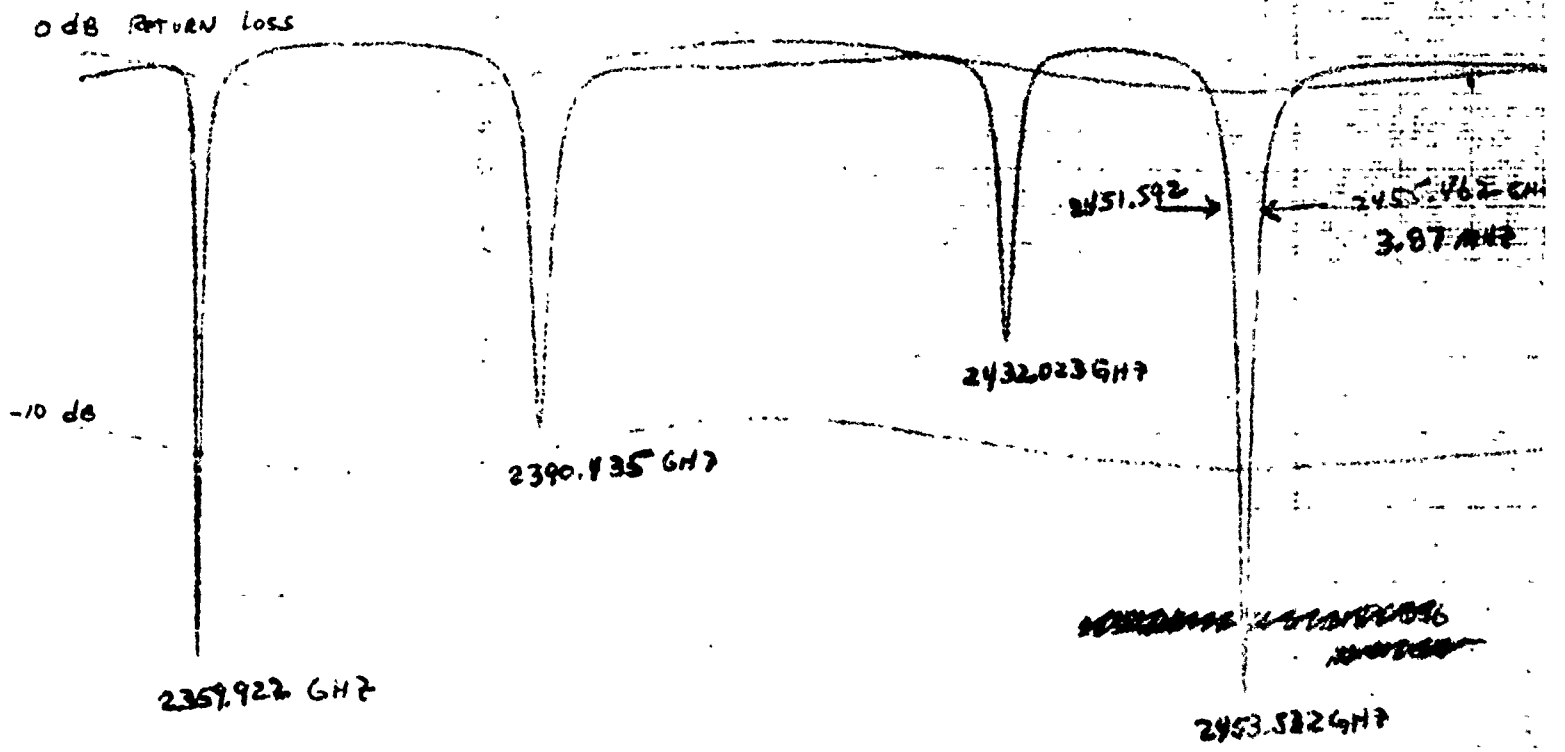
0 dB RETURN LOSS
2351.592
3.87 MHz
2432.023 GHz
-10 dB
2390.135 GHz
2359.922 GHz
2453.522 GHz
-20 dB
-30 dB RETURN LOSS

GEG 10/14/80

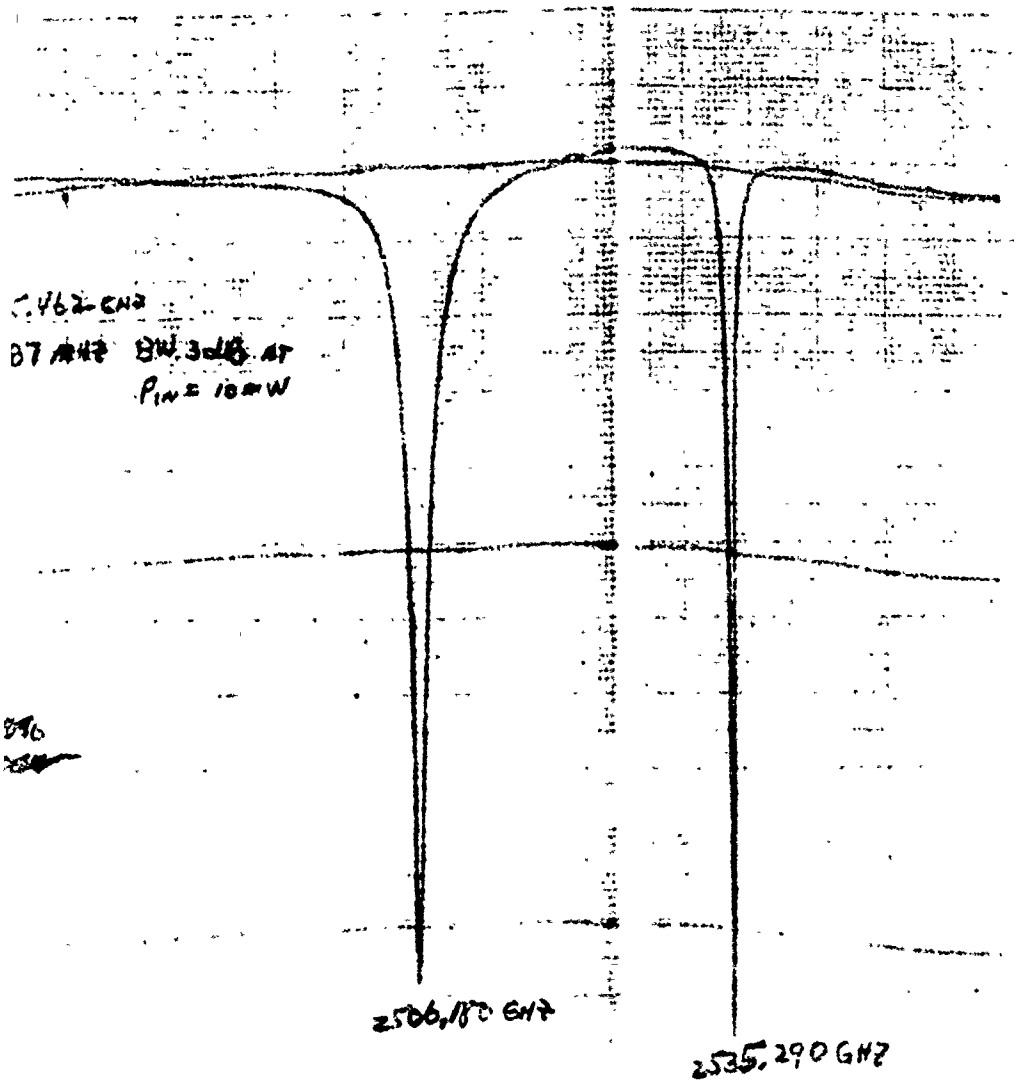

RETURN LOSS
MODE TM01, CAVITY (2 MODE)
INPUT WAVEGUIDE
SHAFT POSITION 4 7/8"
CAVITY PARTS AIR

FIG 4-3

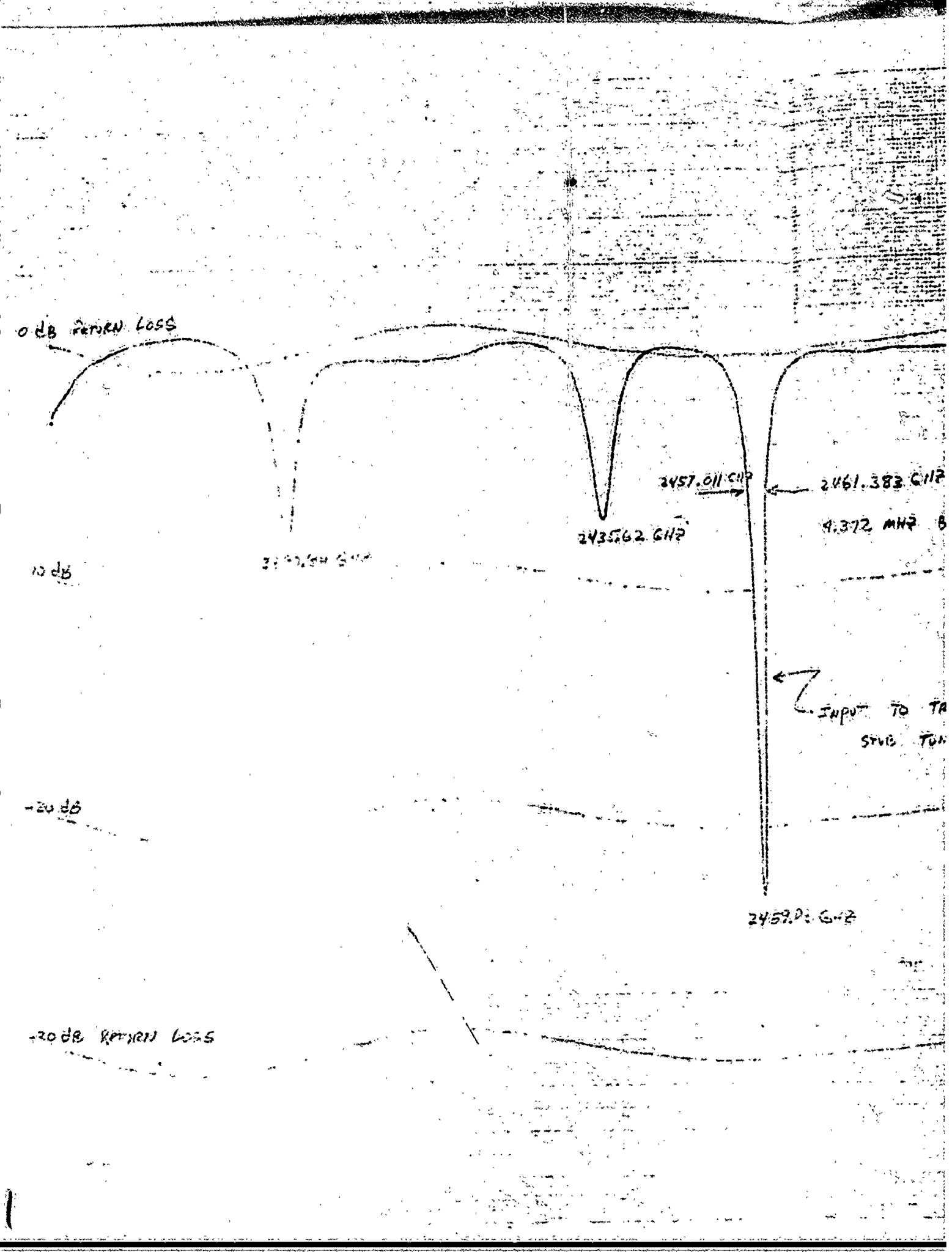
0 dB RETURN LOSS
2457.011 GHz
2461.383 GHz
4.372 MHz
2435.62 GHz
10 dB
INPUT TO
STUB
-20 dB
2459.0 GHz
-20 dB RETURN LOSS

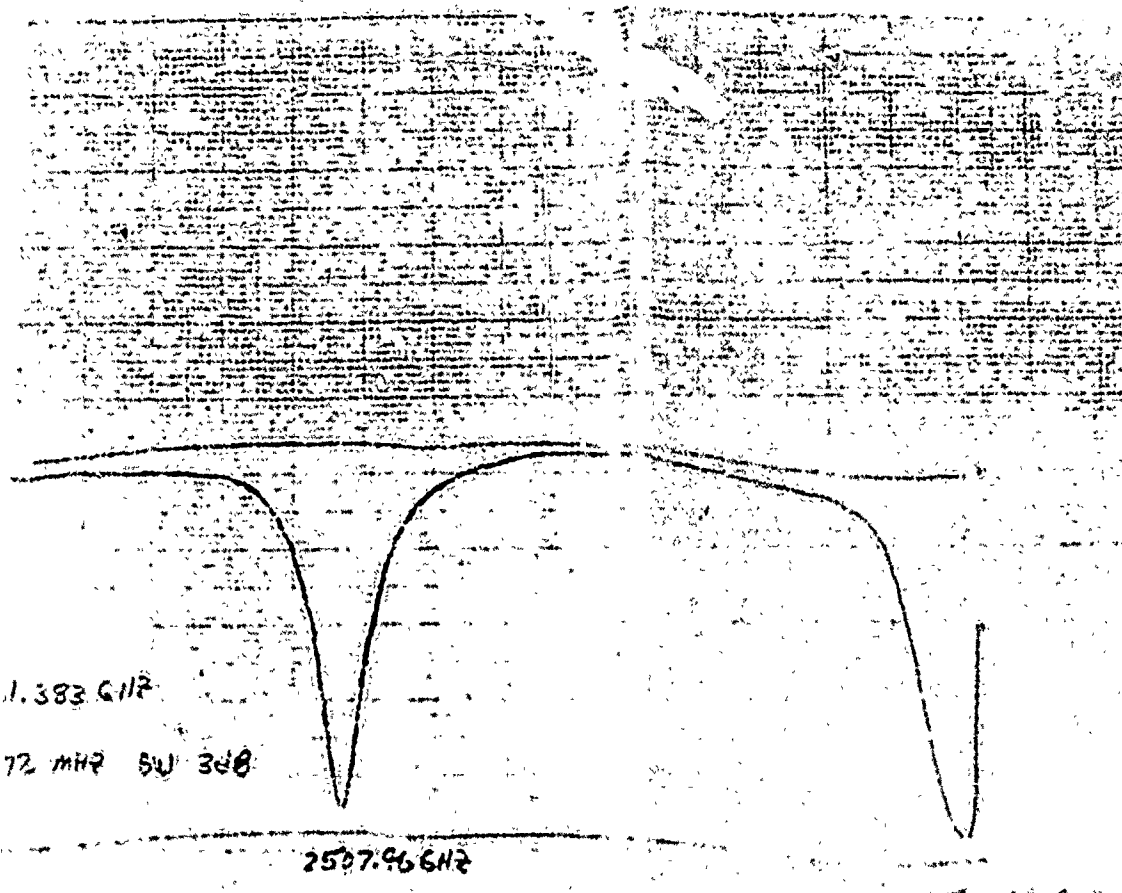

... TO TRIPLE
STUB TUNER

Return Loss
Mode TM01 Cavity (Empty)
Input Waveguide
Short ... 2 3/8"
Cavity ... Pyrex

FIG. 4-4

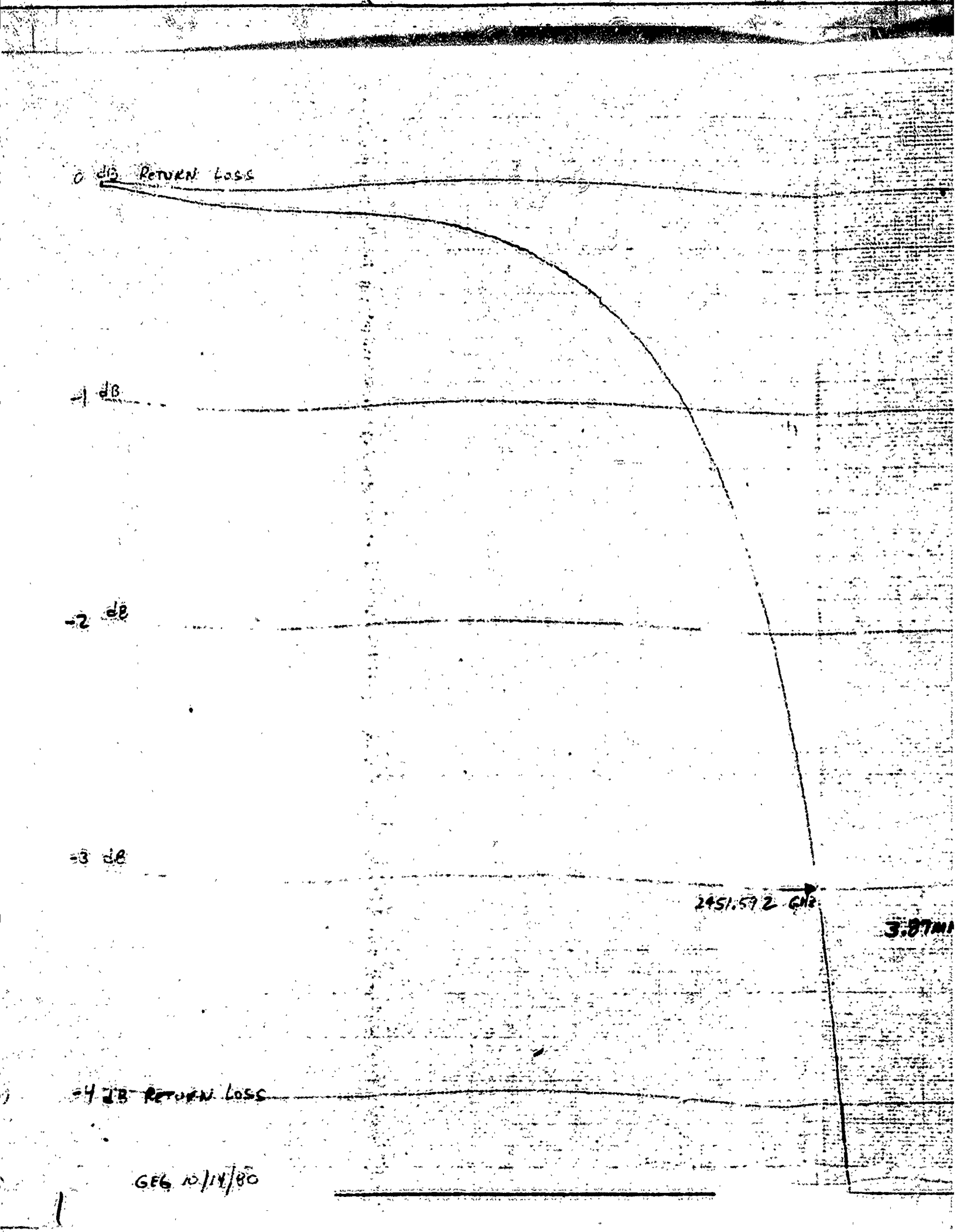
0 dB RETURN LOSS
-1 dB
-2 dB
-3 dB
2451.572 GHz
3.87MH
-4 dB RETURN LOSS
GEG 10/14/80

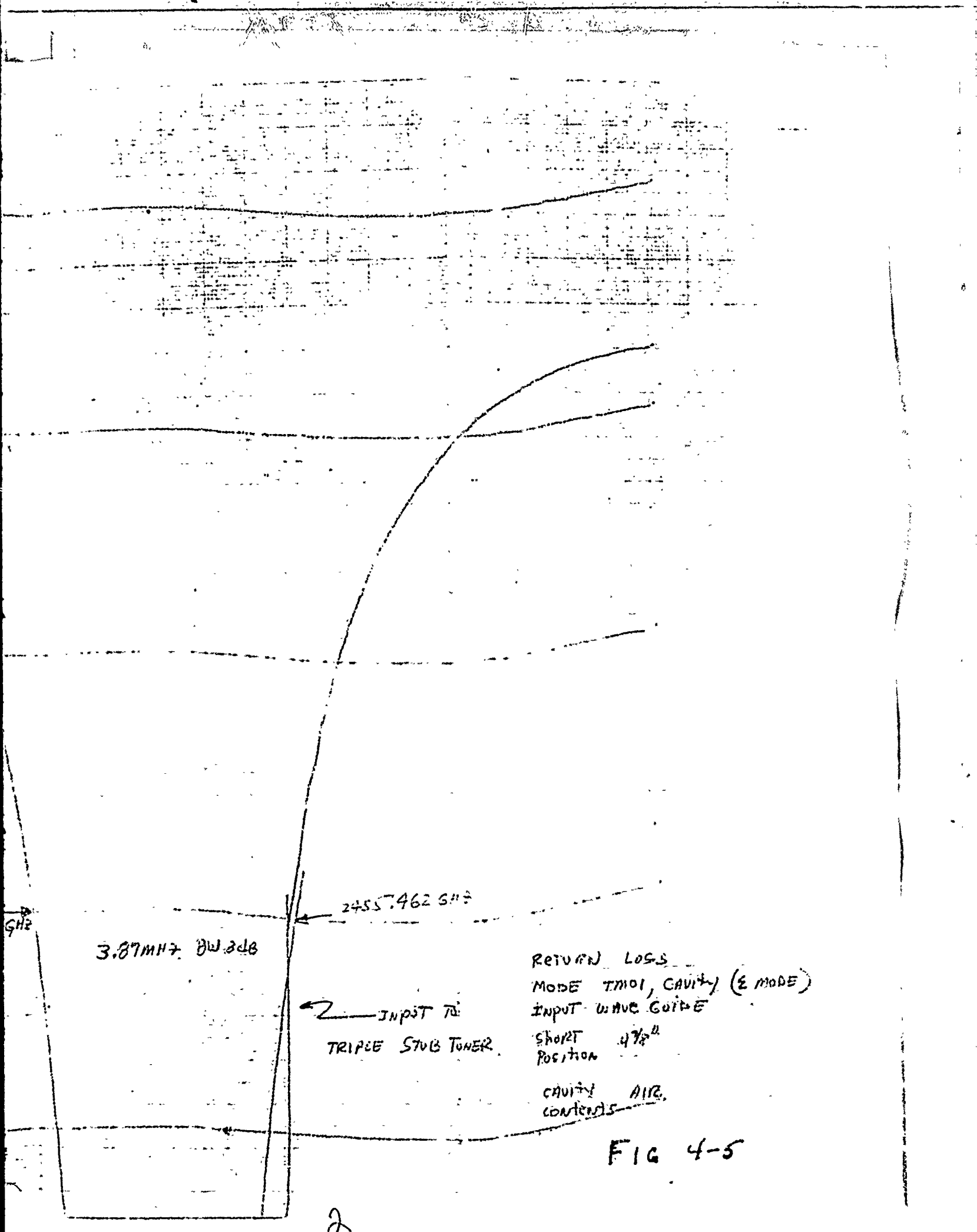
GHz
2455.462 MHz
3.87MHz BW 3dB
INPUT TO
TRIPLE STUB TUNER
RETURN LOSS
MODE TM01, CAVITY (E MODE)
INPUT WAVE GUIDE
SHORT 4 7/8"
POSITION
CAVITY AIR
CONTENTS

FIG 4-5

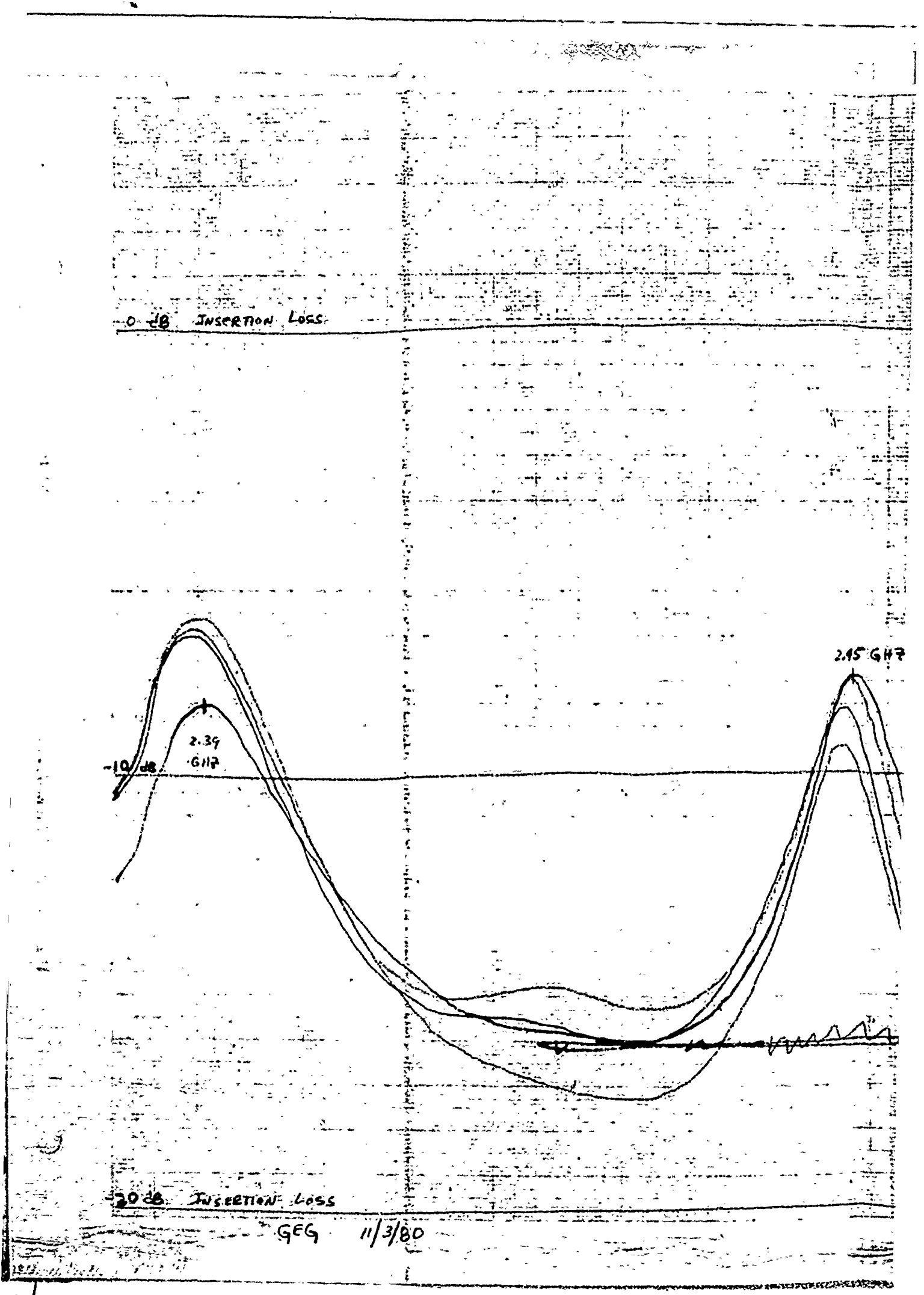
0 dB INSERTION LOSS
2.15 GHz
2.39 GHz
-10 dB
-20 dB INSERTION LOSS
GEG 11/3/80

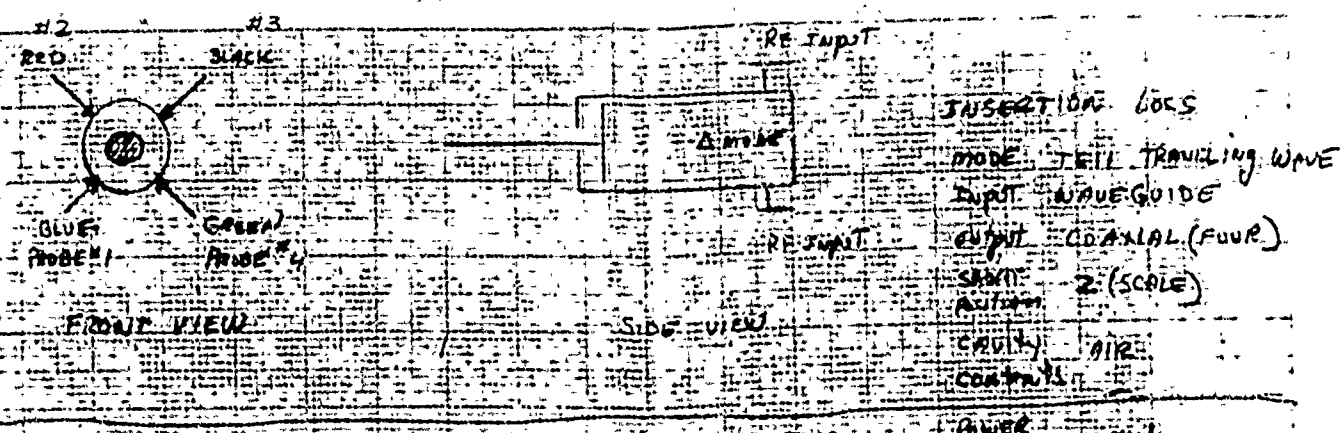

INSERTION LOSS

MODE TE11 TRAVELING WAVE

INPUT WAVEGUIDE

OUTPUT COAXIAL (FEMALE)

SWR 2 (SCALE)

CAVITY AIR

CONTROLS

POWER 10mW

LEVEL

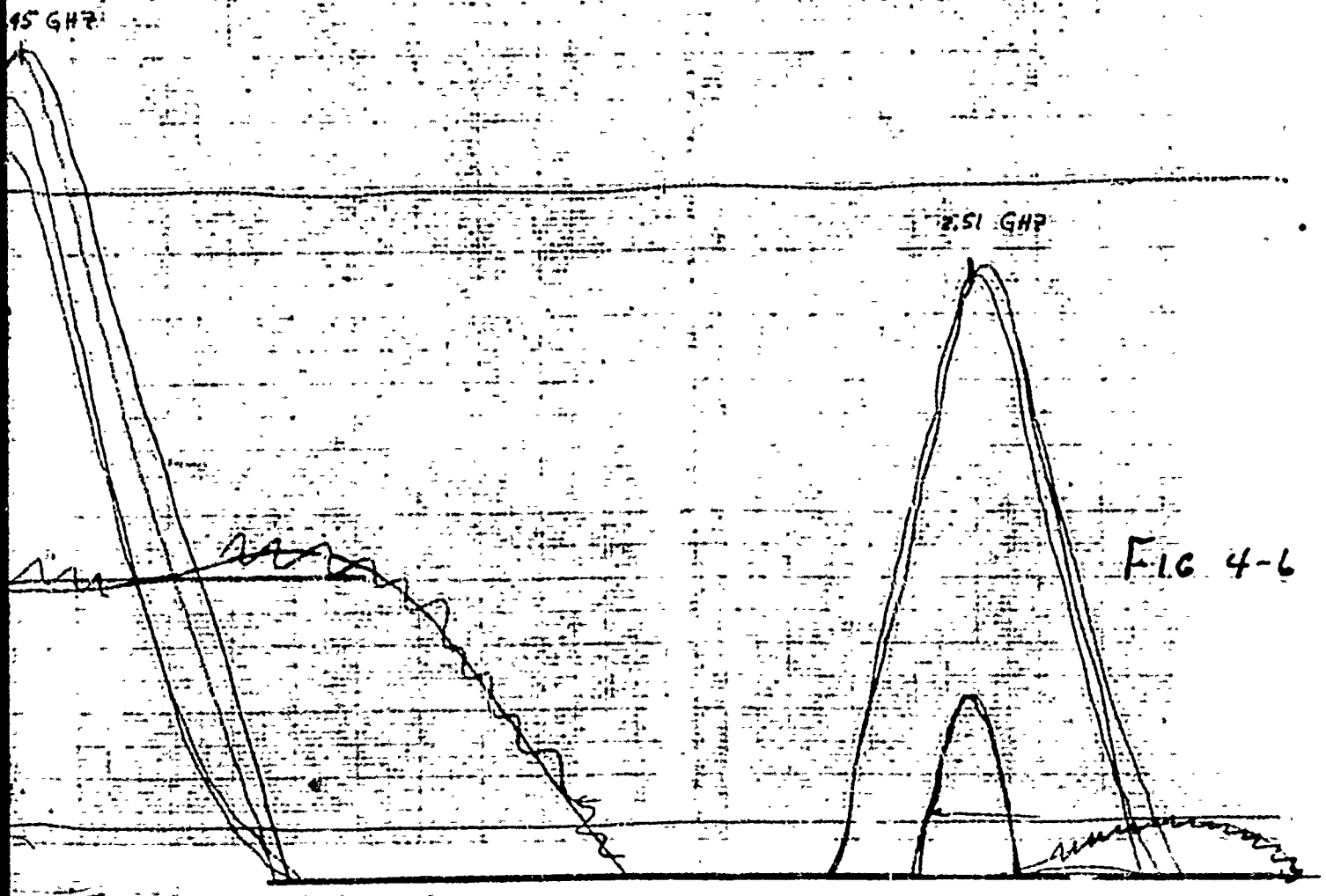

FIG 4-6

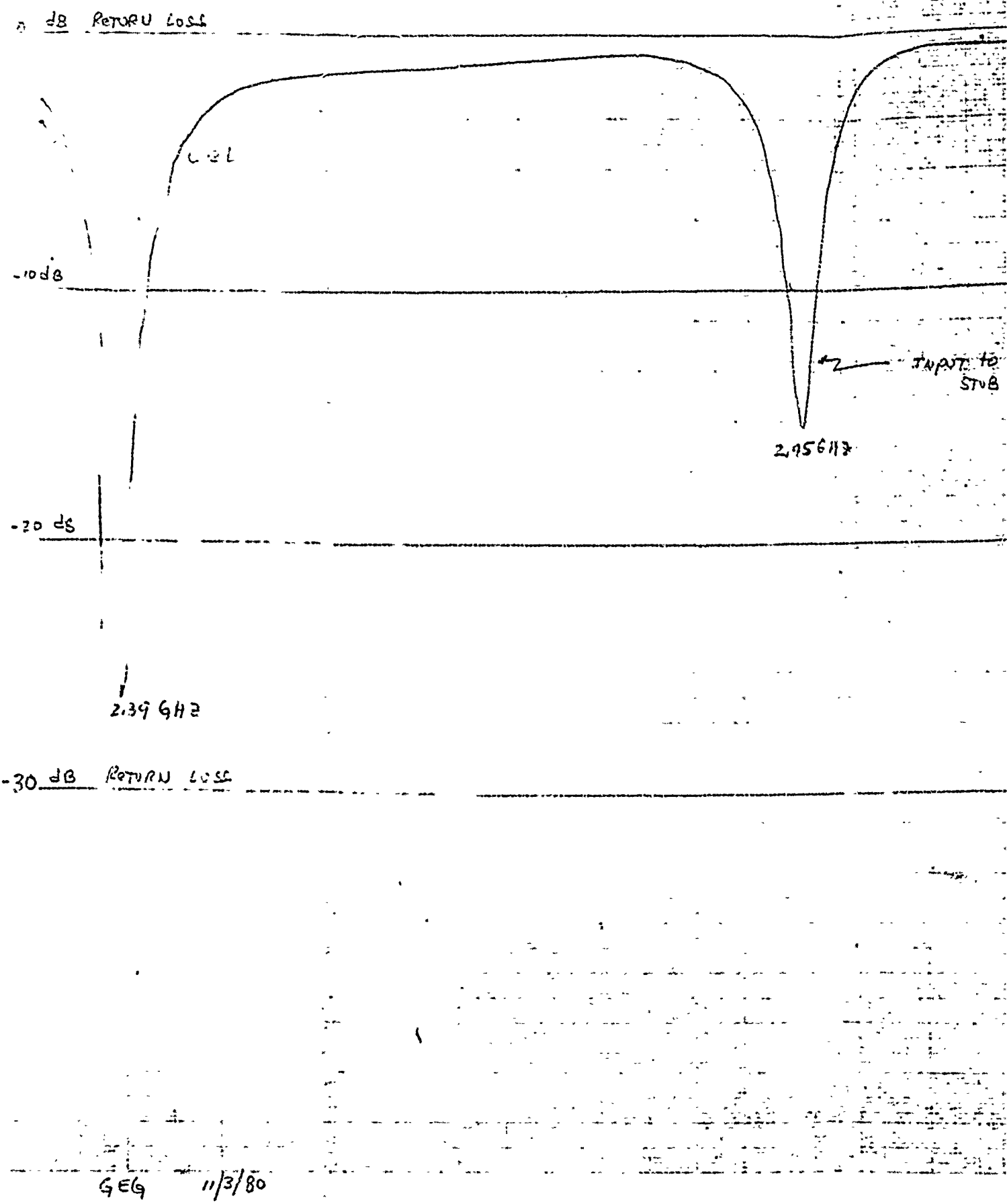
dB RETURN LOSS
-10dB
-20 dB
-30 dB RETURN LOSS
2.156117
INPUT TO STUB
2.39 GHz

GEG 11/3/80

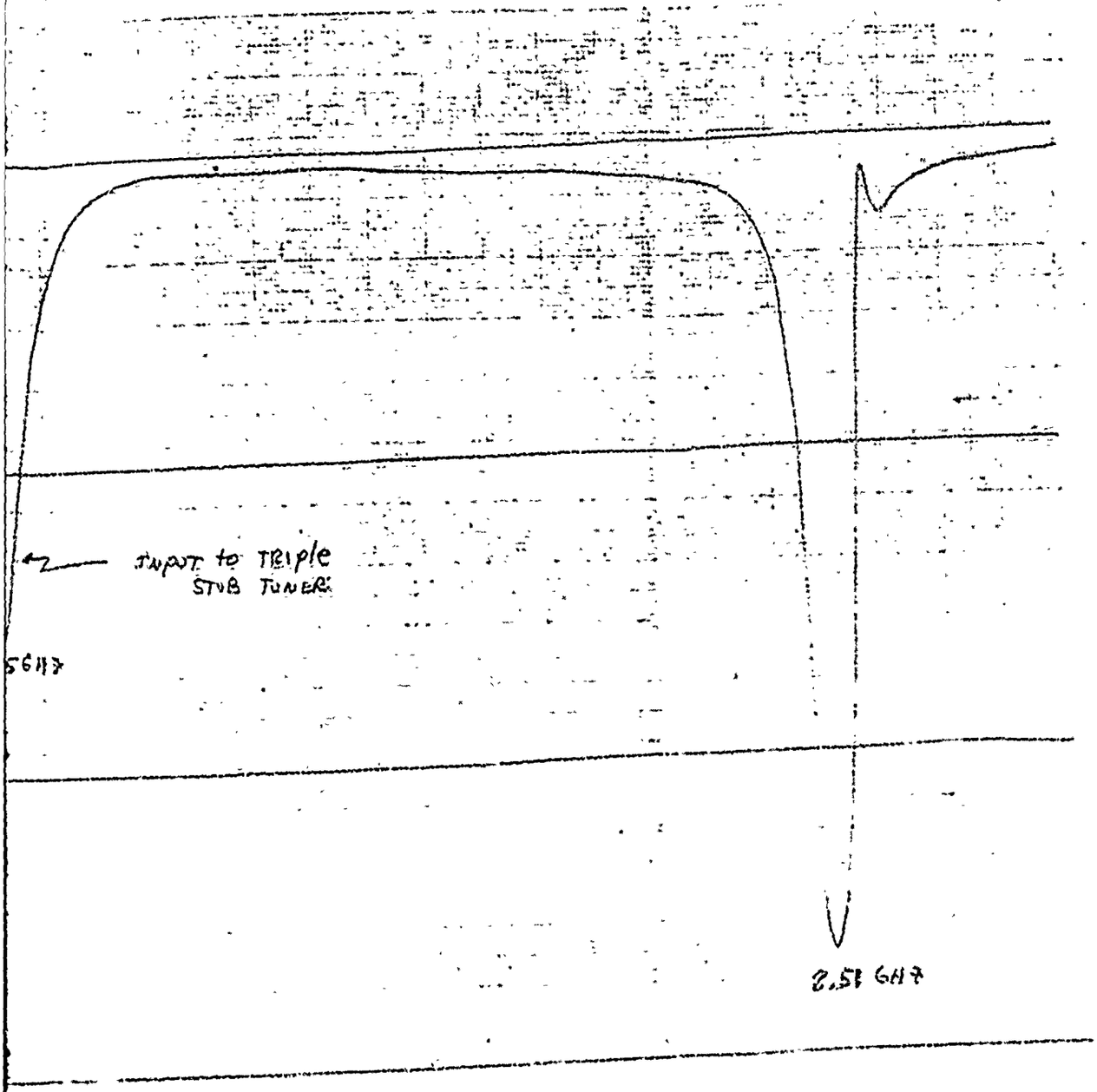

Return Loss

MODE	TE11 Traveling Wave (Δ MODE)
INPUT	WAVEGUIDE
OUTPUT	COAXIAL (PROBE)
SHORT	2 REF, IN ½"
CAVITY CONTENTS	AIR
POWER LEVEL	1 MW

FIG. 4-7

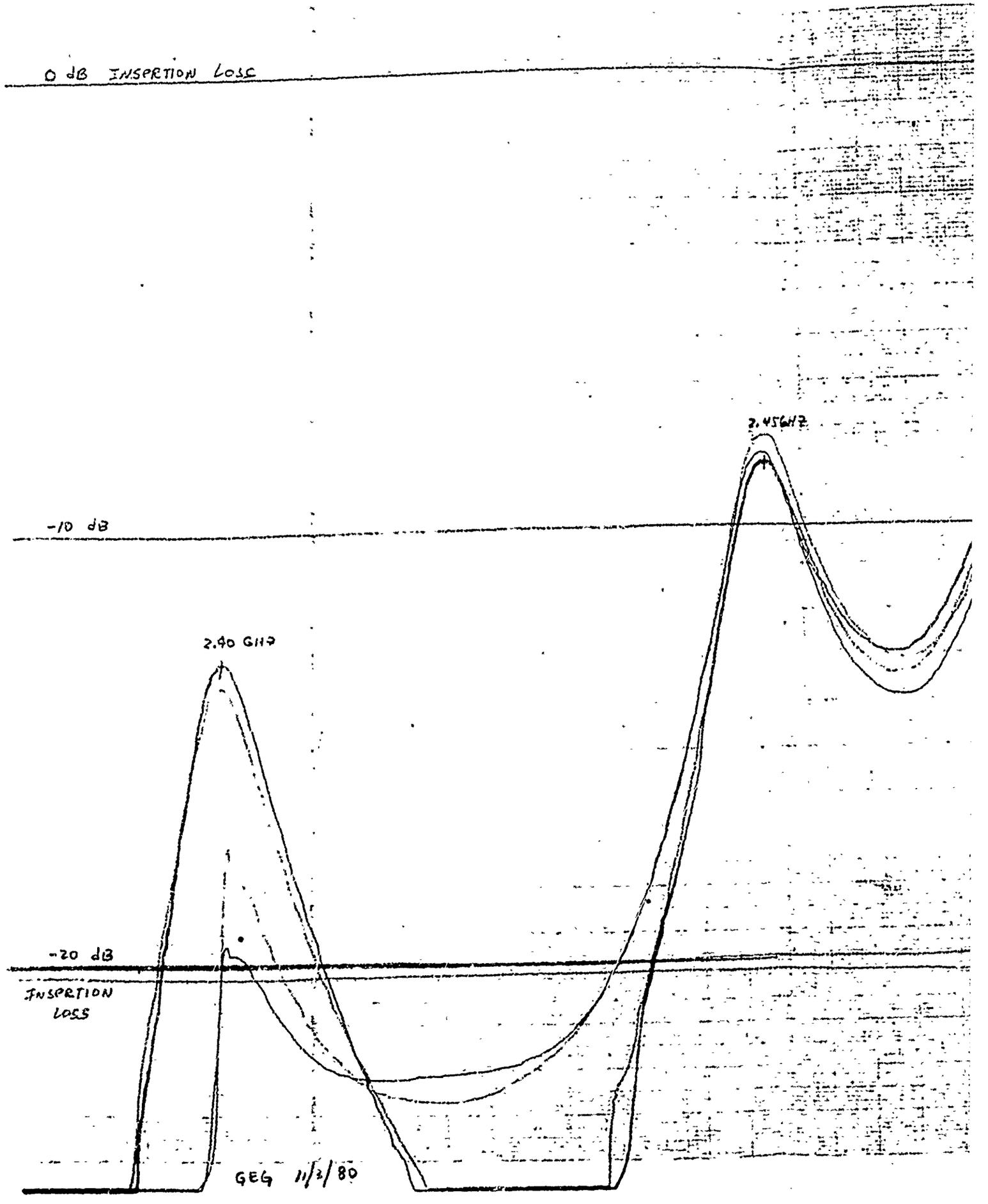
0 dB INSERTION LOSS
-10 dB
-20 dB
INSERTION LOSS
2.40 GHz
2.45GHz
GEG 11/3/80

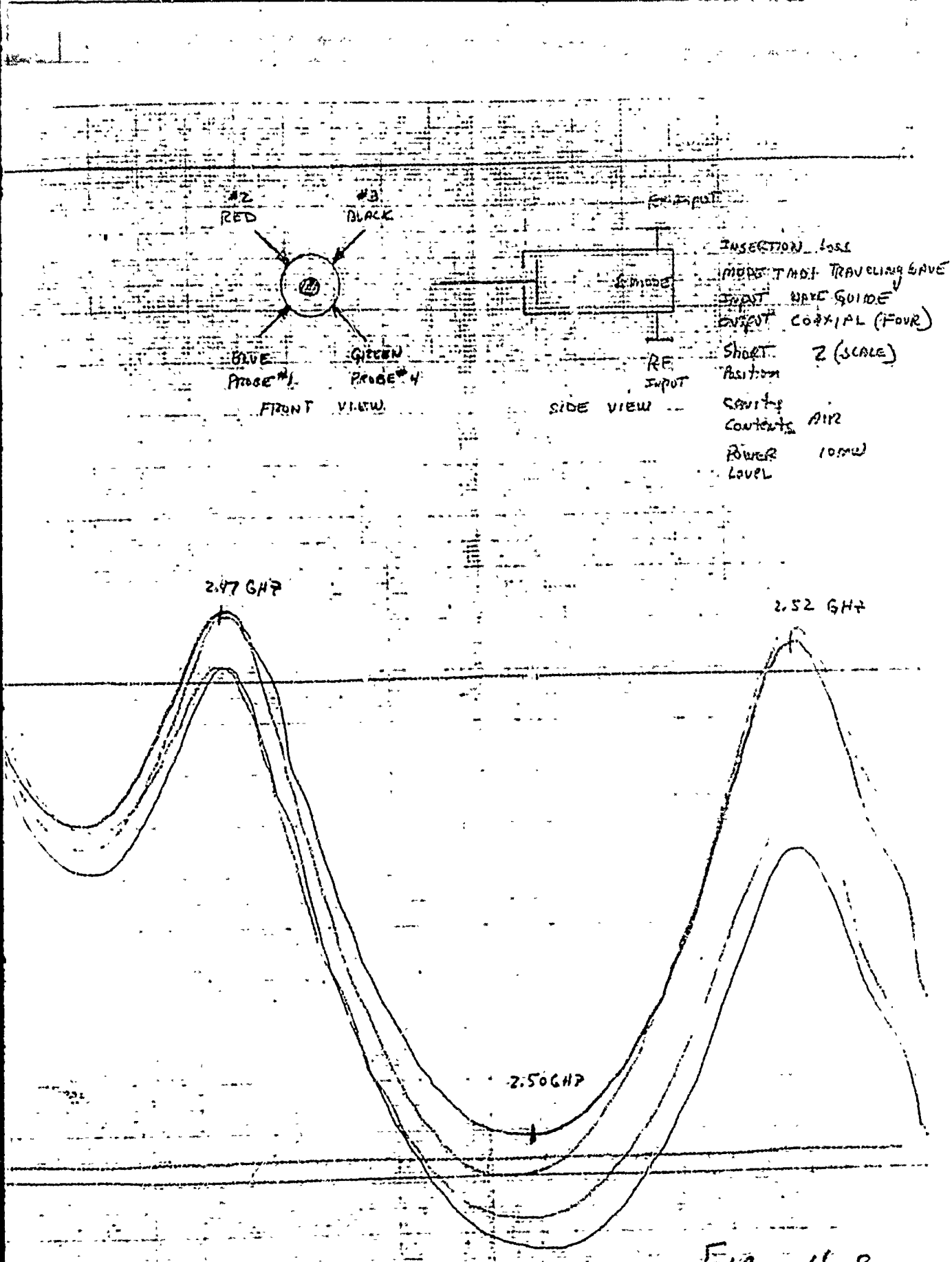
#2
RED
#3
BLACK
BLUE
PROBE #1
GREEN
PROBE #4
FRONT VIEW
SIDE VIEW
RE
INPUT
INSERTION LOSS
MODE TM01 TRAVELING WAVE
INPUT WAVE GUIDE
OUTPUT COAXIAL (FOUR)
SHORT Z (SCALE)
POSITION
CAVITY CONTENTS AIR
POWER LEVEL 10mW
2.47 GHz
2.52 GHz
2.50GHz

FIG. 4-8

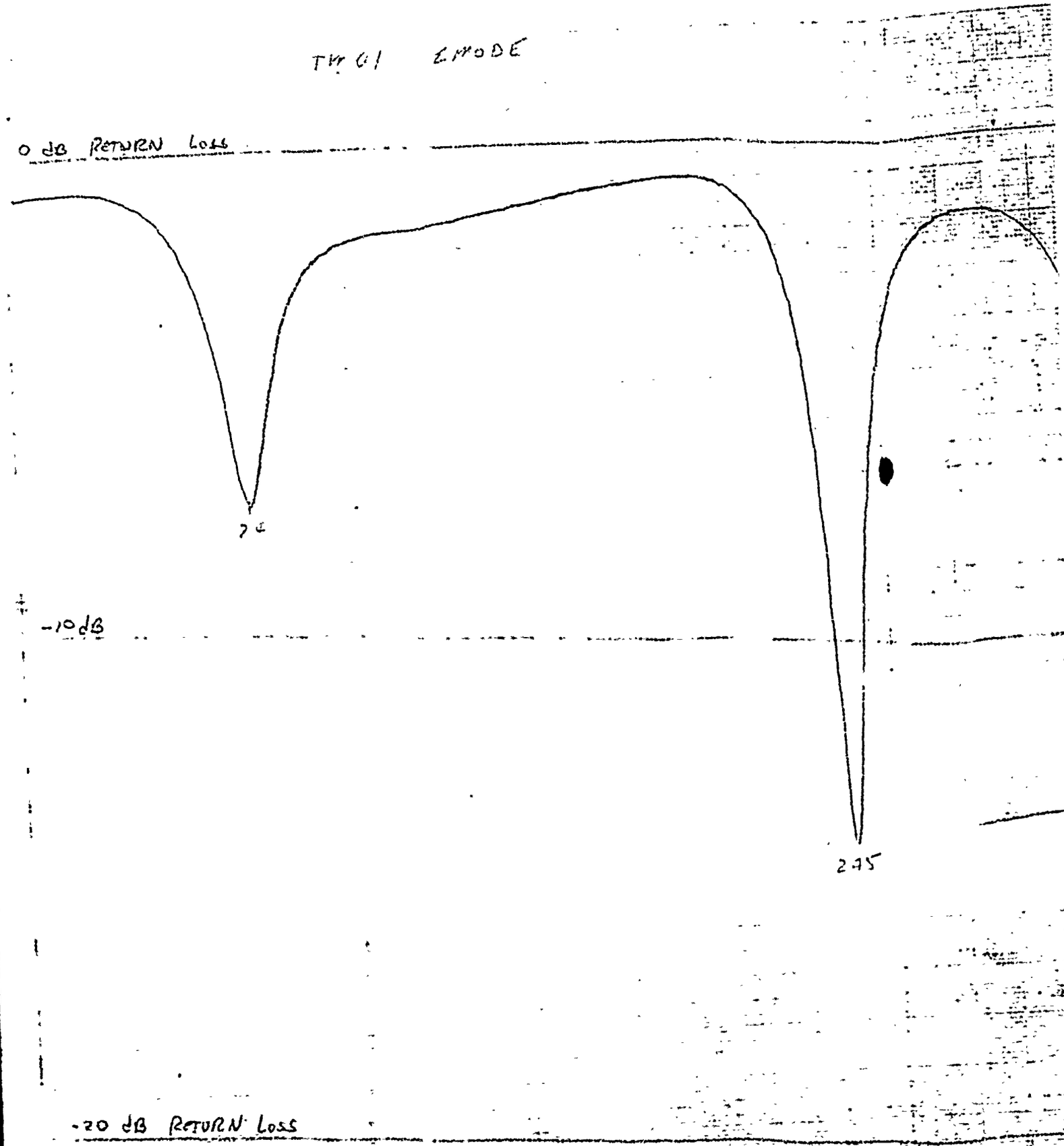
TM 01 E-MODE
0 dB RETURN LOSS
-10 dB
-20 dB RETURN LOSS
2.45

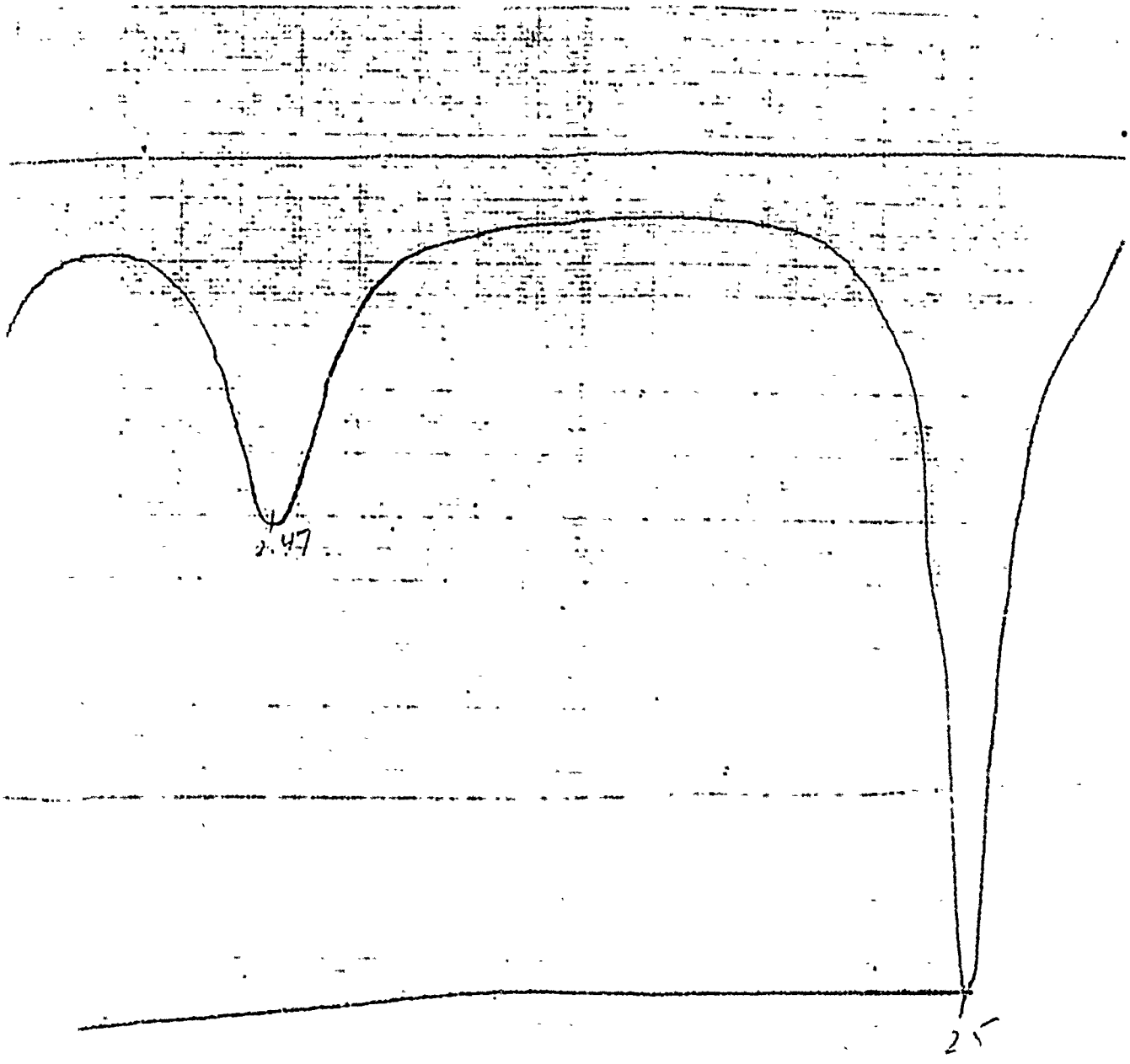

RETURN LOSS
MODE TM01 TRANSMISSION MODE
INPUT

FIG 4-9

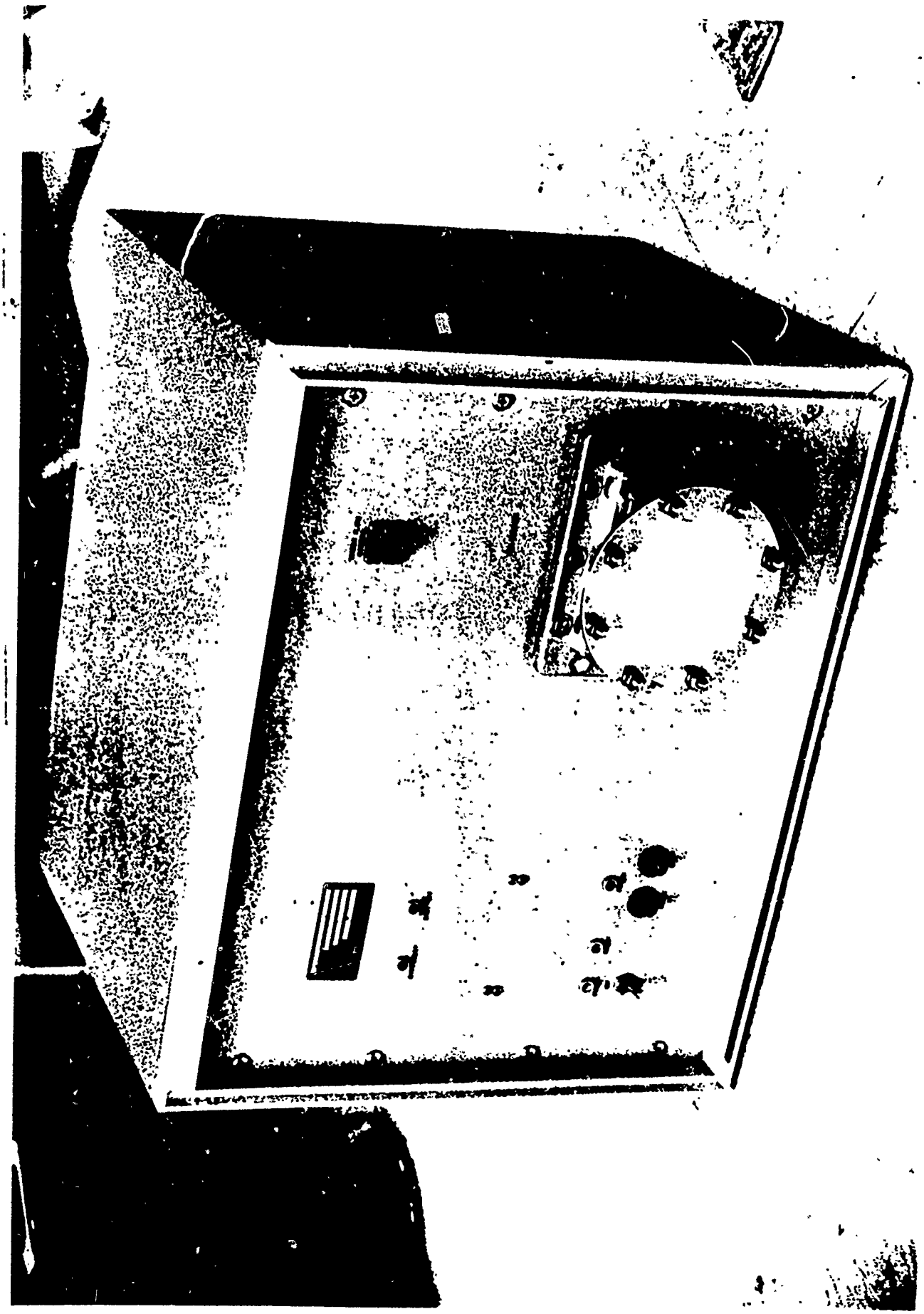

FIG 5 - PHOTO OF RF SOURCE

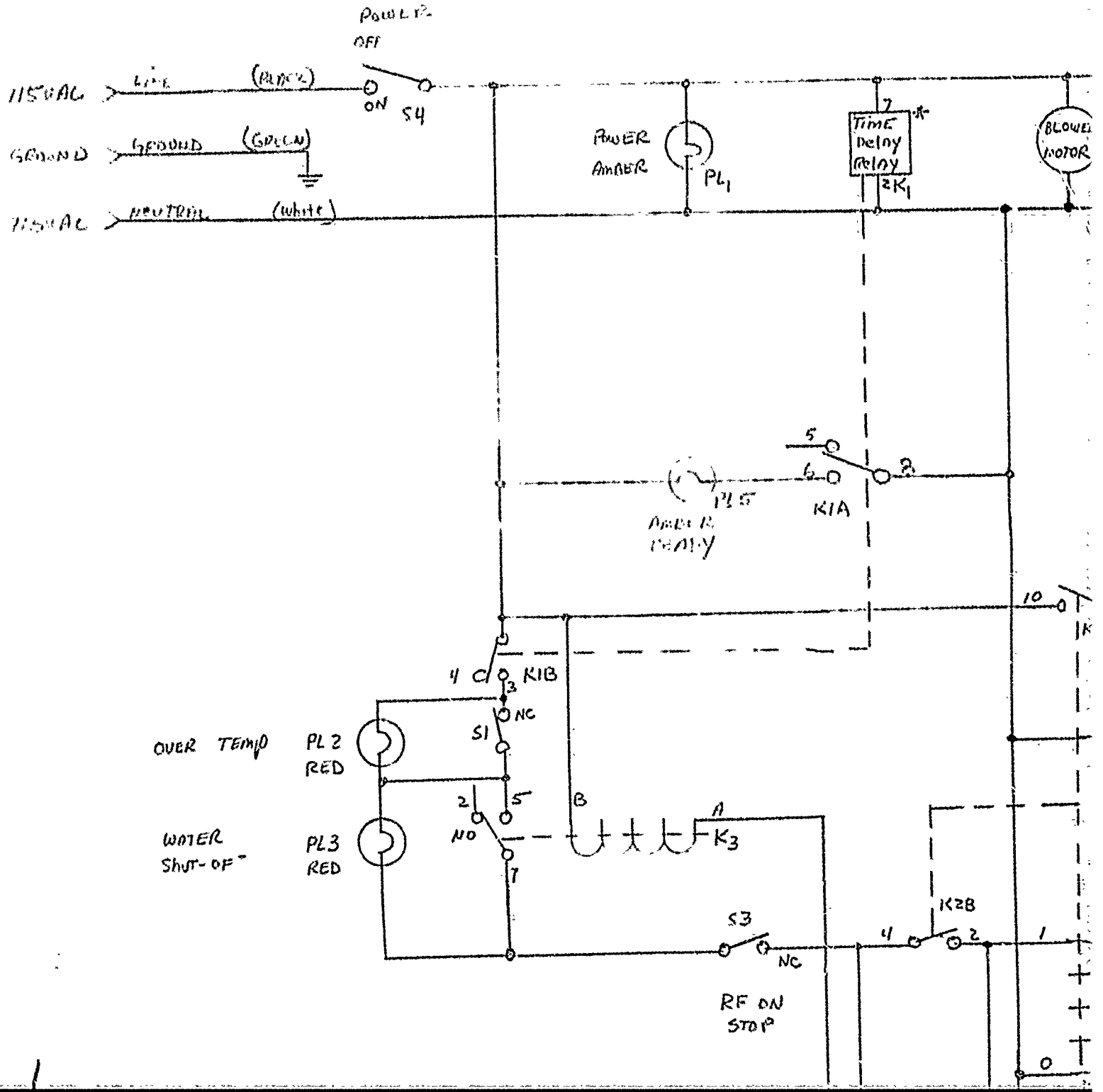
POWER
OFF
115VAC
LINE
(BLACK)
ON
S4
GROUND
GROUND
(GREEN)
115VAC
NEUTRAL
(white)
POWER
AMBER
PL1
TIME
Delay
Relay
2K1
BLOWER
MOTOR
5
6
2
PL5
AMBER
PILOT
K1A
10
4
K1B
3
NC
S1
OVER TEMP
PL2
RED
2
5
B
A
NO
K3
WATER
SHUT-OFF
PL3
RED
1
K2B
S3
4
2
1
NC
RF ON
STOP

REVISIONS

ZONE	LTR	DESCRIPTION

FORM

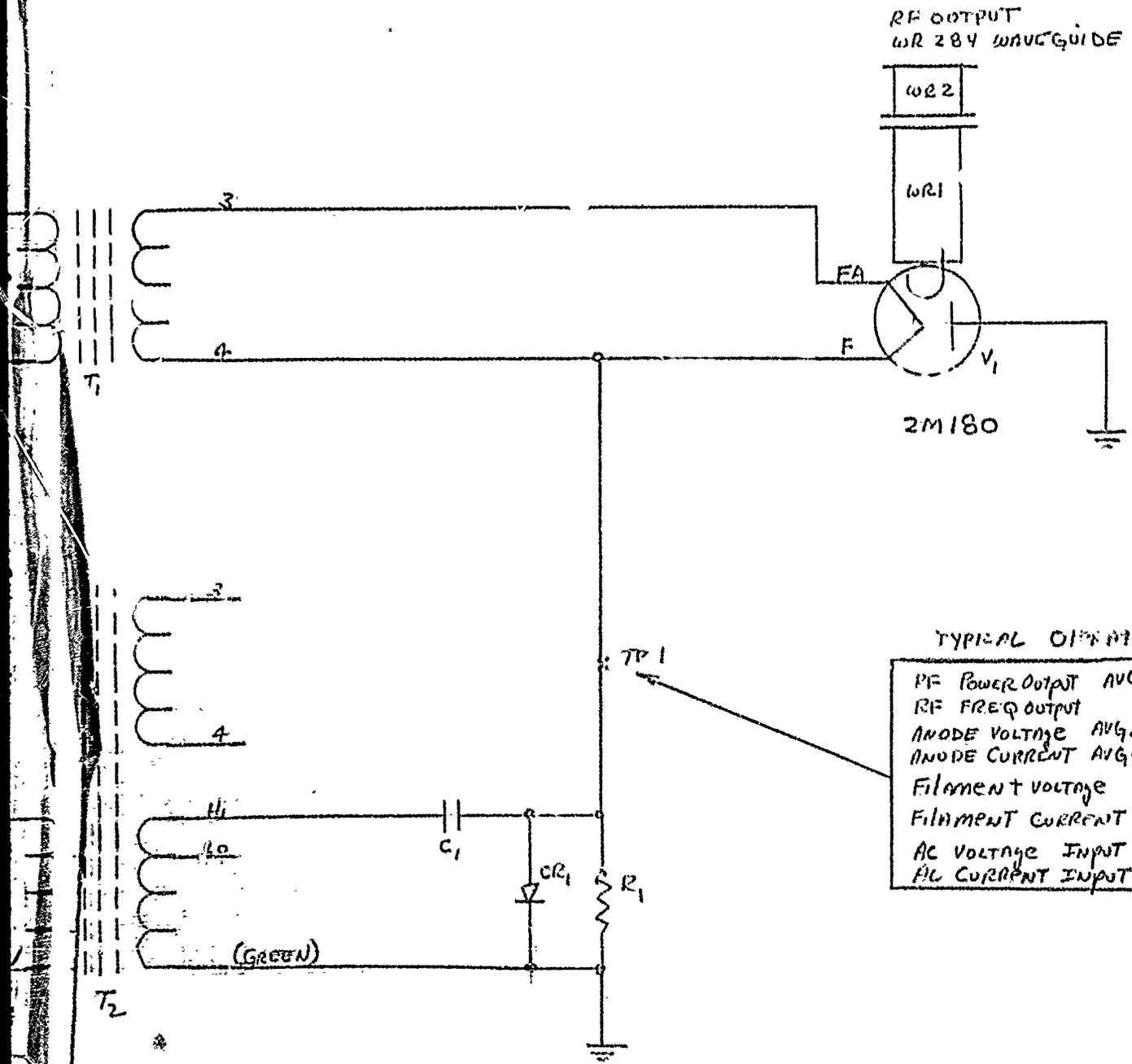

TYPICAL OPERATION DATA

RF POWER OUTPUT AVG.	1.1 KW
RF FREQ OUTPUT	2.45 GHz
ANODE VOLTAGE AVG.	2.05 KVDC
ANODE CURRENT AVG.	0.9 ADC
FILAMENT VOLTAGE	4.4 VAC
FILAMENT CURRENT	16 AAC
AC VOLTAGE INPUT	115 VAC
AC CURRENT INPUT	—

REVISIONS				
ZONE	LTR	DESCRIPTION	DATE	APPROV

OUTPUT
8Y WAVEGUIDE

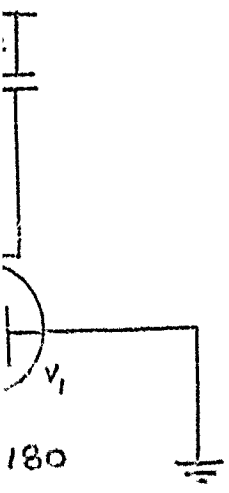

TYPICAL OPERATION DATA

Power Output	AVG.	1.[illegible] KW
FREQ OUTPUT		2.45 GHz
ODE VOLTAGE	AVG.	2.05 KVDC
ODE CURRENT	AVG.	0.9 ADC
lament + VOLTAGE		4.4 VAC
AMENT CURRENT		16 AAC
VOLTAGE INPUT		115 VAC
CURRENT INPUT		———

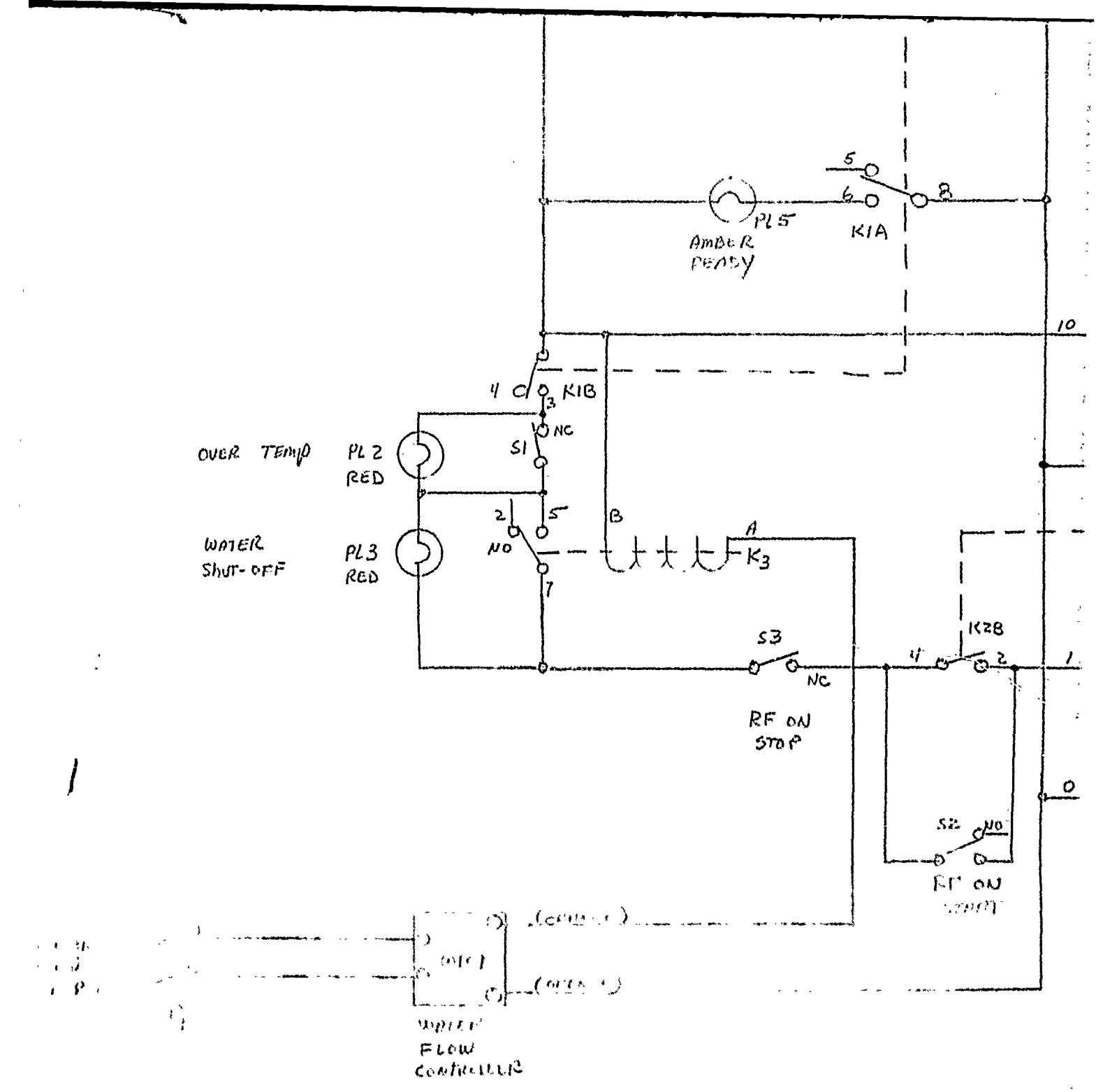

ENGINEERING CHECK LIST

SKETCHING	☐ LOCATE ON GRID. FREEHAND SKETCHING PREFERRED. LOCATE CIRCUIT SYMBOLS FUNCTIONALLY AROUND EACH STAGE. CONNECT STAGES IN LAYERS FROM LEFT-TO-RIGHT ARRANGE TWO OR MORE LAYERS FROM TOP-TO-BOTTOM.	REF DESIG	☐ IDENTIFY EACH SYMBOL BY REFERENCE DESIGNATION PER USA STD Y32.16. FOR DETAIL SEE ESM. ASSIGN REF. DESIG NUMBERS CONSECUTIVELY FROM LEFT TO RIGHT IN FUNCTIONAL SEQUENCE.
SIGNAL FLOW	☐ LOCATE INPUTS AT LEFT, OUTPUTS AT RIGHT (PREFERRED); OR INPUTS AT TOP, OUTPUTS AT BOTTOM; OR ANY COMBINATION OF THE TWO ABOVE.	PARTS IDENT	☐ SPECIFY RESISTANCE, CAPACITANCE AND INDUCTANCE VALUES. USE THE FORM OF FEWEST CIPHERS. SCHEMATIC IDENTITIES MUST AGREE WITH ELECTRICAL PARTS LIST
SYMBOLS	☐ USE CIRCUIT SYMBOLS PER USA STD Y32.2 FOR DETAIL, SEE ENGINEERING STANDARDS MANUAL. USE LOGIC SYMBOLS PER USA STD Y32.13 FOR DETAIL, SEE ENGINEERING STANDARDS MANUAL.	OTHER INFO	☐ ASSIGN FUNCTIONAL IDENTIFICATION TO PARTS, STAGES AND CIRCUITS. INDICATE MECHANICAL LINKAGE, POT ADJUSTMENT AND OPERATING CONTROLS. INDICATE SHIELDING, PAIRING AND CRITICAL GROUND. OUTLINE TERMINAL BOARDS AND SUB ASSEMBLIES.

4

A

3

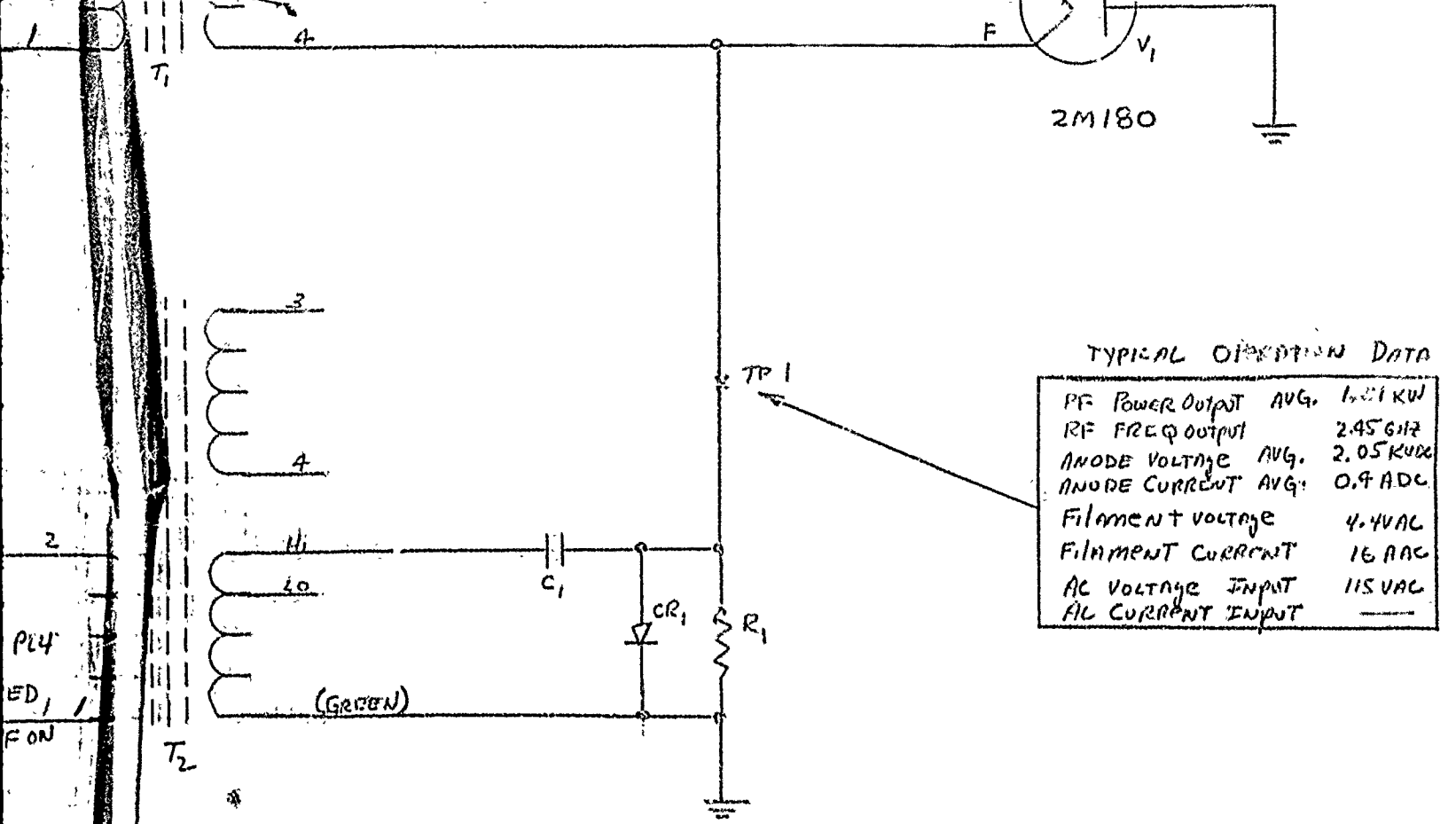

TYPICAL OPERATION DATA

RF POWER OUTPUT	AVG.	1.21 KW
RF FREQ OUTPUT		2.45 GHz
ANODE VOLTAGE	AVG.	2.05 KVDC
ANODE CURRENT	AVG.	0.9 ADC
FILAMENT VOLTAGE		4.4 VAC
FILAMENT CURRENT		16 AAC
AC VOLTAGE INPUT		115 VAC
AC CURRENT INPUT		———

2

* 5 min Delay Relay
Dial Setting 2½
Delay 60 Seconds

OPERATOR INSTRUCTIONS

5

NOTES:
1. PARTIAL REFERENCE DESIGNATIONS ARE SHOWN; FOR COMPLETE DESIGNATION PREFIX WITH UNIT NUMBER AND SUB-ASSEMBLY DESIGNATIONS.
2. UNLESS OTHERWISE SPECIFIED:
ALL RESISTANCE VALUES ARE IN
ALL CAPACITANCE VALUES ARE IN
ALL DIODES ARE
ALL TRANSISTORS ARE
ALL INTEGRATED CKTS ARE

PREPARED IN ACCORDANCE WITH MIL STD 100

LTR	DESCRIPTION	NEXT ASSY	USED ON

APPLICATION

CONTRACT DAAK 70-74-C

APPROVALS SIGNATURE & DATE

DRAWN	
CHECKED	
MECH	
ELECT	
STDS	
R.C.F.M.	

SIZE C | CODE IDENT. 28527

SCALE | SHT

PT

2 1

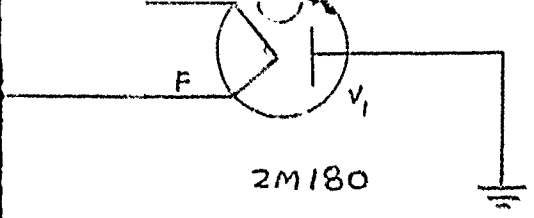

TYPICAL OPERATION DATA

RF Power Output AVG.	1.7 KW
RF FREQ Output	2.45 GHz
ANODE VOLTAGE AVG.	2.05 KVDC
ANODE CURRENT AVG.	0.9 ADC
Filament VOLTAGE	4.4 VAC
FILAMENT CURRENT	16 AAC
AC VOLTAGE INPUT	115 VAC
AC CURRENT INPUT	———

3

Time Delay Relay
Time Current 2½
Relay 60 Sec

PREPARED IN ACCORDANCE WITH MIL STD 100	CONTRACT DAAK 70-79-C	CTI AVIONICS DIVISION	RUTLEY, NEW JERSEY
	APPROVALS SIGNATURE & DATE		
	DRAWN	RF Source	
	CHECKED	Fig 6	6
	MECH		
	ELECT		
NEXT ASSY	USED ON		
APPLICATION		SIZE C	CAGE IDENT NO 28527
		SCALE	CATEGORY
		SHEET	REV

ITT AVIONICS DIVISION NUTLEY, NEW JERSEY

ELECTRICAL PARTS LIST

DRAWING NUMBER

ASSY NAME:
ASSY REF DESIG:

PART OF UNIT: RF SOURCE
UNIT OPER TEMP:

PART OF EQUIP:

PREPARED BY ENGINEERING

APPROVED BY: RELIABILITY - ENGINEERING -

SIZE A

CODE IDENT NO. 28527

SHEET 1 OF 2

REV

1	2	3	4	5	6			7	8
CIRCUIT REF DESIG	PART DESCRIPTION	VALUE & TOL	MFR OR MIL SPEC	MFR OR MIL PART NO. / ITT PART NO.	STRESS RATED	STRESS APPLIED NOM	STRESS APPLIED MAX	REL CODE IDENT	FAIL RATE %
C1	CAPACITOR		LITTON	M10D59					
CR1	DIODE, HIGH VOLTAGE		LITTON	M3D29					
K1	RELAY, TIME DELAY		MAGNECRAFT	W211ACPS0X-8					
K2	RELAY, POWER		LITTON	M16D61					
K3	RELAY		STRUTHERS-DUNN	A283XAXC1					
PL1	PILOT LIGHT, AMBER		LEECRAFT	36EN2313					
PL2	PILOT LIGHT, RED		LEECRAFT	36EN2311					
PL3	PILOT LIGHT, RED		LEECRAFT	36EN2311					
PL4	PILOT LIGHT, RED		LEECRAFT	36EN2311					
PL5	PILOT LIGHT, AMBER		LEECRAFT	36EN2313					

Fig. 7a

ITTAV D6597 ISS. 2/70

ITT AVIONICS DIVISION NUTLEY, NEW JERSEY

ELECTRICAL PARTS LIST

DRAWING NUMBER

ASSY NAME:
ASSY REF DESIG:

PART OF UNIT: RF SOURCE
UNIT OPER TEMP:

PART OF EQUIP:

PREPARED BY ENGINEERING

APPROVED BY:
RELIABILITY -
ENGINEERING -

SIZE A

CODE IDENT NO. 28527

Fig. 7b

SHEET 2 OF 3

REV.

1	2	3	4	5	6			7	8
CIRCUIT REF DESIG	PART DESCRIPTION	VALUE & TOL	MFR OR MIL SPEC	MFR OR MIL PART NO. / ITT PART NO.	STRESS RATED	STRESS APPLIED NOM	STRESS APPLIED MAX	REL CODE IDENT	FAIL RATE %
R1	RESISTOR, BLEEDER		LITTON	M3D12					
S1	SWITCH, THERMAL PROTECTION		LITTON	M4D77					
S2	SWITCH			MS25089-3C 828304					
S3	SWITCH			MS25089-3C 828304					
S4	CIRCUIT BREAKER	25 AMP	POTTER & BRUMFIELD	112-225-101					
T1	TRANSFORMER, FILAMENT		LITTON	M60D75					
T2	TRANSFORMER, HIGH VOLTAGE		LITTON	M60D53					
V1	TUBE, MAGNETRON		PANASONIC	2M180					
WFC1	WATER FLOW CONTROLLER		PRESSURE CONTROL	F103					

ITTAV D6597 ISS. 2/70

ITT AVIONICS DIVISION — NUTLEY, NEW JERSEY

ELECTRICAL PARTS LIST

DRAWING NUMBER

ASSY NAME:
ASSY REF DESIG:

PART OF UNIT: RF SOURCE
UNIT OPER TEMP:

PART OF EQUIP:

PREPARED BY ENGINEERING

APPROVED BY: RELIABILITY - ENGINEERING - [signature]

SIZE: A

CODE IDENT NO.: 28527

SHEET

REV.

1	2	3	4	5	6			7	8
CIRCUIT REF DESIG	PART DESCRIPTION	VALUE & TOL	MFR OR MIL SPEC	MFR OR MIL PART NO. / ITT PART NO.	STRESS RATED	STRESS APPLIED NOM	STRESS APPLIED MAX	REL CODE IDENT	FAIL RATE %
BL1	MOTOR, BLOWER		LITTON	M41D22					
WR1	WAVEGUIDE MAGNETRON COUPLER		ITT	ITT Design					
WR2	WAVEGUIDE TRANSITION WR 430 to WR 284		GERLING MOORE	40-12					

Fig. 7c

Mode	Cavity Contents	Short Position (inches)	Incident Power (watts)	Reflected Power (watts)	Isolated Port (watts)	Power Dissipated In Cavity (watts)
TE-11	Pyrex	4-3/4	1278	40	209	1029
TE-11	Quartz & Carbon	2	1178	89	225	864
TM-01	Empty	4-7/8	1120	186	649	285
TM-01	Pyrex	2-5/16	1266	64	94	1108

FIGURE 4-10 Summary of High Power Measurements

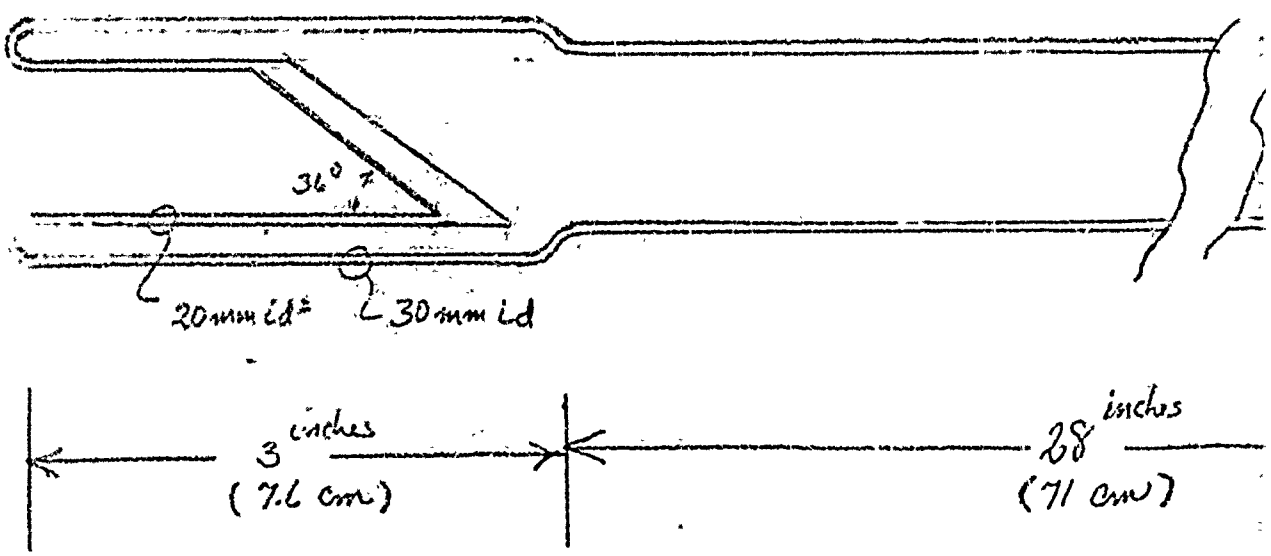
36° ±
20mm id
30mm id

3 inches
(7.6 cm)
28 inches
(71 cm)

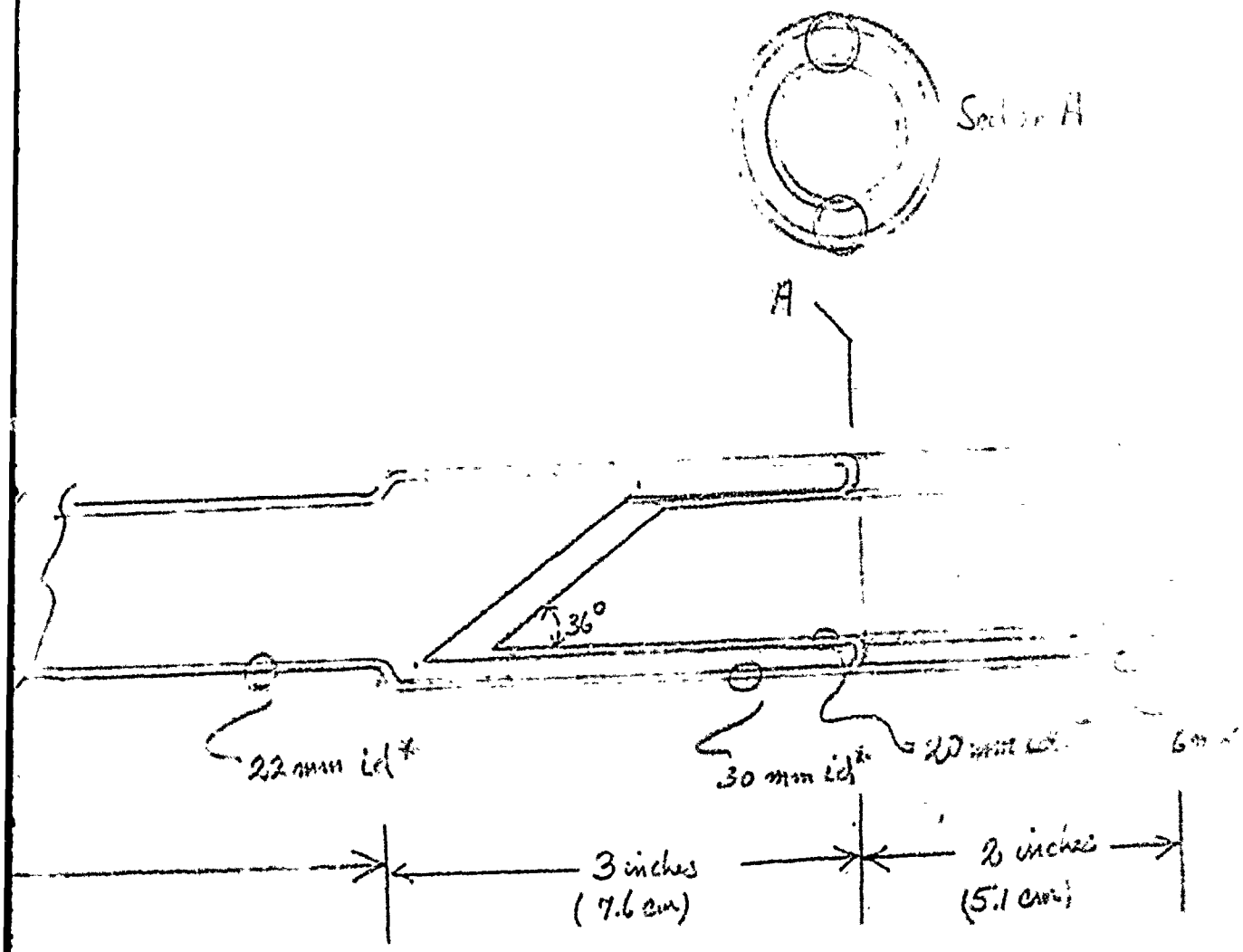

* Matched Clear Fused Quartz tubing Cg 8565.
Single Bore Standard wall.

Window thickness 5 mm. Laser grade Quartz.

APPENDIX II

A PROGRAM FOR THE SOLUTION OF SAHA'S EQUATION

$$\log_{10}\left(\frac{\varepsilon^2}{1-\varepsilon^2}\right) \times P = -5044\frac{E}{T} + \log_{10}\frac{\omega_i\omega_e}{\omega a} - 6.491$$

Program For Saha's Equation

```
000  43 RCL
001  01  01
002  99 PRT
003  43 RCL
004  07  07
005  99 PRT
006  98 ADV
007  43 RCL
008  02  02
009  99 PRT
010  43 RCL
011  12  12
012  65  ×
013  43 RCL
014  13  13
015  55  ÷
016  43 RCL
017  14  14
018  95  =
019  42 STO
020  05  05
021  43 RCL
022  03  03
023  65  ×
024  43 RCL
025  01  01
026  55  ÷
027  43 RCL
028  02  02
029  95  =
030  42 STO
031  08  08
032  43 RCL
033  04  04
034  65  ×
035  53  (
036  43 RCL
037  02  02
038  28 LOG
039  54  )
040  95  =
041  42 STO
042  09  09
043  43 RCL
044  05  05
045  28 LOG
046  95  =
047  42 STO
048  10  10
049  43 RCL
050  07  07
051  28 LOG
052  95  =
053  42 STO
054  08  08
055  53  (
056  43 RCL
057  08  08
058  94 +/-
059  85  +
060  43 RCL
061  09  09
062  85  +
063  43 RCL
064  10  10
065  75  -
066  43 RCL
067  06  06
068  75  -
069  43 RCL
070  11  11
071  54  )
072  22 INV
073  28 LOG
074  95  =
075  42 STO
076  15  15
077  53  (
078  43 RCL
079  15  15
080  55  ÷
081  53  (
082  01  1
083  85  +
084  43 RCL
085  15  15
086  54  )
087  54  )
088  34 fX
089  95  =
090  42 STO
091  16  16
092  99 PRT
093  01  1
094  75  -
095  43 RCL
096  16  16
097  95  =
098  99 PRT
099  53  (
100  43 RCL
101  07  07
102  28 LOG
103  75  -
104  43 RCL
105  19  19
106  75  -
107  43 RCL
108  02  02
109  75  -
110  75  -
111  43 RCL
112  18  18
113  75  -
114  43 RCL
115  20  20
116  54  )
117  22 INV
118  28 LOG
119  95  =
120  42 STO
121  21  21
122  65  ×
123  43 RCL
124  16  16
125  95  =
126  42 STO
127  22  22
128  99 PRT
129  98 ADV
130  69 DP
131  20  20
132  43 RCL
133  00  00
134  65  ×
135  43 RCL
136  17  17
137  95  =.
138  42 STO
139  02  02
140  61 GTO
141  00  00
142  07  07
```

Data Base

```
2.4 01 00
7.4336392-05 01
2.4 03 02
5.044 03 03
2.5 00 04
1. 00 05
6.491 00 06
1.-03 07
2.1930435 01 08
8.4043196 00 09
0. 00 10
-3. 00 11
1. 00 12
2. 00 13
2. 00 14
9.6130725-18 15
3.1005762-09 16
1. 02 17
-2.3779957 01 18
1.9141 00 19
0. 00 20
3.1924896 15 21
9.898557 06 22
```

DATA OUTPUT

```
7.4336392-05 EV      ionization
1.-03 ATMOS

2.4 03 °Kelvin
9.9499451-01 1-e
5.490281-06 e
3.0594524 15 n_e cm^-3

2.5 03
```

APPENDIX III

A PROGRAM FOR DETERMINING THE PARAMETERS OF A CYLINDER WAVE GUIDE CAVITY USING THE TI59 HAND COMPUTER

The parameters of a cylinder wave guide cavity may be calculated from the materials and geometry that make up the cavity. A program has been written that is suitable for a TI 59 hand computer that is equiped with a printer. The notation is defined for the parameters in the tabulation of the storage positions. Table 3.1 below.

The relationships are those used in the MIT Radiation Laboratory series particularly Vol 11 Section 5.4 Vol. 8 Section 11. The interrelations are:

Table 3.1

$$\epsilon_1 = \epsilon' - j\epsilon'' \quad ; \quad \epsilon_1/\epsilon_0 = \epsilon'/\epsilon_0 - j\,\epsilon''/\epsilon_0 \quad \text{for } \mu_1/\mu_0 = 1$$

$$(\epsilon_0/\epsilon_1)^{1/2} C = V \text{ (phase velocity)} = \lambda_1 f_0 \quad ; \quad C = \lambda_0 f_0$$

$$\lambda_c = \frac{\pi D}{\chi_{lm}} (\epsilon'/\epsilon_0)^{1/2} \quad ; \quad \delta = \left(\frac{\lambda_0 \rho}{30}\right)^{1/2} / 2\pi$$

$$\lambda_g/\lambda_0 = \left[\left(\epsilon_1/\epsilon_0 - (\lambda_0/\lambda_{c0})^2\right) \times \left(1 + \left(1 + \left(\frac{\epsilon''/\epsilon_0}{\epsilon'/\epsilon_0 - (\lambda_0/\lambda_{c0})^2}\right)^2\right)^{1/2}\right)/2\right]^{-1/2}$$

$$L = n/2 \,/\, \left((1/\lambda^2) - (\chi_{lm}/\pi D)^2\right)^{1/2}$$

$$Q\,\delta/\lambda_1 = \frac{\left[1 - (l/\chi_{lm})^2\right] \times \left[\chi_{lm}^2 + (n\pi D/2L)^2\right]^{3/2}}{2\pi\left[\chi_{lm}^2 + n^2\pi^2 D^3/4L^3 + (1 - D/L)(n\pi D l/2L\chi_{lm}^2)\right]}$$

Table 3.2

DATA STORAGE POSITIONS FOR CYLINDRICAL WAVE GUIDE CAVITY PROGRAM

Stor	
01	f_o frequency H_z
02	D diameter cm
03	L length cm
04	ρ resistivity of cavity material ohm cm
05	$\varepsilon^1/\varepsilon_o$ real part of the dielectric constant relative to vacuum
06	$\varepsilon^{11}/\varepsilon_o$ imaginary part of the dielectric constant relative to vacuum
07	L/D ratio of the length to diameter of chamber
08	λ_o vacuum wavelength, cm, resulting from applied frequency f_o
09	δ skin depth of the cavity wall, cm
10	c the velocity of light space, cm/sec
11	$120\pi^2$ a constant
12	X_{1m}^{mth} Root of the bessel function $J_1'(x) = 0$, TE mode
13	λ_{co} cutoff wavelength for TE mode in a vacuum cavity, cm
14	λ_q wavelength in guide of TE mode in an ε_o filled cavity, cm
15	α_d attenuation coefficient due to dielectric losses cm^{-1}
16	n the length of the cavity in ½ periods of E_r
19	X_{1m}^{mth} Root of bessel function $J_1(x) = 0$ TM mode
20	λ_{co} cutoff wavelength of TM mode in a vacuum cavity 1 cm
25	$(\varepsilon_o/\mu_o)^{\frac{1}{2}}$
26	$(\lambda_o/\lambda_{co})^2$ TE mode
27	λ_1 wavelength in a medium $\varepsilon_1/\varepsilon_o$ due to f_o, (cm)
28	TE, λ_c cutoff wavelength in an $\varepsilon/\varepsilon_o$ filled TE cavity

Stor (cont'd)

29 l the number of full period variations of E_r as a function of θ

30 $(n\pi D/2L)^2$ for TE cavities

31 Q δ/λ_1 the geometrically dependent component of the cavity quality for the TE mode.

32 Q the quality factor for the TE modes.

33 λ_{co} the cutoff wavelength for an $\varepsilon/\varepsilon_o$ filled TM cavity cm

34 $(\lambda_o/\lambda_{co})^2$ TM mode

35 λ_g the angular wavelength for the TM mode cm

36 α_d the dielectric attenuation in the TM mode cm^{-1}

37 L the length of the TM cavity cm

38 L/D the length to diameter ratio of the TM cavity

39 $(n\pi D/2L)^2$ for TM cavities

40 Q δ/λ the geometrically dependent component of the cavity quality for the TM modes.

41 Q the quality of the TM mode cavities.

PROGRAM FOR TI 58

```
000  25 CLR
001  69 OP
002  00  00
003  04  4
004  03  3
005  01  1
006  03  3
007  04  4
008  02  2
009  01  1
010  07  7
011  00  0
012  00  0
013  69 OP
014  01  01
015  02  2
016  02  2
017  04  4
018  01  1
019  02  2
020  04  4
021  01  1
022  06  6
023  01  1
024  07  7
025  69 OP
026  02  02
027  00  0
028  00  0
029  01  1
030  05  5
031  01  1
032  03  3
033  04  4
034  02  2
035  02  2
036  04  4
037  69 OP
038  03  03
039  03  3
040  07  7
041  04  4
042  05  5
043  00  0
044  00  0
045  00  0
046  00  0
047  00  0
048  00  0
049  69 OP
050  04  04
051  69 OP
052  05  05
053  43 RCL
054  01  01
055  99 PRT
056  43 RCL
057  02  02
058  99 PRT
059  43 RCL
060  03  03
061  43 RCL
062  04  04
063  99 PRT
064  43 RCL
065  05  05
066  99 PRT
067  43 RCL
068  06  06
069  99 PRT
070  43 RCL
071  10  10
072  55  ÷
073  43 RCL
074  01  01
075  95  =
076  42 STO
077  08  08
078  99 PRT
079  43 RCL
080  08  08
081  55  ÷
082  43 RCL
083  05  05
084  34 ΓX
085  95  =
086  42 STO
087  27  27
088  99 PRT
089  53  (
090  43 RCL
091  08  08
092  65  ×
093  43 RCL
094  04  04
095  55  ÷
096  43 RCL
097  11  11
098  54  )
099  34 ΓX
100  95  =
101  42 STO
102  09  09
103  99 PRT
104  98 ADV
105  69 OP
106  00  00
107  03  3
108  07  7
109  01  1
110  07  7
111  00  0
112  02  2
113  00  0
114  02  2
115  00  0
116  00  0
117  69 OP
118  02  02
119  69 OP
120  05  05
121  89  π
122  65  ×
123  43 RCL
124  02  02
125  55  ÷
126  43 RCL
127  12  12
128  99 PRT
129  95  =
130  95  =
131  42 STO
132  13  13
133  99 PRT
134  43 RCL
135  05  05
136  34 ΓX
137  65  ×
138  43 RCL
139  13  13
140  95  =
141  42 STO
142  28  28
143  99 PRT
144  53  (
145  43 RCL
146  08  08
147  55  ÷
148  43 RCL
149  13  13
150  54  )
151  33 X²
152  95  =
153  42 STO
154  26  26
155  43 RCL
156  08  08
157  65  ×
158  53  (
159  53  (
160  43 RCL
161  05  05
162  75  -
163  43 RCL
164  26  26
165  54  )
166  65  ×
167  53  (
168  01  1
169  85  +
170  53  (
171  01  1
172  85  +
173  53  (
174  43 RCL
175  06  06
176  55  ÷
177  53  (
178  43 RCL
179  05  05
180  75  -
181  43 RCL
182  26  26
183  54  )
184  54  )
185  33 X²
186  54  )
187  34 ΓX
188  54  )
189  55  ÷
190  02  2
191  54  )
192  34 ΓX
193  35 1/X
194  95  =
195  42 STO
196  14  14
197  99 PRT
198  43 RCL
199  14  14
200  65  ×
201  43 RCL
202  06  06
203  65  ×
204  89  π
205  55  ÷
206  43 RCL
207  08  08
208  33 X²
209  95  =
210  42 STO
211  15  15
212  99 PRT
213  43 RCL
214  16  16
215  99 PRT
216  43 RCL
```

217	16	16	277	33	X^2	337	65	×	397	65	×
218	55	÷	278	54	)	338	43	RCL	398	53	(
219	53	(	279	65	×	339	27	27	399	53	(
220	02	2	280	53	(	340	55	÷	400	43	RCL
221	65	×	281	43	RCL	341	43	RCL	401	05	05
222	53	(	282	12	12	342	09	09	402	75	-
223	43	RCL	283	33	X^2	343	95	=	403	43	RCL
224	27	27	284	85	+	344	42	STO	404	34	34
225	33	X^2	285	43	RCL	345	32	32	405	54	)
226	35	1/X	286	30	30	346	99	PRT	406	65	×
227	75	-	287	54	)	347	98	ADV	407	53	(
228	43	RCL	288	45	Y^X	348	69	DP	408	01	1
229	13	13	289	01	1	349	00	00	409	85	+
230	33	X^2	290	93	.	350	03	3	410	53	(
231	35	1/X	291	05	5	351	07	7	411	01	1
232	54	)	292	54	)	352	03	3	412	85	+
233	34	$\sqrt{X}$	293	55	÷	353	00	0	413	53	(
234	54	)	294	53	(	354	00	0	414	43	RCL
235	95	=	295	02	2	355	01	1	415	06	06
236	42	STO	296	65	×	356	00	0	416	55	÷
237	03	03	297	89	π	357	02	2	417	53	(
238	99	PRT	298	65	×	358	00	0	418	43	RCL
239	43	RCL	299	53	(	359	00	0	420	75	-
240	03	03	300	43	RCL	360	69	DP	420	65	×
241	55	÷	301	12	12	361	02	02	421	43	RCL
242	43	RCL	302	33	X^2	362	69	DP	422	34	34
243	02	02	303	85	+	363	05	05	423	54	)
244	95	=	304	43	RCL	364	43	RCL	424	54	)
245	42	STO	305	30	30	365	02	02	425	33	X^2
246	07	07	306	55	÷	366	65	×	426	54	)
247	99	PRT	307	43	RCL	367	89	π	427	34	$\sqrt{X}$
248	98	ADV	308	07	07	368	55	÷	428	54	)
249	53	(	309	85	+	369	43	RCL	429	55	÷
250	43	RCL	310	53	(	370	19	19	430	02	2
251	16	16	311	01	1	371	99	PRT	431	54	)
252	65	×	312	75	-	372	95	=	432	34	$\sqrt{X}$
253	89	π	313	43	RCL	373	42	STO	433	35	1/X
254	55	÷	314	07	07	374	20	20	434	95	=
255	53	(	315	35	1/X	375	99	PRT	435	42	STO
256	02	2	316	54	)	376	65	×	436	35	35
257	65	×	317	65	×	377	43	RCL	437	99	PRT
258	43	RCL	318	53	(	378	05	05	438	43	RCL
259	07	07	319	43	RCL	379	33	X^2	439	35	35
260	54	)	320	30	30	380	95	=	440	65	×
261	54	)	321	65	×	381	42	STO	441	43	RCL
262	33	X^2	322	53	(	382	33	33	442	06	06
263	95	=	323	43	RCL	383	99	PRT	443	65	×
264	42	STO	324	29	29	384	53	(	444	89	π
265	30	30	325	55	÷	385	43	RCL	445	55	÷
266	53	(	326	43	RCL	386	08	08	446	43	RCL
267	53	(	327	12	12	387	55	÷	447	08	08
268	01	1	328	54	)	388	43	RCL	448	33	X^2
269	75	-	329	33	X^2	389	20	20	449	95	=
270	53	(	330	54	)	390	54	)	450	42	STO
271	43	RCL	331	95	=	391	33	X^2	451	36	36
272	29	29	332	42	STO	392	95	=	452	99	PRT
273	55	÷	333	31	31	393	42	STO	453	43	RCL
274	43	RCL	334	99	PRT	394	34	34	454	16	16
275	12	12	335	43	RCL	395	43	RCL	455	99	PRT
276	54	)	336	31	31	396	08	08	456	55	÷

```
457  53  (
458  02  2
459  65  ×
460  53  (
461  43  RCL
462  27   27
463  33  X²
464  35  1/X
465  75  -
466  43  RCL
467  20   20
468  33  X²
469  35  1/X
470  54  )
471  34  ΓX
472  54  )
473  95  =
474  42  STO
475  37   37
476  99  PRT
477  43  RCL
478  37   37
479  55  ÷
480  43  RCL
481  02   02
482  95  =
483  42  STO
484  38   38
485  99  PRT
486  98  ADV
487  53  (
488  43  RCL
489  16   16
490  65  ×
491  89  π
492  55  ÷
493  53  (
494  02  2
495  65  ×
496  43  RCL
497  38   38
498  54  )
499  54  )
500  33  X²
501  95  =
502  42  STO
503  39   39
504  53  (
505  43  RCL
506  19   19
507  33  X²
508  85  +
509  43  RCL
510  39   39
511  54  )
512  34  ΓX
513  55  ÷
514  53  (
515  02  2
516  65  ×
517  89  π
518  65  ×
519  53  (
520  01  1
521  85  +
522  43  RCL
523  38   38
524  35  1/X
525  54  )
526  54  )
527  95  =
528  42  STO
529  40   40
530  99  PRT
531  65  ×
532  43  RCL
533  27   27
534  55  ÷
535  43  RCL
536  09   09
537  95  =
538  42  STO
539  41   41
540  99  PRT
541  98  ADV
542  91  R/S
543  61  GTO
544  01   01
545  05   05
546  91  R/S
```

Table 3.3

PRINT OUT

```
WAVE GUIDE CAVITY
2450000000.      fo
   10.8402       D
.0000063694      ρ
         1.      ε'/ε0
         0.      ε"/ε0
12.23636735      λ0
12.23636735      λ1
.0002565287      δ

    TE11
     1.841       x11
18.49836648      λco
18.49836648      λc
16.31603604      λg
         0.      αd
         1.      n
 8.15801802      L
.7525708031      L/D

.2762474574      Qδ/λ1
13176.94899      Q

    TM01
     2.405       x01
14.16028802      λco
14.16028802      λc
24.31400837      λg
         0.      αd
         1.      n
12.15700418      L
1.121474159      L/D

.2341565538      Qδ/λ1
11169.22123      Q
```

The computer instruction are given for a partition of 559.49 i.e. 49 data registers are allocated to information storage. Table 3.2 indicates the instructions required. Table 3.3 is a printout of the program solution that is used in section //.

APPENDIX IV

T159
Plasma Resistivity Program

Program

```
000   43 RCL
001   00  00
002   99 PRT
003   43 RCL
004   01  01
005   99 PRT
006   53  (
007   53  (
008   53  (
009   43 RCL
010   05  05
011   65  ×
012   43 RCL
013   00  00
014   54  )
015   45 Y×
016   03  3
017   54  )
018   55  ÷
019   53  (
020   89  π
021   65  ×
022   43 RCL
023   01  01
024   54  )
025   54  )
026   34 √X
027   65  ×
028   01  1
029   93  .
030   05  5
031   55  ÷
032   53  (
033   43 RCL
034   03  03
035   65  ×
036   43 RCL
037   04  04
038   65  ×
039   53  (
040   43 RCL
041   02  02
042   45 Y×
043   03  3
044   54  )
045   54  )
046   95  =
047   42 STO
048   10  10
049   99 PRT
050   43 RCL
051   10  10
052   23 LNX
053   95  =
054   42 STO
055   11  11
056   99 PRT
057   43 RCL
058   11  11
059   65  ×
060   43 RCL
061   06  06
062   55  ÷
063   53  (
064   43 RCL
065   00  00
066   45 Y×
067   01  1
068   93  .
069   05  5
070   54  )
071   95  =
072   42 STO
073   12  12
074   99 PRT
075   98 ADV
076   91 R/S
077   81 RST
```

Data File

```
          7.  03    00
          1.  11    01
4.80217-10    02    02
          1.  00    03
          1.  00    04
1.38024-16    05    05
       6.53 03    06
          0.  00    07
          0.  00    08
          0.  00    09
2.2950001  04    10
1.0041073  01    11
1.1195571-01    12
```

Output

```
          7.  03   T °K
          1.  11   n_e cm^-3
2.2950001  04   Λ
1.0041073  01   ln Λ
1.1195571-01   ρ ohm cm
```